Structural Mechanics of Class 1 Viral Membrane Fusion Proteins

Mark A. Benhaim

A dissertation

submitted in partial fulfillment of the

requirements for the degree of

Doctor of Philosophy

University of Washington

2020

Reading Committee:

Kelly K. Lee, Chair

Abhinav Nath

Miklos Guttman

Program Authorized to Offer Degree:

Medicinal Chemistry

University of Washington

Abstract

Structural Mechanics of Class 1 Viral Membrane Fusion Proteins

Mark A. Benhaim

Chair of the Supervisory Committee:

Dr. Kelly K. Lee

Medicinal Chemistry

Protein-mediated membrane fusion is a highly regulated biological process essential for cellular and organismal functions and infection by enveloped viruses. During viral entry, the membrane fusion reaction is catalyzed by specialized protein machinery on the viral surface. These viral fusion proteins undergo a series of dramatic structural changes during membrane fusion where they engage, remodel, and ultimately fuse with the host membrane. The structural and dynamic nature of these conformational changes and their impact on the membranes have long-eluded characterization. Furthermore, the native pre-fusion structural and conformational dynamics of these fusion machines remains unclear as the conventional structural approaches employed by structural biologists are not well suited for studying these dynamic protein machines on the viral surface. The objective of this dissertation is to characterize the complete mechanism of Influenza virus hemagglutinin (HA) fusion activation and membrane fusion, and to profile and characterize the structural and conformational dynamics of the HIV-1 Env fusion glycoprotein on the viral surface. In chapter 2 I use continuous labeling HDX-MS to characterize the structural dynamics and conformational homogeneity of the HIV-1 Env fusion glycoprotein on the surface of two distinct engineered and authentic viral vaccine platforms. By

HDX-MS we observed significant amounts of non-native Env present in one vaccine platform, whereas all Env present in the other resembled trimeric Env in the closed conformation. In chapter 3, I use pulse labeling HDX-MS to characterize the mechanism of HA fusion activation and HA mediated membrane fusion *in situ* using whole infectious virions. Our data reveal how concurrent reorganizations at the HA1 receptor binding domain interface and HA2 fusion subunit produce a dynamic fusion intermediate ensemble in full-length HA. In contrast, the soluble HA ectodomain transitions directly to the post-fusion state with no observable intermediate. These data provide unprecedented insight into the structural mechanics of HA which has served as the prototypical class 1 viral fusion protein and informed our understanding about how all class 1 viral fusion proteins function. In chapter 4 I present developments and improvements on the HDX-MS workflows that will enable more complete characterizations of HA's mechanism and the structural and conformational dynamics of other class 1 viral fusion proteins. Together these works have dramatically furthered our understanding of the structural mechanics of class 1 fusion proteins and lay the foundation for future studies on influenza virus and other enveloped viruses and their membrane fusion machinery.

Table of Contents

Acknowledgments

I would like to express my most sincere thanks and gratitude to all of those who have contributed towards the success and completion of this dissertation.

Firstly, I would like to thank my supervisor and mentor Dr. Kelly Lee. Throughout the entirety of my work you have supported all aspects of my work, growth, and development. There is no question that I am who I am today because of your work and mentorship. I could not have imagined having a better boss than you. You let me explore my own research interests and fostered my development as a scientist. Our constant conversations, discussions, arguments, and bets were some of the fondest memories I have from the past 6 years. I look forward to continuing those conversations in the future, whether they be about science, or more importantly baking.

I would also like to thank Natalie K. Garcia who served as my mentor during the early years in lab. Without you I would have been completely lost, and it is because of you that I was able to do the work contained in this dissertation. You taught me how to think critically, be analytically minded, and importantly carry out everything I do with care, caution, and diligence. You were, and will always be, the best teacher I have ever had.

I would like to thank Dr. Miklos Guttman as well. I owe all my expertise in HDX-MS and MS to you. You are such an incredible scientist and person, I learned so much just being around you all these years. You are a constant inspiration; I have never met someone who is as hard working as yourself. I cannot think of anyone who is more deserving of the success they have than you.

I would also like to thank my committee members for their guidance and encouragement throughout this process: Dr. William Atkins, Dr. Abhinav Nath, Dr. Miklos Guttman, and Dr. Neil King. I have so greatly enjoyed working with each of you and being able to learn from you. Thank you all for the opportunities you have given me and the successes you have enabled me to achieve.

I would like to thank all the members of the Lee Lab: Long Gui, James Williams, Natalie Garcia, Tad Davenport, Nancy Hom, Vidya Mangala Prasad, Eddie Hodge, Alec Mileant, Adam Nguyen, Sally Kephart, Chengbo Chen, and Klaus Lovendahl. I could not have asked for a better group of people to have shared this journey with. You all have helped me grow into a better scientist and person, and I will cherish the time we spent together.

Finally, I would be no where without the support of those closest to me. To my Mom, you are the most amazing woman I know. I am who I am today because of you, without question. Those days walking around the yard and digging up bugs, endless trips to the Science Museum, and constant encouragement to ask questions and look beneath the surface were the beginnings of my journey as a scientist. To my brother, David, you are my best friend – you always have been and always will be. I have always looked up to you, and you have been a constant source of encouragement and inspiration. It was by following your footsteps and example that I have been able to achieve in life. To the memory of my Father, David. While I never had the opportunity to know you, I feel so lucky to be your son. The highest compliment I ever receive is hearing how much alike we are. To my wife, Nicole, you are my partner, my best friend, and biggest supporter. Thank you for your unending patience and love, without which I would have failed long ago. I cannot wait for what our future holds. And to my cats, Camas and Joop, you have taught me basically nothing, you have taken everything you can get your hands on, you have kept me up at night, and woken me up way too early in the morning. But I cannot imagine what my life would be like without you. Your highly conditional love keeps me going, and I cannot wait to see you when I leave every day – because I know you will be there, hungry, needy, and loving.

Chapter 1. Introduction

Portions of the text in this chapter have been modified and reproduced with permissions from:

Benhaim, M.A.; Lee, K.K. New Biophysical Approaches Reveal the Dynamics and Mechanics of Type I Viral Fusion Machinery and Their Interplay with Membranes. *Viruses* **2020**, *12*, 413.

1.1 Overview

The process of protein-mediated membrane fusion is essential for a range of cellular and organismal functions. It is involved in synaptic signaling, cellular communication, intra- and extra-cellular vesicle trafficking, mitochondrial homeostasis, sexual reproduction, embryogenesis, and infection by enveloped viruses [1-6]. Enveloped viruses, like all viruses, are non-living biological infectious agents comprised of a nucleic acid genome encapsulated in a protective shell. Unique to enveloped viruses, however, is the host derived lipid membrane surrounding the viral core. Enveloped viruses acquire this lipid envelope from their hosts during assembly as new viral progeny are released from infected cells. Infection by all enveloped viruses requires fusion of the viral and host membranes in order to deliver the viral genome and replication machinery across the host cell membrane to a suitable subcellular location and initiate an infection cycle. Enveloped viruses have evolved specialized protein machinery that drive this process to completion by undergoing a series of large-scale conformational changes in response to one or more activation triggers [7]. The nature of these changes and the resulting impact on the membranes themselves have long-eluded characterization, but new structural and biophysical techniques are providing a detailed glimpse into the structural changes carried out by the protein machinery as well as revealing the interplay of proteins and membranes during fusion. Collectively, the advances offer unprecedented new structural and mechanistic insights into this fundamental biological process and the viral protein machinery involved.

1.2 Anatomy of an Enveloped Virus: Influenza A virus

The influenza A virus belongs to the Orthomyxoviridae family of pleomorphic enveloped viruses and features a negative-sense, single stranded, segmented RNA genome [8]. Influenza A virus' eight genome segments are packaged in the viral core in complex with viral polymerases and nucleoproteins (Figure 1.1). The ribonucleic complex is contained within a capsid composed of the M1 matrix protein which lines the inside of the viral membrane. The M2 matrix proton channel lies within the viral membrane and is responsible for acidifying the viral lumen which is critical for delivering the viral replication complex to the target cell cytosol during infection. Two virally encoded glycoproteins decorate the surface of the influenza A virus; hemagglutinin (HA), which mediates attachment and entry into host cells, and neuraminidase (NA), which facilitates release of progeny virions from infected cells. HA is the dominant surface antigen and is the primary antigenic target for neutralizing antibodies.

1.3 Structure, Function, and Classifications of Viral Fusion Proteins

Protein mediated membrane fusion is a highly regulated biological process essential for cellular and organismal functions and infection by enveloped viruses. During viral entry the membrane fusion reaction is catalyzed by specialized protein machinery on the viral surface. All viral fusion proteins encode the same basic functionality; activate in response to a specific trigger(s), engage the target host membrane, draw the host membrane into close apposition with the viral membrane, and induce the membranes to merge. Viral membrane fusion proteins are classified into three distinct structural classes, with the class I fusion proteins being the best characterized to date [1, 4, 7, 9]. Among the class I fusion proteins, the Influenza virus hemagglutinin (HA) is the most widely studied and has served as the foundation upon which much of our understanding of viral membrane fusion proteins has been built. Class II fusion proteins are found in a range of viruses including flaviviruses and alphaviruses including Dengue, Zika, Chikungunya viruses, and even have been identified in eukaryotic cell-cell fusion systems

[10-13]. Class III fusion proteins are found in rhabdoviruses (such as Rabies and Vesicular Stomatatis virus G glycoproteins), herpesviruses (Herpes Simplex virus 1 gB protein), and most recently baculovirus [13-17]. While the individual folds exhibited by these classes are completely different, they share common functional traits in that all adopt a pre-fusion conformation prior to activation in which one terminus of the protein is anchored in the virus membrane by a transmembrane domain and a second membrane active component, either a fusion peptide or loop, is sequestered from interacting with membranes (Figure 1.2) [13]. A trigger, such as exposure to low pH in endosomes or receptor binding, induces the machinery to reorganize into a post-fusion state in which the two membrane active components are colocalized.

A defining characteristic of class I and II viral fusion proteins is that the pre-fusion conformation is metastable, or high-energy, with respect to the low-energy post-fusion conformation [4, 7, 18]. This ultimately results in an irreversible transition to the post-fusion state. Indeed many early pioneering studies on influenza HA led to the development of the "spring-loaded" mechanistic model for viral membrane fusion that is the prevailing way in which these machines are considered to function (discussed in detail below) [18-29]. In this model, class I fusion proteins function analogously to taut springs that are poised in a high energy state that, once triggered, rapidly and irreversibly "spring" or refold to the low energy, post-fusion state.

While membrane fusion is a thermodynamically favorable process, it requires an input of free energy to dehydrate the phospholipid headgroups as they are drawn into close apposition during fusion [2, 18, 30, 31]. This repulsive "hydration force" presents a kinetic barrier to fusion that prevents spontaneous, aberrant fusion events from occurring. This renders the membrane fusion reaction a tightly controlled biological process [13, 32-34]. The fusion peptides (class I) or fusion loops (class II) are believed to facilitate this reorganization of bound water while the free energy released from the exothermic refolding of the fusion proteins from the metastable pre-fusion to the low-energy post-

fusion state is harnessed to remodel, induce curvature and local defects in the lipid bilayer, and drive the membranes together [13, 18, 34-39]. The class III rhabdovirus G proteins are an exception to this general trend and exhibit reversible pH-dependent conformational switching [14, 16].

Until recently, static structures of the pre- and post-fusion states of isolated fusion protein ectodomains and low-resolution biophysical or spectroscopic measurements were the primary pieces of information that informed our models of membrane fusion. While the static structures provide defined endpoints for the conformational change that drives membrane fusion, they cannot tell us how these conformational changes occur and how these proteins interact with and perturb the lipid membrane during fusion. Furthermore, these static structural models do not capture or convey the innate dynamic motions and conformations sampled by these fusion proteins at rest in the pre-fusion state. This disparity is exemplified by recent solution state biophysical and structural studies of the influenza HA and HIV-1 Env fusion glycoproteins and will be discussed in detail in subsequent sections [19, 40-47]. A central focus of this thesis is to dissect the structural mechanism by which a class I fusion protein, influenza HA, becomes activated and reorganizes to catalyze the membrane fusion reaction. Furthermore, we have sought to characterize the structural and conformational dynamics of various class I viral fusion proteins under near native conditions on the surface of authentic and engineered viral systems.

1.4 Structural Organization of Class I Fusion Proteins

Class I viral fusion proteins are homotrimeric glycoproteins that decorate the viral envelope. These proteins are synthesized as inactive single chain polypeptide precursors that assemble into trimers and are proteolytically processed by host cell proteases into their functional, metastable pre-fusion states [4, 7, 48-50]. Proteolytic processing can take place during viral assembly, maturation, and/or entry depending on the specific virus. In the case of influenza, the uncleaved and fusion incompetent HA

glycoprotein trimer, HA0, is primarily processed by extracellular trypsin-like proteases after new virions are released from infected cells [20, 23, 29, 48, 49]. HA's from highly pathogenic avian Influenza viruses often contain a polybasic motif at their cleavage site and are processed by endogenous proteases, such as furin, in the trans-Golgi network [8, 51, 52]. The resulting functional HA assembly is a homotrimer of disulfide-linked heterodimers consisting of a receptor binding subunit, HA1, and a membrane fusion subunit, HA2 (Figure 1.2 A). The newly formed N-terminus of HA2 includes the highly conserved hydrophobic fusion peptide which becomes sequestered in a pocket within the central helical bundle of HA2 in the pre-fusion conformation (Figure 1.2 A) [21, 23, 27, 29, 53]. The C-terminus of HA2 is anchored in the viral membrane by a helical transmembrane domain [54]. The HA1 globular head contains a sialic acid receptor binding site positioned at the apex of the trimer in the pre-fusion conformation.

Class I fusion proteins are linked by a common architectural feature of their post-fusion states; a six helix bundle featuring a trimer of hairpins that positions the C-terminal viral membrane anchor and N-terminal fusion peptide together (Figure 1.2 A and B) [1, 4, 7]. The structures for the pre- and post-fusion states of the influenza virus HA ectodomain were the first of any viral fusion protein to be solved by X-ray crystallography [1, 4, 6, 55]. In the years since, pre- and post-fusion structures of many class I viral fusion proteins from diverse viruses have been solved. These structures have revealed architecturally conserved features amongst class I fusion proteins [1, 4, 55]. To date, pre- and post-fusion structures have been determined for the Influenza HA, human immunodeficiency virus (HIV-1) Env, coronavirus (CoV) S, Ebola virus GP, Lassa virus GPC, Parainfluenza virus (PIV5) F protein, and Respiratory Syncytial virus (RSV) F proteins (Figure 1.2 A and B) [56-65]. While the pre-fusion structures of these diverse fusion proteins differ in size and elaborations, they share a conserved organization and architecture of their fusion subunits which feature two central heptad repeats that reorganize to form the three hairpins at the core of the six-helix bundle in the post-fusion state bringing the viral and host

target membranes together (Figure 1.2 A and B) [7, 13]. Furthermore, in the pre-fusion state the fusion subunits for these viral fusion proteins exhibit extensive interactions with the head domains that, as for influenza HA, could be interpreted to help "clamp" the fusion subunit in its pre-triggered conformation (Figure 1.2 A and B).

1.5 Dissecting HA's Structure and Function as a "Spring-Loaded" Fusion Protein

Infection by influenza virus begins when HA binds sialic acid on cell surface receptors through a low affinity high avidity interaction triggering uptake into cells by receptor mediated endocytosis or macropinocytosis [29]. As the endosomal lumen becomes increasingly acidic, low pH triggers a cascade of conformational changes throughout HA that culminate in the irreversible reorganization to the post-fusion conformation and fusion of the viral and host endosomal membranes together (Figure 1.2 A) [22].

The conventional mechanistic model describing HA's membrane fusion activity suggests that two dominant stabilizing interactions within HA, termed the "clamp" and "hook", act to maintain the metastable pre-fusion conformation [18]. In this model put forth by Carr and Kim, the HA1 globular head acts as a stabilizing "clamp" on the high-energy and spring-loaded HA2 fusion domain. The HA1 globular head rests atop the HA2 apex where HA1 forms stabilizing contacts with the HA2 B-loop (Figure 1.2 A). N- and C-terminal segments of HA1 form extended quaternary contacts with the HA2 A-helix and B-loop and are likely important for maintaining the pre-fusion conformation (Figure 1.2 A) [18, 28, 40]. The sequestered N-terminal HA2 fusion peptide forms a "hook" lashing the central helices of adjacent HA2 protomers together. According to this model, once activated by low pH, these interactions become destabilized and release the high-energy spring-loaded HA2 fusion domain which rapidly and irreversibly reorganizes to the post-fusion state.

Comparison of the pre- and post-fusion crystal structures of the HA ectodomain reveals the dramatic conformational changes that occur as a result of this reorganization (Figure 1.2 A). In the post-

fusion state, the central B-loop segment of HA2 has converted from an extended coil to a helix that extends the central helical bundle [28, 40]. As a result, the fusion peptide is projected towards the target host membrane. Structures of post-fusion HA2 revealed that C-terminal portions of the subunit also refold. In this case, a helix converts to a turn, which enables the C-terminal "leash" attached to the viral membrane anchor to run along the groove formed by the helical bundle. This "leash in the groove" interaction was shown to be necessary for drawing the two membrane active components together, leading the viral and target into close contact and inducing them to merge [66]. These structures provided the beginning and endpoints of the pathway the fusion machinery takes, but neither in fact reflects the nature of the fusogenic, activated forms of the HA trimer that are involved in manipulating the membranes during fusion. Likewise, fluorescence spectroscopy and circular dichroism studies have shown that HA fusion-activation leads to population of discernable intermediates rather than transitioning directly and irreversibly from pre- to post-fusion states [67-70]. Furthermore, these studies show that not all HAs respond to activation in the same way and some require different pH conditions to fully activate [70]. While these studies provided valuable information on how influenza HA responds to activation conditions, nearly all the studies to date have lacked sufficient resolution to characterize the structure of any intermediate or to resolve the specific conformational changes that occur. Thus the "spring-loaded" mechanistic model, and the characterization of HA implied therein, became rooted in the field's conceptualization of how class 1 fusion proteins behave and function.

1.6 Evolving Perspectives and Alternative Models of HA Fusion Activation

Many class I viral fusion proteins mediate both viral attachment and entry through their receptor binding and membrane fusion activities. In some cases, such as with HIV-1 Env, these functions are intimately linked as receptor and coreceptor binding events act as triggers for membrane fusion. In other cases, such as influenza HA, evidence suggests that receptor binding transduces a signal to the

fusion domain priming it for fusion activation; however, triggering of the membrane fusion activity requires exposure to low pH as in the endosome [19, 71].

The process of fusion protein activation and the means by which the fusion trigger is communicated across domains are not well understood for the majority of class I viral fusion proteins. Indeed, for the best-characterized system, HA, structural and biophysical data that reveals details of fusion activation and membrane fusion have only recently become available.

To date, technical limitations have hindered researchers' abilities to directly observe fusion intermediates with adequate resolution. One of the earliest and most informative studies performed by White and Wilson, used a panel of antibodies against HA to determine the sequence of early structural rearrangements that occur during HA fusion activation [24]. This approach, however, was limited to resolving changes significant enough to expose the antibody epitope and was unable to definitively resolve the complete sequence of events or identify any fusion intermediates. Using antibodies as probes also has the potential to perturb the behavior of the system due to their strong interactions with the antigen and their large size. Despite these limitations, White and Wilson concluded that there were likely two sequential conformational changes that occur throughout HA during fusion activation; reorganization of the HA2 stem region followed by a dissociation of the HA1 globular head domains leading to opening of the HA apex. Furthermore, White and Wilson demonstrated that activation of the soluble Bromelain released HA ectodomain (BHA) was slightly faster than detergent solubilized C-HA suggesting that full-length membrane associated HA behaves differently than BHA during activation. This study was the first to suggest there was a sequence of conformational changes during fusion activation and that there likely exist intermediate states along the fusion pathway.

The antibody monitored changes in HA structure seemed to contradict an "HA1 uncaging" model for hemagglutinin activation that suggests this fusion protein's activation is initiated by the dissociation of HA1 globular head domains, which would necessarily precede HA2 triggering. This uncaging model is

supported by data showing that dissociation of the HA1 globular head is essential for HA's membrane fusion activity [24-26, 72]. Forced dissociation of the HA1 globular head by heat, or denaturant, results in HA2 reorganizing to the post-fusion state and expression of HA without HA1 yields post-fusion HA2 stumps [24-26, 72]. Furthermore, preventing HA1's dissociation either through the introduction of interprotomer disulfide bonds or antibody binding renders HA non-fusogenic, but these restraints still enable the HA2 fusion peptide to release and interact with target membranes [25, 26, 72-74]. Ultimately, none of these studies directly probe the sequence of conformational changes that occur during HA fusion activation but rather proved that HA1 dissociation is required for HA to be fully fusion active.

Recent direct observations of HA fusion intermediates and the membrane fusion process, enabled by advances in cryo-EM, sm-FRET, and structural mass spectrometry have begun to challenge these long-standing conceptions about HA's, and possibly all class I viral fusion proteins', mechanisms of fusion activation and membrane fusion. In 2012 using cryo-electron tomography, Fontana et al. observed low pH-induced morphological changes in full length HA on the virus surface that suggested reorganization of the HA2 fusion domain preceded dissociation of the HA1 globular head and that these changes were reversible, within a certain window in time, upon return to neutral pH [75]. In tomographic data collection, a series of projection images of a sample are taken over a range of angles and recombined computationally to produce the 3D image volume. From these reconstructed tomograms, localized 3D volumes for similar objects can be extracted and averaged together, as is done in traditional single particle cryo-EM, yielding higher resolution information than can be gathered from individual tomograms [76]. The sub-tomogram averaged structures of fusion active HA generated by Fontana et al. lacked sufficient structural resolution to elucidate detailed structural changes that had occurred. However, the morphological changes observed were consistent with those suggested to occur during the so called "fusion peptide release" mechanism of HA fusion activation, similar to those put forth by

White and Wilson nearly 30 years earlier [24, 73, 75]. In contrast to the long held and conventional "HA1 uncaging" model, an alternative fusion peptide release model posits that first the HA2 fusion domain becomes activated by low pH, releasing the fusion peptide from sequestration where it is free to engage the target membrane prior to complete dissociation of the HA1 globular head [73].

More recently, Garcia et al. sought to understand the dynamic structural changes that occur throughout the soluble HA ectodomain at low pH at the threshold of fusion activation using hydrogen/deuterium-exchange mass spectrometry (HDX-MS) [77]. HDX-MS is a solution state biophysical and structural technique that monitors the accessibility of amide hydrogens along the protein backbone. HDX-MS directly monitors dynamic structural changes and motion throughout a protein that are otherwise invisible to other structural approaches [78-81]. At low pH conditions approaching fusion activation, dynamic changes across HA were observed where the HA1-HA1 trimeric interface became bolstered and the HA2 fusion peptide proximal subdomain became more dynamic. The authors concluded that at increasingly acidic condition, prior to activation, HA becomes primed for fusion peptide release, adding further support to this emerging mechanistic model. These recent studies suggest that in the early stages of fusion activation HA adopts a dynamic fusion peptide released intermediate state [19, 24, 30, 75, 77, 82-85].

Yet, the high-resolution structure of any fusion intermediate eluded characterization; in part due to the structural heterogeneity and purported transient nature of these intermediate states. Despite these monumental challenges, Benton et al. used single-particle cryo-EM to determine the first high-resolution structures of HA fusion intermediates. Their study is the first to present atomic resolution structural information for any fusion protein intermediate. By rapidly freezing acid activated HA in vitreous ice Benton et al. were able to capture the early stages of HA's conformational changes in stunning detail [40]. Their data reveals a sequence of concerted structural changes occurring throughout the HA ectodomain whereby dilation of HA1 protomeric interface is linked to reorganization of the HA2

fusion peptide proximal subdomain [40]. The authors concluded that a structured loop in the N-terminal F'-domain of HA1 forms critical contacts with the HA2 fusion peptide proximal subdomain and A-helix in the pre-fusion conformation that are broken as the HA1 trimeric interface dilates upon acid activation. Prior to complete reorganization of HA2, the fusion peptide is released from its pocket within the central helices and becomes disordered, evident from a loss of electron density and decreased local resolution around the fusion peptide proximal subdomain. Benton et al. suggest that once HA2 becomes fully activated, it rapidly reorganizes into the extended pre-hairpin helical intermediate driven by the loop-to-helix conformational change. Their structures provide the first high-resolution characterization of the pre-hairpin intermediate for any fusion protein and inform on the subsequent fold back conformational change to the post-fusion trimer of hairpins. In contrast to other recent biophysical and structural studies, Benton et al. did not observe any intermediates between the fusion peptide released pre-fusion like "dilated form 2" and pre-hairpin intermediate states [19, 40, 86]. While these structures show, in unparalleled detail, never before seen interactions and structural changes that are critical for understanding the mechanism of HA fusion activation and membrane fusion; the soluble HA ectodomain is known to behave markedly different that full length HA on the viral surface during fusion activation and does not adopt fusion intermediates seen in full length HA (discussed in detail in subsequent sections)[24, 86]. Furthermore, structurally heterogenous samples like this are refractory to analysis by single-particle cryo-EM, as heterogenous particles or classes lacking defined secondary structure are excluded from analysis and the resulting structures represent a subset of the total population. Nevertheless, this work further cements the importance of the "clamp" and "hook" interactions in regulating HA's structure and function during fusion activation and adds further support to an evolving hybrid mechanistic model for HA fusion activation and HA mediated membrane fusion.

1.7 Direct Monitoring of the Transitions Between Conformational States

While atomic resolution static structure models provide the highest level of detail for a proteins structure, they are less suited for characterizing protein dynamics and motion. Researchers have recently turned towards approaches such as single molecule-FRET (sm-FRET), that enable the study of proteins motions. Using sm-FRET, Das et al. directly observed, for the first time, an obligate and highly dynamic fusion intermediate for influenza HA [19]. By producing virus like particles (VLPs) where, on each VLP, a single HA trimer bore one pair of FRET labels, the authors were able to monitor, in real time, the dynamic structural changes that occurred in HA2 during low pH induced fusion activation and membrane fusion. Their data showed that, even at neutral pH, HA was remarkably dynamic and reversibly transitions between at least two distinct states. These pre-fusion conformational dynamics suggest that the fusion peptide is much more mobile than previously indicated, however this mobility was potentially influenced by the proximity of the FRET label to the fusion peptide [77]. During fusion activation, in the absence of a target membrane, HA was observed to reversibly transition through a long-lived, obligate fusion intermediate before irreversibly transitioning to the post-fusion conformation. When a target membrane was present, HA transitioned to the same intermediate state; however, the subsequent transition to the irreversible post-fusion state was significantly faster. While this approach cannot definitively resolve the detailed structure of each state, sm-FRET monitoring yields information describing the dynamic behavior and lifetimes of each state reported by the relative positioning of the FRET dye pairs. Furthermore, by inferring the position of each FRET label based upon its attachment residue, authors were able to develop structural models that correspond to each FRET state. The resulting mechanistic model put forth by the authors describing HA fusion activation and membrane fusion provided a detailed glimpse into the intermediate states and transitions for this long-studied fusion protein. Despite the advances, much about the molecular mechanisms and structural nature of HA fusion activation remains poorly understood.

1.8 Visualizing Viral Membrane Fusion in Action

Thus far I have reviewed the structure of class I viral fusion proteins and their mechanisms of fusion activation and the conformational changes that occur during the membrane fusion reaction. However, these topics have largely been discussed outside the context of the actual membrane fusion reaction. While the mechanics of viral fusion proteins, namely influenza HA, have been intensively studied, the biophysical and structural mechanics of the membranes themselves have eluded characterization. The role of the viral fusion protein in the membrane fusion reaction can be distilled, quite simply, down to; engaging the host target membrane, generating the required free energy through structural reorganization to be able to bring the two membranes into close apposition, perturb the membranes, and induce them to merge. The conventional model for influenza virus HA-mediated membrane fusion suggests that HA deforms the membranes while bringing them into close contact resulting in formation of the hemifusion state, where the outer leaflets of each membrane have joined, and the inner leaflets remain separate [7, 34, 87-96]. How HA mediates formation of the hemifusion state and how hemifusion proceeds to a fusion pore is not well understood, however. Furthermore, until recently it was not known which membrane, that of the virus or cell or both, was being primarily perturbed and remodeled during fusion [87, 97-99]. Direct structural characterization of the membrane fusion reaction and elucidation of the sequence of membrane remodeling by the fusion proteins has only recently become possible [87, 88, 100-103]. Cryo-EM has proven invaluable for developing our understanding of viral morphology, entry mechanisms, and fusion protein structure [55, 75, 87, 88, 101-107]. Cryo-ET is uniquely suited for the direct imaging of protein and membrane structural changes during protein-mediated membrane fusion [75, 76, 87-90, 95, 100, 101, 104, 108].

The power and utility of this approach was demonstrated by in 2010 where the ultrastructure of influenza virus membrane fusion intermediates was imaged using whole virions and synthetic membrane vesicles [87]. The cryo-ET images suggested that fusion initiates when fusion-active HA, after

grappling to the target membrane and upon refolding to a post-fusion hairpin configuration, creates highly curved, localized dimples in the target membrane as it is drawn towards the more rigid, matrix protein-reinforced, viral membrane. Density surrounding the dimples corresponded to a set of 2-8 HAs that coordinated the junction between membranes. This figure was in good agreement with previous findings that estimated the stoichiometry of viral fusion proteins required for membrane fusion [39, 109-114]. The cryo-tomograms conclusively showed that during membrane fusion the viral membrane remains largely unperturbed, under the mildly acidic pH conditions examined, due to the influenza M1 presence of an intact matrix protein layer [87]. Thus, the majority of membrane remodeling at that early stage is focused on the target membrane. Only when acidic pH was further lowered, did the M1 layer dissociates from the viral membrane as would need to occur to free the lipid bilayer to complete fusion during the late stages of fusion. This study was among the first to directly image the membrane ultrastructure during fusion.

The advent of the direct electron detector for use in cryo-electron microscopy, which afforded greater sensitivity and the ability to correct for sample blurring due to beam-induced sample movement and mechanical drift, enabled high resolution information to be retained when imaging biological complexes while limiting sample degradation from high electron exposures. For studies of membrane fusion, it became possible for example to consistently resolve the individual membrane leaflets of a lipid bilayer [90]. Using cryo-ET, Gui et al. sought to sequence the influenza virus membrane fusion reaction and characterize the membrane ultrastructure at each stage of the fusion process using multiple pH conditions and varied target membrane compositions [90]. The authors identified and characterized the interactions between influenza virions and liposomes and monitored the population of fusion intermediate states over time (Figure 1.3).

In addition to the initial point-like contact mediated by a small number of HA trimers, intermediates formed by extended regions of membranes in direct contact with each other emerged prior to

formation of fusion pores that allowed transfer of the viral RNP segments into the merged virus-liposome vesicles (Figure 1.3). Through analysis of the population kinetics, the putative sequence of intermediate states traversed during fusion was inferred. Interestingly, in that study, hemifusion was very rarely observed; it was concluded that the hemifusion state is likely unstable and transiently populated during fusion [90]. These results challenge prior observations of the hemifusion state in past studies, which relied primarily on fluorescence monitored membrane fusion with cell surface-expressed HA, which may not replicate the density and organization of HA on virions and also lack the important M1 matrix layer [91-93]. Some studies have suggested that hemifusion represents an unproductive off-pathway state for protein mediated membrane fusion [115, 116]. While this remains a subject of debate, studies of SNARE protein mediated membrane fusion show that while hemifusion is often observed, it may function as a metastable trap [115, 116].

Gui et al. suggest that for influenza virus membrane fusion, activated HA first engages the target membrane through its exposed fusion peptide forming bridging contacts between the two opposing membranes (Figure 1.3 A). Subsequent HA refolding induces dimpling in the target membrane as it is drawn towards the matrix reinforced viral membrane leading to formation of localized close contact zones between the two membranes, which the authors suggest may serve to minimize the initial energetic penalty incurred from dehydrating the membrane surface (Figure 1.3 A and B) [37, 98]. The contact zone then expands to form an extended tightly docked interface between the two outer membrane leaflets (Figure 1.3 A and B). Similar extended interface contacts have been observed during SNARE protein mediated membrane fusion and the GTP dependent alastin fusion protein [2, 31, 115-119]. Higher levels of cholesterol or inclusion of lipids found in mature endosomes in the target membrane were found to promote formation of these extended interfaces [90]. The tightly docked membranes transitioned to the post-fusion state thus supporting the authors' conclusion that these extended interfaces are a critical stage along the fusion reaction [89, 90, 92].

Membrane composition contributes to how the membrane fusion reaction proceeds and what intermediate structures are stably populated and enriched throughout [37, 87, 89, 92, 95, 96, 98, 120, 121]. A separate recent cryo-ET study of influenza virus membrane fusion with synthetic liposomes, where the liposome composition differed from that used by Gui et al., found hemifused virus-liposome complexes in high abundance [89]. While both cryo-ET studies concluded that cholesterol is critically important for productive and complete fusion to occur, their conflicting results regarding how prevalent hemifused membranes are indicate that membrane composition can have a significant influence on the apparent membrane remodeling takes during fusion.

One aspect that makes clear the need to study whole influenza virions to understand the fusion process relates to the role of the M1 matrix protein layer. While classically HA has been considered the prime mediator of fusion, M1 likewise appears to play an important role in regulating the order of events as well as the ability for the virus membrane to deform and complete fusion [90]. At increasingly acidic conditions the previously well-ordered M1 matrix layer dissociates from the viral membrane conferring plasticity to the lipid bilayer and greater lateral mobility of HAs engaged in fusion [87, 122]. The HA transmembrane domain (TMD) and cytoplasmic tail are believed to interact with the M1 matrix layer, thus dissociation of the matrix layer and abolition of this interaction would free the HA TMD enabling it to mobilize and recombine with the HA2 fusion peptide as the fusion reaction proceeds to completion [87, 123, 124].

These cryo-ET studies present the most complete observations describing viral protein-mediated membrane fusion to date and taken together with recent observations on the structural mechanics of HA fusion activation these studies show how new approaches are providing unprecedented views into mechanisms of protein-mediated membrane fusion.

1.9 Divergent Mechanism of Fusion Protein Activation

Indeed, HA serves as the prototypical class I viral fusion protein and the system against which all other class I fusion proteins are compared. However, low pH activation of HA is relatively simple when compared to other class I fusion proteins with more varied and complex activation modes [9]. For example, the HIV-1 Env fusion glycoprotein is activated by two successive receptor binding events [4, 46, 64, 125-128]. Env first binds the CD4 receptor on the surface of T-cells which induces reorganization of the gp120 receptor binding domain and exposure of the co-receptor binding site enabling binding of either CCR5 or CXCR4 [7, 128]. Recently cryo-EM, sm-FRET, and HDX-MS have been used to characterize the structure of Env in the apo and CD4 bound conformations, illuminating how CD4 binding induces long range conformational changes throughout Env priming it for coreceptor binding [46, 64, 125-127]. Remarkably, Env is capable of dynamically sampling multiple conformations at rest, including an "open" CD4-bound like state [64, 125-127]. While these studies have revealed valuable information about Env structural dynamics, little is known about how coreceptor binding activates Env during membrane fusion.

Other class I fusion proteins are activated by similarly complex mechanisms. The S fusion glycoprotein of some coronaviruses, including the novel SARS2-CoV, is activated by receptor binding and proteolytic processing [50, 58, 59, 129]. CoV-S is first proteolytically activated during biogenesis producing the cleaved metastable pre-fusion conformation [50, 59]. CoV-S mediated membrane fusion requires both receptor binding and a secondary proteolytic activation that occurs in the endosome during viral entry [50, 58, 59, 129]. However, it is not known how these events act to activate the S protein for membrane fusion. Furthermore, activation of both HIV-1 Env and CoV-S occur via all or nothing events rather than a gradated activation like influenza HA. Thus, our understanding of how HA

becomes activated cannot be generalized to other class I fusion proteins that do not share the same activation mode.

Fusion activation of paramyxovirus F proteins is unique amongst class I fusion proteins as receptor binding is facilitated by another surface glycoprotein [56, 130, 131]. There are two prevailing hypothesis describing how paramyxovirus F protein activation occurs through the interaction with the receptor binding protein (HN, H, or G protein). The dissociation or clamp hypothesis suggests that the fusion and attachment proteins are associated on the viral surface before receptor binding and that this interaction acts to stabilize the F protein in the metastable pre-fusion conformation, similar to how the RBDs of other class I fusion proteins act as a "clamp" and the fusion domain [130, 131]. Upon receptor binding, the fusion protein dissociates and becomes fusion active. Alternatively, the provocateur hypothesis suggests that the fusion and attachment proteins exist freely on the viral surface and that, upon receptor binding, they associate, and the F protein becomes fusion active. One key difference between these two hypotheses is that in the dissociation/clamp hypothesis the interaction between attachment and fusion protein is stabilizing, whereas in the provocateur hypothesis this interaction acts to destabilize the F protein [130, 131].

Ultimately, little is known about the mechanisms of activation for fusion proteins other than influenza HA. While their triggers are known, until recently it was not well understood how those triggers are communicated and what the conformational changes are that occur during membrane fusion. However, as previously discussed, solution state structural and biophysical approaches such as HDX-MS and sm-FRET are enabling researchers to interrogate the structural biology of increasingly complex systems.

Recently, Das et al. sought to characterize the dynamic conformational changes that occur another class I fusion protein, the Ebola virus GP fusion glycoprotein, resulting from a set of activating factors [41]. Once internalized into cells by macropinocytosis, the low pH conditions of the endosome activate

cellular proteases that cleave and remove the large heavily glycosylated mucin-like domain and glycan cap from GP [41, 132-135]. Once cleaved, GP binds the Niemann-Pick C1 (NPC1) receptor, which is required for entry, becomes activated and mediates membrane fusion through a currently unknown mechanism [132, 136, 137]. While endosomal pH and Ca^{2+} levels have been implicated in Ebola entry and GP mediated fusion, their molecular basis for their impact on GP structure and dynamics were not known [138]. Using sm-FRET Das et al. monitored dynamic structural changes in the GP2 fusion domain that were induced by NPC1 receptor binding, exposure to low pH, and Ca^{2+} [41]. The authors observed that receptor binding, low pH, and Ca^{2+} act synergistically to promote membrane fusion. Furthermore, low pH and Ca^{2+} induced dynamic and reversible conformational changes in GP that prime GP for NPC1 binding. Once bound to the receptor, GP transitioned irreversibly to a conformation that was consistent with the post-fusion state. Thus, the authors conclude that low pH and endosomal Ca^{2+} act to prime GP for receptor binding following removal of the glycan cap by promoting transition to the receptor binding competent intermediate state. NPC1 binding induces reorganization of GP into a fusion active intermediate state and the subsequent transition to the irreversible post-fusion state. This study presented the first direct evidence for how multiple fusion activation factors serve to regulate and prime a fusion protein's activity. While the detailed molecular mechanisms underlying these observed conformational changes remain to be understood, the study of Ebola GP further highlighted the power and versatility of the sm-FRET approach and demonstrated how this approach can be used to better understand the dynamic mechanisms of fusion protein activation *in situ* beyond the simpler systems such as influenza HA. This approach thus appears to be well-suited for use in studies of fusion proteins with complex and multicomponent activation mechanisms such as SARS CoV-S and Lassa GPC [50, 58, 139-146].

1.10 Goals of this Dissertation

The studies and methodology discussed throughout this introduction have outlined how emerging structural and biophysical approaches have provided insight into the mechanisms by which class 1 viral fusion proteins, specifically influenza HA, become activated and catalyze the membrane fusion reaction during viral entry beyond what classical high-resolution structural approaches are capable of. Despite these advances, our understanding of influenza virus membrane fusion and the structural mechanics of HA fusion activation are still incomplete. To gain a complete mechanistic understanding of fusion protein activation and function, detailed resolution of structural reorganization throughout the fusion protein and sequencing of conformational events traversed by HA *in situ* is needed. This dissertation aims to characterize the structural dynamics of HA during fusion activation on intact virions using pulse labeling HDX-MS and cryo-ET. This approach enables us to monitor and dissect the nature and sequence of the conformational changes that occur throughout the entire HA fusion machinery during activation on intact virions and in the soluble isolated ectodomain forms. To date no detailed structural analysis describing how different regions of HA1 and HA2 respond to acidic pH once the fusion machinery is triggered has been available. We also aim to characterize the structural and conformational dynamics of the HIV-1 Env fusion glycoprotein on the surface of authentic and engineered viral particles intended for use as vaccine immunogens by continuous labeling HDX-MS. Together these works demonstrate the power and utility of HDX-MS as a tool to study the structure and function of viral fusion proteins *in situ.*

1.11 Figures

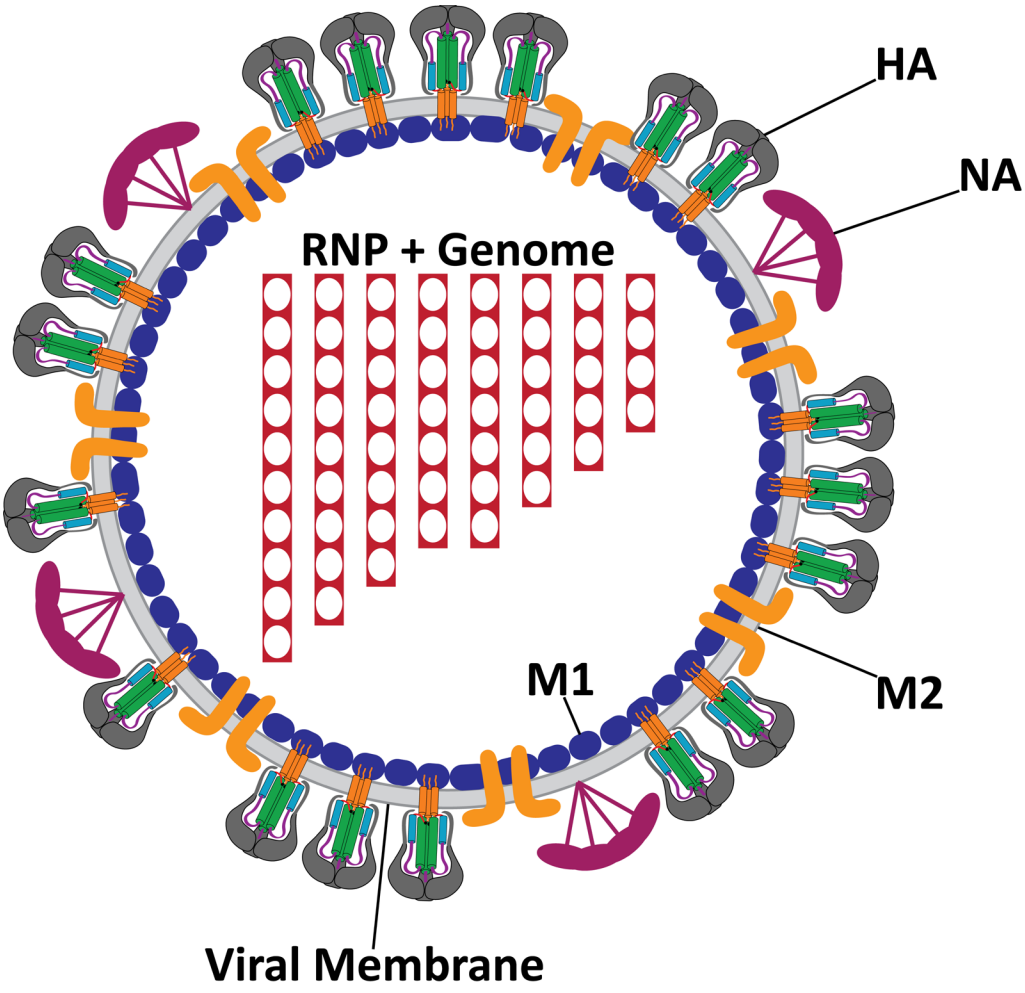

Figure 1.1 Anatomy of Influenza A Virus. Cartoon representation of an influenza A virion. The segmented RNA genome and nucleoprotein complex is surrounded by the matrix M1 layer which lines the inside of the host derived lipid membrane. The matrix M2 proton channel traverses the viral membrane. The hemagglutinin (HA) and neuraminidase (NA) glycoproteins decorate the viral surface.

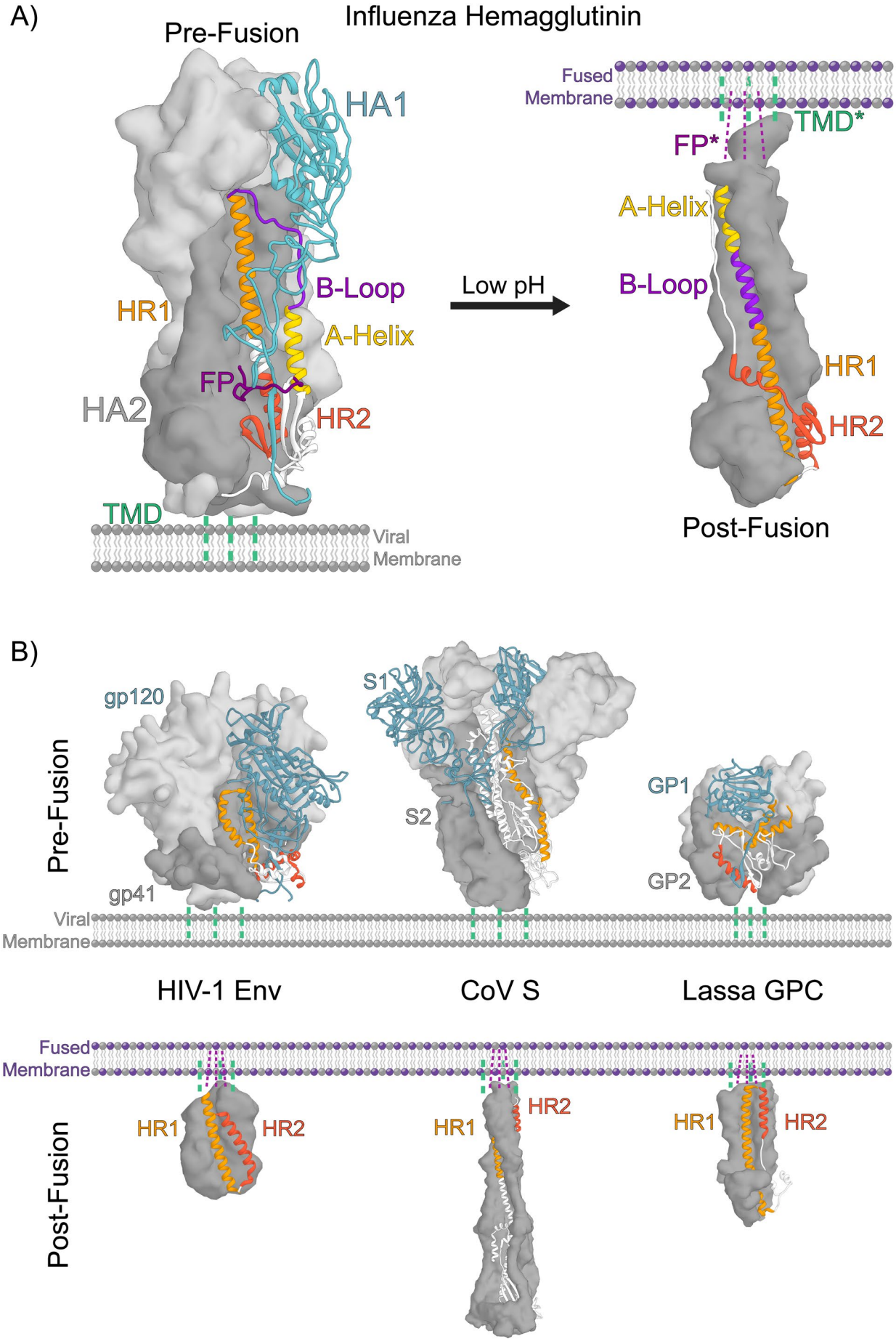
A)
Influenza Hemagglutinin
Pre-Fusion
HA1
B-Loop
HR1
A-Helix
FP
HA2
HR2
TMD
Viral
Membrane
Low pH
Fused
Membrane
TMD*
FP*
A-Helix
B-Loop
HR1
HR2
Post-Fusion
B)
gp120
gp41
S1
S2
GP1
GP2
Pre-Fusion
Viral
Membrane
HIV-1 Env
CoV S
Lassa GPC
Fused
Membrane
HR1
HR2
HR1
HR2
HR1
HR2
Post-Fusion

Figure 1.2 Architecture of a Class I Fusion Protein. A) The structures Influenza Hemagglutinin (HA) fusion protein in the pre-fusion (PDB 3HMG) and post-fusion (PDB 1QU1) states highlight the dramatic pH dependent reorganization that drives the membrane fusion reaction. The pre-fusion state is metastable with respect to the post-fusion state. In the pre-fusion state the HA1 receptor binding domain (RBD) (shown in light grey volume and blue ribbon) forms a "clamp" interaction with the HA2 fusion subunit thereby stabilizing the high-energy "spring-loaded" HA2 fusion domain (highlighted by the HA1-HA2 interface shown in grey). The HA2 N-terminal fusion peptide (FP shown in dark magenta) forms a "hook" within the fusion domain lashing adjacent protomers together. Once destabilized by low pH these interactions are lost and HA reorganizes to the post-fusion state where they N-terminal FP and transmembrane domain (TMD) are colocalized in the newly fused membrane. The post-fusion state is characterized by the trimer of hairpins formed by the two heptad repeat regions (HR1 and HR2). B) Comparison of the pre-fusion (top) and post-fusion (bottom) structures of diverse class I fusion proteins reveals the conservation of core architectural features including the "clamp" interaction between the RBD and fusion domain and reorganization of the two heptad repeats into a trimer of hairpins. Shown are the pre- and post-fusion structures of the HIV-1 Env (PDB 5FUU and 1I5X), Coronavirus (CoV) S (PDB 5W9J and 6B3O), and Lassa virus GPC (PDB 5VK2 and 5OMI). Figure reproduced with permission from [147].

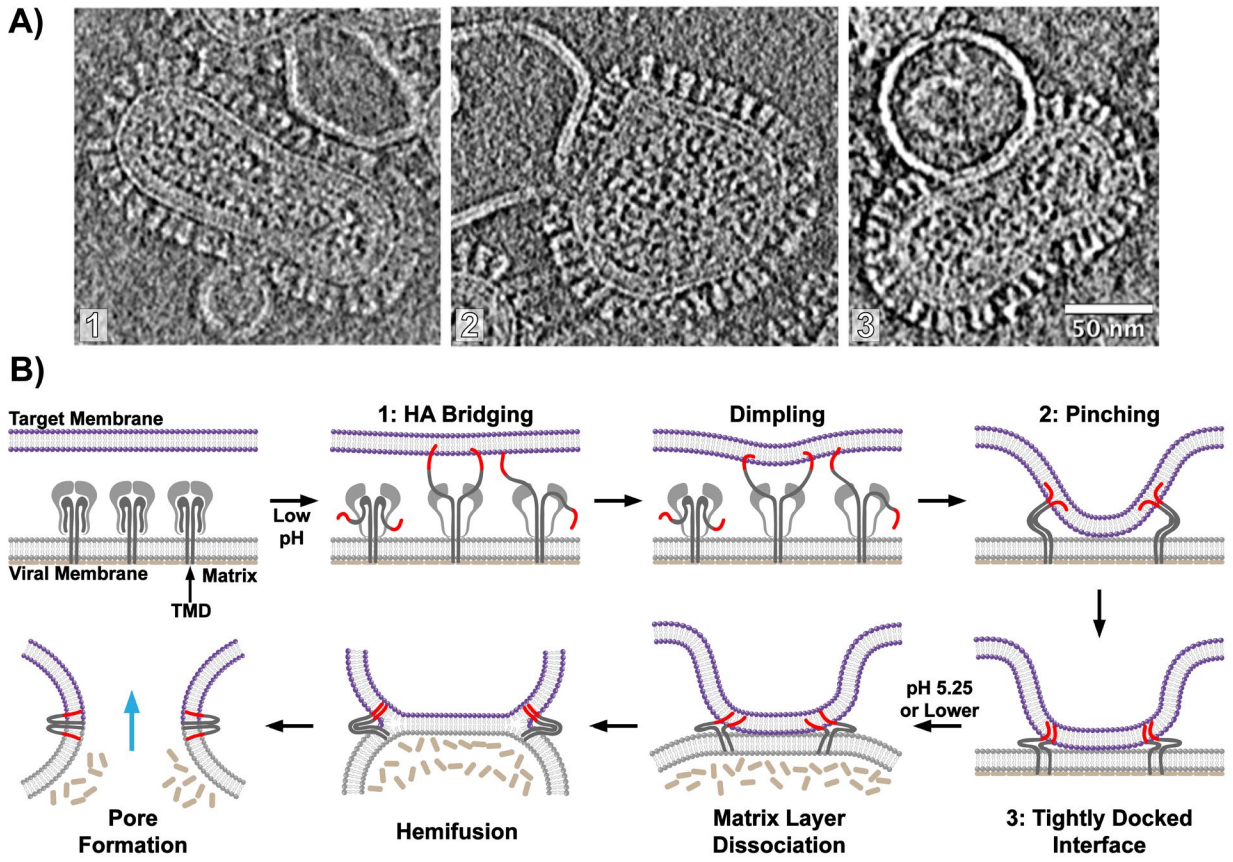

Figure 1.3 Visualizing Influenza Virus Membrane Fusion. Intermediates throughout the membrane fusion were visualized by cryo-ET and the sequence of membrane remodeling was elucidated. A) Cryo-ET images highlight key intermediates during membrane fusion including HA bridging (1), membrane pinching (2), and formation of a tightly docked interface (3) (left to right) (scale bar = 50 nm). B) Cartoon model describing the membrane ultrastructure and sequence of intermediates during influenza viral membrane fusion. Figure reproduced with permission from [147].

References

1. White, J.M., et al., *Structures and mechanisms of viral membrane fusion proteins: multiple variations on a common theme.* Crit Rev Biochem Mol Biol, 2008. **43**(3): p. 189-219.
2. Südhof, T.C. and J.E. Rothman, *Membrane fusion: grappling with SNARE and SM proteins.* Science, 2009. **323**(5913): p. 474-7.
3. McNew, J.A., et al., *GTP-dependent membrane fusion.* Annu Rev Cell Dev Biol, 2013. **29**: p. 529-50.
4. Rey, F.A. and S.M. Lok, *Common Features of Enveloped Viruses and Implications for Immunogen Design for Next-Generation Vaccines.* Cell, 2018. **172**(6): p. 1319-1334.
5. Segev, N., O. Avinoam, and B. Podbilewicz, *Fusogens.* Curr Biol, 2018. **28**(8): p. R378-R380.
6. Jahn, R., T. Lang, and T.C. Sudhof, *Membrane fusion.* Cell, 2003. **112**(4): p. 519-33.
7. Colman, P.M. and M.C. Lawrence, *The structural biology of type I viral membrane fusion.* Nat Rev Mol Cell Biol, 2003. **4**(4): p. 309-19.
8. Klenk, H.D. and R. Rott, *The molecular biology of influenza virus pathogenicity.* Adv Virus Res, 1988. **34**: p. 247-81.
9. White, J.M. and G.R. Whittaker, *Fusion of Enveloped Viruses in Endosomes.* Traffic, 2016. **17**(6): p. 593-614.
10. Hernandez, J.M. and B. Podbilewicz, *The hallmarks of cell-cell fusion.* Development, 2017. **144**(24): p. 4481-4495.
11. Li, Y. and Y. Modis, *A novel membrane fusion protein family in Flaviviridae?* Trends Microbiol, 2014. **22**(4): p. 176-82.
12. Modis, Y., *Relating structure to evolution in class II viral membrane fusion proteins.* Curr Opin Virol, 2014. **5**: p. 34-41.
13. Harrison, S.C., *Viral membrane fusion.* Virology, 2015. **479-480**: p. 498-507.
14. Backovic, M. and T.S. Jardetzky, *Class III viral membrane fusion proteins.* Curr Opin Struct Biol, 2009. **19**(2): p. 189-96.
15. Kadlec, J., et al., *The postfusion structure of baculovirus gp64 supports a unified view of viral fusion machines.* Nat Struct Mol Biol, 2008. **15**(10): p. 1024-30.
16. Roche, S., et al., *Crystal structure of the low-pH form of the vesicular stomatitis virus glycoprotein G.* Science, 2006. **313**(5784): p. 187-91.
17. Backovic, M., R. Longnecker, and T.S. Jardetzky, *Structure of a trimeric variant of the Epstein-Barr virus glycoprotein B.* Proc Natl Acad Sci U S A, 2009. **106**(8): p. 2880-5.
18. Carr, C.M., C. Chaudhry, and P.S. Kim, *Influenza hemagglutinin is spring-loaded by a metastable native conformation.* Proc Natl Acad Sci U S A, 1997. **94**(26): p. 14306-13.
19. Das, D.K., et al., *Direct Visualization of the Conformational Dynamics of Single Influenza Hemagglutinin Trimers.* Cell, 2018. **174**(4): p. 926-937 e12.
20. Klenk, H.D., et al., *Activation of influenza A viruses by trypsin treatment.* Virology, 1975. **68**(2): p. 426-39.
21. Wilson, I.A., J.J. Skehel, and D.C. Wiley, *Structure of the haemagglutinin membrane glycoprotein of influenza virus at 3 A resolution.* Nature, 1981. **289**(5796): p. 366-73.
22. Skehel, J.J., et al., *Changes in the conformation of influenza virus hemagglutinin at the pH optimum of virus-mediated membrane fusion.* Proc Natl Acad Sci U S A, 1982. **79**(4): p. 968-72.
23. White, J., J. Kartenbeck, and A. Helenius, *Membrane fusion activity of influenza virus.* Embo j, 1982. **1**(2): p. 217-22.
24. White, J.M. and I.A. Wilson, *Anti-peptide antibodies detect steps in a protein conformational change: low-pH activation of the influenza virus hemagglutinin.* J Cell Biol, 1987. **105**(6 Pt 2): p. 2887-96.

25. Godley, L., et al., *Introduction of intersubunit disulfide bonds in the membrane-distal region of the influenza hemagglutinin abolishes membrane fusion activity.* Cell, 1992. **68**(4): p. 635-45.
26. Kemble, G.W., et al., *Intermonomer disulfide bonds impair the fusion activity of influenza virus hemagglutinin.* J Virol, 1992. **66**(8): p. 4940-50.
27. Carr, C.M. and P.S. Kim, *A spring-loaded mechanism for the conformational change of influenza hemagglutinin.* Cell, 1993. **73**(4): p. 823-32.
28. Chen, J., J.J. Skehel, and D.C. Wiley, *N- and C-terminal residues combine in the fusion-pH influenza hemagglutinin HA(2) subunit to form an N cap that terminates the triple-stranded coiled coil.* Proc Natl Acad Sci U S A, 1999. **96**(16): p. 8967-72.
29. Skehel, J.J. and D.C. Wiley, *Receptor binding and membrane fusion in virus entry: the influenza hemagglutinin.* Annu Rev Biochem, 2000. **69**: p. 531-69.
30. Boonstra, S., et al., *Hemagglutinin-Mediated Membrane Fusion: A Biophysical Perspective.* Annu Rev Biophys, 2018. **47**: p. 153-173.
31. Francois-Martin, C., J.E. Rothman, and F. Pincet, *Low energy cost for optimal speed and control of membrane fusion.* Proc Natl Acad Sci U S A, 2017. **114**(6): p. 1238-1241.
32. Monck, J.R. and J.M. Fernandez, *The exocytotic fusion pore.* J Cell Biol, 1992. **119**(6): p. 1395-404.
33. Chanturiya, A., L.V. Chernomordik, and J. Zimmerberg, *Flickering fusion pores comparable with initial exocytotic pores occur in protein-free phospholipid bilayers.* Proc Natl Acad Sci U S A, 1997. **94**(26): p. 14423-8.
34. Chernomordik, L.V. and M.M. Kozlov, *Mechanics of membrane fusion.* Nat Struct Mol Biol, 2008. **15**(7): p. 675-83.
35. Lorieau, J.L., J.M. Louis, and A. Bax, *The complete influenza hemagglutinin fusion domain adopts a tight helical hairpin arrangement at the lipid:water interface.* Proc Natl Acad Sci U S A, 2010. **107**(25): p. 11341-6.
36. Nanavati, C., et al., *The exocytotic fusion pore modeled as a lipidic pore.* Biophys J, 1992. **63**(4): p. 1118-32.
37. Aeffner, S., et al., *Energetics of stalk intermediates in membrane fusion are controlled by lipid composition.* Proc Natl Acad Sci U S A, 2012. **109**(25): p. E1609-18.
38. Kemble, G.W., T. Danieli, and J.M. White, *Lipid-anchored influenza hemagglutinin promotes hemifusion, not complete fusion.* Cell, 1994. **76**(2): p. 383-91.
39. Blumenthal, R., et al., *Dilation of the influenza hemagglutinin fusion pore revealed by the kinetics of individual cell-cell fusion events.* J Cell Biol, 1996. **135**(1): p. 63-71.
40. Benton, D.J., et al., *Structural transitions in influenza haemagglutinin at membrane fusion pH.* Nature, 2020.
41. Das, D.K., et al., *Conformational changes in the Ebola virus membrane fusion machine induced by pH, Ca2+, and receptor binding.* PLoS Biol, 2020. **18**(2): p. e3000626.
42. Yang, Z., et al., *Asymmetric opening of HIV-1 Env bound to CD4 and a coreceptor-mimicking antibody.* Nat Struct Mol Biol, 2019. **26**(12): p. 1167-1175.
43. Lu, M., et al., *Associating HIV-1 envelope glycoprotein structures with states on the virus observed by smFRET.* Nature, 2019. **568**(7752): p. 415-419.
44. Wang, H., et al., *Partially Open HIV-1 Envelope Structures Exhibit Conformational Changes Relevant for Coreceptor Binding and Fusion.* Cell Host Microbe, 2018. **24**(4): p. 579-592 e4.
45. Stadtmueller, B.M., et al., *DEER Spectroscopy Measurements Reveal Multiple Conformations of HIV-1 SOSIP Envelopes that Show Similarities with Envelopes on Native Virions.* Immunity, 2018. **49**(2): p. 235-246 e4.
46. Guttman, M., et al., *CD4-induced activation in a soluble HIV-1 Env trimer.* Structure, 2014. **22**(7): p. 974-84.

47. Munro, J.B., et al., *Conformational dynamics of single HIV-1 envelope trimers on the surface of native virions.* Science, 2014. **346**(6210): p. 759-63.
48. Lazarowitz, S.G. and P.W. Choppin, *Enhancement of the infectivity of influenza A and B viruses by proteolytic cleavage of the hemagglutinin polypeptide.* Virology, 1975. **68**(2): p. 440-54.
49. Chen, J., et al., *Structure of the hemagglutinin precursor cleavage site, a determinant of influenza pathogenicity and the origin of the labile conformation.* Cell, 1998. **95**(3): p. 409-17.
50. Tortorici, M.A. and D. Veesler, *Structural insights into coronavirus entry.* Adv Virus Res, 2019. **105**: p. 93-116.
51. Vey, M., et al., *Hemagglutinin activation of pathogenic avian influenza viruses of serotype H7 requires the protease recognition motif R-X-K/R-R.* Virology, 1992. **188**(1): p. 408-13.
52. Klenk, H.D. and W. Garten, *Host cell proteases controlling virus pathogenicity.* Trends Microbiol, 1994. **2**(2): p. 39-43.
53. Bullough, P.A., et al., *Structure of influenza haemagglutinin at the pH of membrane fusion.* Nature, 1994. **371**(6492): p. 37-43.
54. Benton, D.J., et al., *Influenza hemagglutinin membrane anchor.* Proc Natl Acad Sci U S A, 2018. **115**(40): p. 10112-10117.
55. Rossmann, M.G., *Structure of viruses: a short history.* Q Rev Biophys, 2013. **46**(2): p. 133-80.
56. Welch, B.D., et al., *Structure of the cleavage-activated prefusion form of the parainfluenza virus 5 fusion protein.* Proc Natl Acad Sci U S A, 2012. **109**(41): p. 16672-7.
57. Hastie, K.M., et al., *Structural basis for antibody-mediated neutralization of Lassa virus.* Science, 2017. **356**(6341): p. 923-928.
58. Walls, A.C., et al., *Cryo-electron microscopy structure of a coronavirus spike glycoprotein trimer.* Nature, 2016. **531**(7592): p. 114-117.
59. Walls, A.C., et al., *Tectonic conformational changes of a coronavirus spike glycoprotein promote membrane fusion.* Proc Natl Acad Sci U S A, 2017. **114**(42): p. 11157-11162.
60. Swanson, K.A., et al., *Structural basis for immunization with postfusion respiratory syncytial virus fusion F glycoprotein (RSV F) to elicit high neutralizing antibody titers.* Proc Natl Acad Sci U S A, 2011. **108**(23): p. 9619-24.
61. McLellan, J.S., et al., *Structure of respiratory syncytial virus fusion glycoprotein in the postfusion conformation reveals preservation of neutralizing epitopes.* J Virol, 2011. **85**(15): p. 7788-96.
62. Malashkevich, V.N., et al., *Core structure of the envelope glycoprotein GP2 from Ebola virus at 1.9-A resolution.* Proc Natl Acad Sci U S A, 1999. **96**(6): p. 2662-7.
63. Lee, J.E., et al., *Structure of the Ebola virus glycoprotein bound to an antibody from a human survivor.* Nature, 2008. **454**(7201): p. 177-82.
64. Lee, J.H., G. Ozorowski, and A.B. Ward, *Cryo-EM structure of a native, fully glycosylated, cleaved HIV-1 envelope trimer.* Science, 2016. **351**(6277): p. 1043-8.
65. Lu, M., et al., *Structural and functional analysis of interhelical interactions in the human immunodeficiency virus type 1 gp41 envelope glycoprotein by alanine-scanning mutagenesis.* J Virol, 2001. **75**(22): p. 11146-56.
66. Park, H.E., J.A. Gruenke, and J.M. White, *Leash in the groove mechanism of membrane fusion.* Nat Struct Biol, 2003. **10**(12): p. 1048-53.
67. Wharton, S.A., et al., *Conformational aspects of the acid-induced fusion mechanism of influenza virus hemagglutinin. Circular dichroism and fluorescence studies.* J Biol Chem, 1988. **263**(9): p. 4474-80.
68. Korte, T. and A. Herrmann, *pH-dependent binding of the fluorophore bis-ANS to influenza virus reflects the conformational change of hemagglutinin.* Eur Biophys J, 1994. **23**(2): p. 105-13.

69. Korte, T., et al., *Transient changes of the conformation of hemagglutinin of influenza virus at low pH detected by time-resolved circular dichroism spectroscopy.* J Biol Chem, 1997. **272**(15): p. 9764-70.
70. Korte, T., et al., *Conformational intermediates and fusion activity of influenza virus hemagglutinin.* J Virol, 1999. **73**(6): p. 4567-74.
71. Schrauwen, E.J., et al., *Amino Acid Substitutions That Affect Receptor Binding and Stability of the Hemagglutinin of Influenza A/H7N9 Virus.* J Virol, 2016. **90**(7): p. 3794-9.
72. Chen, J., et al., *A soluble domain of the membrane-anchoring chain of influenza virus hemagglutinin (HA2) folds in Escherichia coli into the low-pH-induced conformation.* Proc Natl Acad Sci U S A, 1995. **92**(26): p. 12205-9.
73. Blijleven, J.S., et al., *Mechanisms of influenza viral membrane fusion.* Semin Cell Dev Biol, 2016. **60**: p. 78-88.
74. Williams, J.A., et al., *Dissection of epitope-specific mechanisms of neutralization of influenza virus by intact IgG and Fab fragments.* J Virol, 2017.
75. Fontana, J., et al., *Structural changes in Influenza virus at low pH characterized by cryo-electron tomography.* J Virol, 2012. **86**(6): p. 2919-29.
76. Briggs, J.A., *Structural biology in situ--the potential of subtomogram averaging.* Curr Opin Struct Biol, 2013. **23**(2): p. 261-7.
77. Garcia, N.K., et al., *Dynamic changes during acid-induced activation of influenza hemagglutinin.* Structure, 2015. **23**(4): p. 665-76.
78. Garcia, N.K. and K.K. Lee, *Dynamic Viral Glycoprotein Machines: Approaches for Probing Transient States That Drive Membrane Fusion.* Viruses, 2016. **8**(1).
79. Guttman, M. and K.K. Lee, *Isotope Labeling of Biomolecules: Structural Analysis of Viruses by HDX-MS.* Methods Enzymol, 2016. **566**: p. 405-26.
80. Benhaim, M., K.K. Lee, and M. Guttman, *Tracking Higher Order Protein Structure by Hydrogen-Deuterium Exchange Mass Spectrometry.* Protein Pept Lett, 2019. **26**(1): p. 16-26.
81. Hodge, E.A., M.A. Benhaim, and K.K. Lee, *Bridging protein structure, dynamics, and function using hydrogen/deuterium-exchange mass spectrometry.* Protein Sci, 2019.
82. Leikina, E., et al., *Reversible stages of the low-pH-triggered conformational change in influenza virus hemagglutinin.* EMBO J, 2002. **21**(21): p. 5701-10.
83. Xu, R. and I.A. Wilson, *Structural characterization of an early fusion intermediate of influenza virus hemagglutinin.* J Virol, 2011. **85**(10): p. 5172-82.
84. Lin, X., et al., *Order and disorder control the functional rearrangement of influenza hemagglutinin.* Proc Natl Acad Sci U S A, 2014. **111**(33): p. 12049-54.
85. Lin, X., et al., *Lowered pH Leads to Fusion Peptide Release and a Highly Dynamic Intermediate of Influenza Hemagglutinin.* J Phys Chem B, 2016. **120**(36): p. 9654-60.
86. Benhaim, M., et al., *Structural monitoring of a transient intermediate in the hemagglutinin fusion machinery on influenza virions.* Sci Adv, 2020.
87. Lee, K.K., *Architecture of a nascent viral fusion pore.* EMBO J, 2010. **29**(7): p. 1299-311.
88. Fontana, J. and A.C. Steven, *Influenza virus-mediated membrane fusion: Structural insights from electron microscopy.* Arch Biochem Biophys, 2015. **581**: p. 86-97.
89. Chlanda, P., et al., *The hemifusion structure induced by influenza virus haemagglutinin is determined by physical properties of the target membranes.* Nat Microbiol, 2016. **1**(6): p. 16050.
90. Gui, L., et al., *Visualization and Sequencing of Membrane Remodeling Leading to Influenza Virus Fusion.* J Virol, 2016. **90**(15): p. 6948-62.
91. Chernomordik, L.V. and M.M. Kozlov, *Membrane hemifusion: crossing a chasm in two leaps.* Cell, 2005. **123**(3): p. 375-82.

92. Biswas, S., et al., *Cholesterol promotes hemifusion and pore widening in membrane fusion induced by influenza hemagglutinin.* J Gen Physiol, 2008. **131**(5): p. 503-13.
93. Risselada, H.J., G. Bubnis, and H. Grubmuller, *Expansion of the fusion stalk and its implication for biological membrane fusion.* Proc Natl Acad Sci U S A, 2014. **111**(30): p. 11043-8.
94. Grunewald, K., *Viral fusion: how Flu induces dimples on liposomes.* EMBO J, 2010. **29**(7): p. 1165-6.
95. Calder, L.J. and P.B. Rosenthal, *Cryomicroscopy provides structural snapshots of influenza virus membrane fusion.* Nat Struct Mol Biol, 2016. **23**(9): p. 853-8.
96. Chernomordik, L.V. and M.M. Kozlov, *Protein-lipid interplay in fusion and fission of biological membranes.* Annu Rev Biochem, 2003. **72**: p. 175-207.
97. Efrat, A., L.V. Chernomordik, and M.M. Kozlov, *Point-like protrusion as a prestalk intermediate in membrane fusion pathway.* Biophys J, 2007. **92**(8): p. L61-3.
98. Kuzmin, P.I., et al., *A quantitative model for membrane fusion based on low-energy intermediates.* Proc Natl Acad Sci U S A, 2001. **98**(13): p. 7235-40.
99. Kozlov, M.M. and L.V. Chernomordik, *A mechanism of protein-mediated fusion: coupling between refolding of the influenza hemagglutinin and lipid rearrangements.* Biophys J, 1998. **75**(3): p. 1384-96.
100. Maurer, U.E., B. Sodeik, and K. Grunewald, *Native 3D intermediates of membrane fusion in herpes simplex virus 1 entry.* Proc Natl Acad Sci U S A, 2008. **105**(30): p. 10559-64.
101. Caston, J.R., *Conventional electron microscopy, cryo-electron microscopy and cryo-electron tomography of viruses.* Subcell Biochem, 2013. **68**: p. 79-115.
102. Zhou, Z.H., *Structures of viral membrane proteins by high-resolution cryoEM.* Curr Opin Virol, 2014. **5**: p. 111-9.
103. Bai, X.C., G. McMullan, and S.H. Scheres, *How cryo-EM is revolutionizing structural biology.* Trends Biochem Sci, 2015. **40**(1): p. 49-57.
104. Harris, A., et al., *Influenza virus pleiomorphy characterized by cryoelectron tomography.* Proc Natl Acad Sci U S A, 2006. **103**(50): p. 19123-7.
105. Calder, L.J., et al., *Structural organization of a filamentous influenza A virus.* Proc Natl Acad Sci U S A, 2010. **107**(23): p. 10685-90.
106. Hryc, C.F., D.H. Chen, and W. Chiu, *Near-atomic-resolution cryo-EM for molecular virology.* Curr Opin Virol, 2011. **1**(2): p. 110-7.
107. Chang, J., et al., *Reconstructing virus structures from nanometer to near-atomic resolutions with cryo-electron microscopy and tomography.* Adv Exp Med Biol, 2012. **726**: p. 49-90.
108. Stass, R., S.L. Ilca, and J.T. Huiskonen, *Beyond structures of highly symmetric purified viral capsids by cryo-EM.* Curr Opin Struct Biol, 2018. **52**: p. 25-31.
109. Clague, M.J., C. Schoch, and R. Blumenthal, *Delay time for influenza virus hemagglutinin-induced membrane fusion depends on hemagglutinin surface density.* J Virol, 1991. **65**(5): p. 2402-7.
110. Danieli, T., et al., *Membrane fusion mediated by the influenza virus hemagglutinin requires the concerted action of at least three hemagglutinin trimers.* J Cell Biol, 1996. **133**(3): p. 559-69.
111. Bentz, J., *Minimal aggregate size and minimal fusion unit for the first fusion pore of influenza hemagglutinin-mediated membrane fusion.* Biophys J, 2000. **78**(1): p. 227-45.
112. Günther-Ausborn, S., et al., *Role of hemagglutinin surface density in the initial stages of influenza virus fusion: lack of evidence for cooperativity.* J Virol, 2000. **74**(6): p. 2714-20.
113. Mittal, A., T. Shangguan, and J. Bentz, *Measuring pKa of activation and pKi of inactivation for influenza hemagglutinin from kinetics of membrane fusion of virions and of HA expressing cells.* Biophys J, 2002. **83**(5): p. 2652-66.

114. Ellens, H., et al., *Fusion of influenza hemagglutinin-expressing fibroblasts with glycophorin-bearing liposomes: role of hemagglutinin surface density.* Biochemistry, 1990. **29**(41): p. 9697-707.
115. Diao, J., et al., *Synaptic proteins promote calcium-triggered fast transition from point contact to full fusion.* Elife, 2012. **1**: p. e00109.
116. Hernandez, J.M., et al., *Membrane fusion intermediates via directional and full assembly of the SNARE complex.* Science, 2012. **336**(6088): p. 1581-4.
117. Christensen, S.M., M.W. Mortensen, and D.G. Stamou, *Single vesicle assaying of SNARE-synaptotagmin-driven fusion reveals fast and slow modes of both docking and fusion and intrasample heterogeneity.* Biophys J, 2011. **100**(4): p. 957-67.
118. McDargh, Z.A., A. Polley, and B. O'Shaughnessy, *SNARE-mediated membrane fusion is a two-stage process driven by entropic forces.* FEBS Lett, 2018. **592**(21): p. 3504-3515.
119. Imig, C., et al., *The morphological and molecular nature of synaptic vesicle priming at presynaptic active zones.* Neuron, 2014. **84**(2): p. 416-31.
120. Tamm, L.K., J. Crane, and V. Kiessling, *Membrane fusion: a structural perspective on the interplay of lipids and proteins.* Curr Opin Struct Biol, 2003. **13**(4): p. 453-66.
121. Légaré, S. and P. Lagüe, *The influenza fusion peptide promotes lipid polar head intrusion through hydrogen bonding with phosphates and N-terminal membrane insertion depth.* Proteins, 2014. **82**(9): p. 2118-27.
122. Stauffer, S., et al., *Stepwise priming by acidic pH and a high K+ concentration is required for efficient uncoating of influenza A virus cores after penetration.* J Virol, 2014. **88**(22): p. 13029-46.
123. Ali, A., et al., *Influenza virus assembly: effect of influenza virus glycoproteins on the membrane association of M1 protein.* J Virol, 2000. **74**(18): p. 8709-19.
124. Ruigrok, R.W., et al., *Membrane interaction of influenza virus M1 protein.* Virology, 2000. **267**(2): p. 289-98.
125. Ward, A.B. and I.A. Wilson, *Insights into the trimeric HIV-1 envelope glycoprotein structure.* Trends Biochem Sci, 2015. **40**(2): p. 101-7.
126. Ma, X., et al., *HIV-1 Env trimer opens through an asymmetric intermediate in which individual protomers adopt distinct conformations.* Elife, 2018. **7**.
127. Torrents de la Pena, A., et al., *Similarities and differences between native HIV-1 envelope glycoprotein trimers and stabilized soluble trimer mimetics.* PLoS Pathog, 2019. **15**(7): p. e1007920.
128. Pancera, M., A. Changela, and P.D. Kwong, *How HIV-1 entry mechanism and broadly neutralizing antibodies guide structure-based vaccine design.* Curr Opin HIV AIDS, 2017. **12**(3): p. 229-240.
129. Walls, A.C., et al., *Structure, Function, and Antigenicity of the SARS-CoV-2 Spike Glycoprotein.* Cell, 2020.
130. Porotto, M., et al., *Regulation of paramyxovirus fusion activation: the hemagglutinin-neuraminidase protein stabilizes the fusion protein in a pretriggered state.* J Virol, 2012. **86**(23): p. 12838-48.
131. Jardetzky, T.S. and R.A. Lamb, *Activation of paramyxovirus membrane fusion and virus entry.* Curr Opin Virol, 2014. **5**: p. 24-33.
132. Lee, J.E. and E.O. Saphire, *Ebolavirus glycoprotein structure and mechanism of entry.* Future Virol, 2009. **4**(6): p. 621-635.
133. Chandran, K., et al., *Endosomal proteolysis of the Ebola virus glycoprotein is necessary for infection.* Science, 2005. **308**(5728): p. 1643-5.
134. Schornberg, K., et al., *Role of endosomal cathepsins in entry mediated by the Ebola virus glycoprotein.* J Virol, 2006. **80**(8): p. 4174-8.

135. Nanbo, A., et al., *Ebolavirus is internalized into host cells via macropinocytosis in a viral glycoprotein-dependent manner.* PLoS Pathog, 2010. **6**(9): p. e1001121.
136. Carette, J.E., et al., *Ebola virus entry requires the cholesterol transporter Niemann-Pick C1.* Nature, 2011. **477**(7364): p. 340-3.
137. Simmons, J.A., et al., *Ebolavirus Glycoprotein Directs Fusion through NPC1+ Endolysosomes.* J Virol, 2016. **90**(1): p. 605-10.
138. Nathan, L., et al., *Calcium Ions Directly Interact with the Ebola Virus Fusion Peptide To Promote Structure-Function Changes That Enhance Infection.* ACS Infect Dis, 2020. **6**(2): p. 250-260.
139. Jae, L.T., et al., *Virus entry. Lassa virus entry requires a trigger-induced receptor switch.* Science, 2014. **344**(6191): p. 1506-10.
140. Cohen-Dvashi, H., et al., *Molecular Mechanism for LAMP1 Recognition by Lassa Virus.* J Virol, 2015. **89**(15): p. 7584-92.
141. Cohen-Dvashi, H., et al., *Role of LAMP1 Binding and pH Sensing by the Spike Complex of Lassa Virus.* J Virol, 2016. **90**(22): p. 10329-10338.
142. Li, S., et al., *Acidic pH-Induced Conformations and LAMP1 Binding of the Lassa Virus Glycoprotein Spike.* PLoS Pathog, 2016. **12**(2): p. e1005418.
143. Cao, W., et al., *Identification of alpha-dystroglycan as a receptor for lymphocytic choriomeningitis virus and Lassa fever virus.* Science, 1998. **282**(5396): p. 2079-81.
144. Rojek, J.M. and S. Kunz, *Cell entry by human pathogenic arenaviruses.* Cell Microbiol, 2008. **10**(4): p. 828-35.
145. Hastie, K.M. and E.O. Saphire, *Lassa virus glycoprotein: stopping a moving target.* Curr Opin Virol, 2018. **31**: p. 52-58.
146. Hulseberg, C.E., et al., *Lamp1 Increases the Efficiency of Lassa Virus Infection by Promoting Fusion in Less Acidic Endosomal Compartments.* MBio, 2018. **9**(1).
147. Benhaim, M.A. and K.K. Lee, *New Biophysical Approaches Reveal the Dynamics and Mechanics of Type I Viral Fusion Machinery and Their Interplay with Membranes.* Viruses, 2020. **12**(4).

Chapter 2. HDX-MS Analysis of Viral Fusion Proteins *In Situ*

Portions of the text in this chapter have been modified and reproduced with permissions from:

† Hodge EA, Benhaim MA, Lee KK. Bridging Protein Structure, Dynamics, and Function Using Hydrogen/Deuterium-Exchange Mass Spectrometry. *Protein Science* 2020;29(4):843-855. doi:10.1002/pro.3790

‡ Benhaim MA, Lee KK, Guttman M. Tracking Higher Order Protein Structure by Hydrogen-Deuterium Exchange Mass Spectrometry", *Protein & Peptide Letters* (2019) 26: 16. doi:10.2174/0929866526666181212165037

2.1 Introduction†

As previously discussed, high-resolution three-dimensional structures of macromolecular complexes have deepened our understanding of their assembly and construction. However, proteins are dynamic molecules that are constantly in motion. These motions range from small fluctuations in local structure to large scale conformational rearrangements between distinct structural states. Despite the fact that these dynamic motions and structural rearrangements are critical for protein function, we do not yet fully understand how these motions and conformational changes contribute to protein structure and function [1]. This is especially true for viral fusion proteins and particularly relevant to immunogen design and understanding how viral fusion proteins interact with our immune system and their cellular receptors. In order to fully understand how viral fusion proteins function, we need to understand the dynamic structural changes that lead to functionally distinct and antigenically relevant conformations. In recent years Hydrogen/Deuterium-exchange Mass Spectrometry (HDX-MS) has developed into a powerful solution-state structural technique that enables the study of macromolecular protein complexes under native conditions. HDX-MS enables one to interrogate protein structure and function by directly monitoring backbone amide solvent accessibility in solution, which is sensitive to protein structural and conformational dynamics [2]. In this chapter I will present an overview of the fundamental theory behind HDX-MS and outline its practical applications; highlighting how recent

advances in technology have expanded the capabilities of HDX-MS enabling interrogation of protein structure *in situ*.

The Biophysics of HDX-MS: Fundamental Theory†

Protein motion is constant and ranges from large-scale, slower structural rearrangements to rapid, transient fluctuations in local structure [3]. These innate, often subtle, dynamic motions across the protein backbone are fundamental to protein function but cannot be probed readily by most structural techniques [4]. The intrinsic chemical rate of deuterium exchange of a residue's amide group is primarily dependent on temperature, pH, and the particular type of amino acid. Under physiological conditions the exchange rates for fully exposed amide hydrogens range from 10^1 to 10^3 s^{-1} [5]. On top of this, HDX-MS applied to proteins is sensitive to the accessibility, or exposure, of backbone amide hydrogens resulting from a protein's conformation and can change in response to protein motion and structural dynamics [5, 6]. In native proteins, the accessibility of a backbone amide hydrogen is largely dependent on hydrogen bonding and local secondary structure, as well as solvent accessibility [6, 7]. Backbone amide hydrogens more exposed to deuterated solvent will exchange faster than those occluded in the protein core. Similarly, those amide hydrogens engaged in stable hydrogen bonds are protected from deuterium and will exchange more slowly. Local fluctuations in protein structure transiently expose backbone amide hydrogens to deuterium. The propensity for exposed amide hydrogens in a peptide segment to exchange with deuterium is related to how frequently and for how long they exist in an exposed, exchange-competent state with respect to the chemical rate of exchange [6]. These transitions are monitored under equilibrium conditions during continuous labeling HDX-MS experiments [8]. Briefly, in such an experiment, a protein is diluted into a deuterated solution for various amounts of time, ranging from seconds to hours or days. The exchange reaction is then quenched by dropping the solution pH to 2.5 and 0°C, where the labeling rate is at its minimum [6, 9-11]. The labeled

protein is digested into peptide fragments which are separated and analyzed by liquid chromatography coupled to mass spectrometry (LC-MS). The reverse phase LC separation must be performed quickly and under quench conditions to limit back exchange of the deuterium label with water in solution. The extent of labeling is straightforward to analyze by mass spectrometry as uptake of a single deuteron produces a Dalton increase in mass.

Under physiological conditions, the majority of local protein motion is faster than the HDX labeling rate and thus leads to gradual incorporation of deuterium onto the peptide backbone (Figure 2.1 A). So-called "EX2 kinetics" is observed when the interconversion rate between a peptide's protected, exchange-incompetent and exposed, exchange-competent state is faster than the labeling rate [6, 12, 13]. In this case, rapid opening and closing events allow only a subset of the collectively exposed amide hydrogens to exchange during any single transition to the exchange competent state. These rapid fluctuations are characterized by unimodal mass spectra envelopes that gradually shift to higher masses with time. Over time the entire peptide segment will become deuterated after repeatedly sampling the exposed, exchange-competent state. The rate and extent of a peptide's deuterium uptake under EX2 kinetics is interpretable in terms of local structural dynamics, motion, and flexibility (Figure 2.1 A). Furthermore, by characterizing how this exchange profile changes with environment, upon ligand binding, or between homologous proteins, one can begin to appreciate and dissect the structural basis for protein function and behavior.

Large scale structural rearrangements, including reversible interconversion between conformations, can also be monitored by HDX-MS (Figure 2.1 B)[14]. As a protein changes conformation, the rate and extent of HDX will shift in accordance with the local structure of each state. These types of protein motion are typically slow (on the order of milliseconds to seconds) and highly correlated across segments of the amide backbone. In an HDX labeling experiment, this behavior manifests as multimodal isotopic distributions with unique HDX populations for each structural state, and is termed EX1 kinetics

[13, 15-17]. For example, if a region in a protein reversibly interconverts between a “closed” protected (exchange-incompetent) and an “open” exposed (exchange-competent) state, with the residues in this segment switching conformations in a concerted manner, this would be readily apparent by HDX-MS (Figure 2.1 B). The amide hydrogens in the “closed” state would be protected from exchange and visible as a lower mass population in the spectra, whereas those that had transitioned to the exposed state would be evidenced as a deuterated higher mass population in the spectra. As the protein reversibly transitions between these states, the individual HDX populations will ultimately converge on the fast exchanging exposed state, enabling one to determine the rate of conversion between states and their relative half-lives (Figure 2.1 B). More generally, EX1 kinetics is indicative of correlated local structural changes or motion occurring slower than the labeling rate; meaning multiple amide hydrogens in a peptide segment adopt a relatively long-lived exchange competent state and become deuterated together [13, 18]. In reality, EX1 exchange kinetics are rarely observed under physiological conditions because one’s ability to resolve EX1 kinetics is dependent on the rate of interconversion between the protected-exchange incompetent and exposed-exchange competent state being slower than the labeling rate [13, 18].

EX1 exchange kinetics commonly manifests as abnormally broad mass envelopes, where the two HDX states are not dissimilar enough from one another to produce visually distinct populations. Analysis by binomial fitting is sensitive to changes in mass envelope width and can therefore detect the presence of two similar, coexisting HDX states and characterize their individual exchange profiles through bimodal deconvolution. The presence of bimodal spectra in HDX-MS data does not always correspond to EX1 kinetics arising from large scale conformational changes, reversible interconversion between states, or local coordinated motion. It can also be indicative of conformational heterogeneity resulting from sample impurity or degradation, mixed populations from unsaturated ligand binding, and even back exchange from chromatographic carryover and improper sample handling [10, 19, 20].

One of the advantages of HDX-MS is that it is applicable to nearly any protein system of interest[21]‡. With the high sensitivity of modern mass spectrometers, the limits of detection are sufficient to enable comprehensive studies with very little sample requirements; nowadays, a few hundred picomoles of protein is sufficient. HDX is now routinely used to study large protein assemblies, heavily glycosylated proteins, and membrane proteins, all of which can be challenging targets for most structural techniques. Furthermore, HDX-MS can be used to study protein structure in highly complex biological matrices such as in blood serum or on the surface of whole cells and viruses [14, 21, 22]. This chapter is focused on the development of an HDX-MS workflow for studying the structural and conformational dynamics of the HIV-1 Env fusion glycoprotein *in situ* using authentic and engineered viral systems.

2.2 Results and Discussion

VSV-Env-ΔG Vaccine Candidate Evaluated by ns-ET and HDX-MS

The work presented here was done in collaboration with Joanne DeStefano at the IAVI AIDS Vaccine Design and Development Laboratory. All electron microscopy and tomography presented here was performed by Dr. Long Gui and Dr. James Williams.

The HIV-1 Env fusion glycoprotein is the sole antigenic target on the surface of HIV and is essential for mediating entry into host cells. High resolution structural studies have revealed that Env dynamically samples multiple, functionally and antigenically distinct, conformations at rest [23-37]. These conformational dynamics are essential for Env's function as a viral fusion protein and as a vaccine immunogen. However, our understanding of Env's conformational dynamics has largely been informed through the study of stabilized soluble Env ectodomain trimers, termed SOSIPs, as native Env has a high propensity to misfold [24, 25, 28, 29, 31-34, 38-42]. Furthermore, Env is present in low abundance on the surface of HIV-1 virions [37]. While a typical influenza virion is decorated with hundreds of copies HA; HIV-1 virions are sparsely decorated with between 10-20 copies of Env [37, 43, 44]. Thus

researchers often use engineered virus like particles (VLPs) or infectious viruses, such as vesicular stomatitis virus (VSV), psuedotyped with HIV-1 Env in place of the VSV-G protein (henceforth referred to as VSV-Env-ΔG) [28-30, 32, 45-51].

These platforms provide researchers with a means of studying various components of HIV biology and Env function; including isolation of and evaluation of neutralizing antibodies against Env using infectious virions under accessible biosafety conditions [45, 47, 49-51]. Furthermore, these platforms are currently being evaluated as potential HIV-1 vaccine platforms as recent attempts using subunit-based vaccines have had limited success [39, 47, 49-55]. However, the structure and homogeneity of Env present on these VSV-Env-ΔG psudeotyped virions, and other VLP platforms, is rarely characterized. In order to create a safe and effective vaccine against HIV-1, it is imperative that Env be present in the correct conformation so that broadly neutralizing antibodies can be elicited and that minimal non-native Env is present to avoid eliciting non-neutralizing antibodies [23, 24, 27, 39-42, 49, 52-57]. Thus, we have developed an HDX-MS workflow to characterize the structure and dynamics of native Env on the surface of intact virions. In combination with negative stain electron microscopy and tomography imaging this approach can assess virion ultrastructure, Env surface density, and Env conformation.

Analysis of Virion Ultrastructure and Env Surface Density

VSV-Env-ΔG particles were first imaged by negative stain electron microscopy (ns-EM) to assess sample quality and homogeneity (Figure 2.2 A). By ns-EM many particles were in high abundance and appeared coated with a dense array of surface proteins; however, under these conditions the surface proteins could not be definitively identified as Env trimers. Thus, we turned to cyro-EM and cryo-ET in order to obtain higher resolution information and avoid artifacts associated with ns-EM. Attempts to image VSV-Env-ΔG particles by cryo-EM were unsuccessful despite numerous attempts to optimize

freezing conditions. The VSV-Env-ΔG samples were purified in buffer containing 5% trehalose as a means of stabilizing viral particles. We believed this buffer additive was affecting sample vitrification and contributed to poor freezing conditions. We attempted to remove the trehalose by dialysis and imaged the resulting VSV-Env-ΔG particles by ns-EM. However, we discovered that dialysis and removal of the stabilizing buffer additive resulted in significant damage to viral particles and widespread shedding of surface proteins.

Thus, we turned to negative stain electron tomography (ns-ET) in order to visualize the viral particles in 3D and characterize the abundance and conformation of the surface proteins. By ns-ET we observed a significant amount of shed BG505 Env trimers. When free from the viral surface BG505 Env trimers preferentially orient themselves on the grid in a top down orientation, as was observed for these free trimers. These free Env trimers are easily identified due to their distinct morphology and resemble the soluble BG505 SOSIP trimer. Obtaining similar views of the BG505 trimer on the viral surface using ns-ET was complicated by technical limitations (i.e. the missing wedge problem) and high background noise [58]. However, we were able to observe some side-views of the surface proteins which strongly resemble Env trimers (Figure 2.2 B and C)[37]. We also observed a significant amount of elongated and disordered surface proteins which likely correspond to misfolded Env monomers or dimers. Ultimately, we were unable to definitively resolve Envs structure and conformation on the viral surface by ns-EM and ns-ET. Furthermore, negative stain sample preparation can result in perturbation of protein structure and likely contributed to particle disruption and Env conformation [59, 60]. Thus, in order to obtain an unbiased characterization of Env's conformation and homogeneity we turned to HDX-MS.

In Situ HDX-MS Analysis of BG505 Env on VSV-Env-ΔG VLPs

Typically, HDX-MS analysis requires that your protein of interest be conformationally homogenous so that the deuterium exchange can be attributed to a single species; in this case trimeric

BG505 Env on the surface of VSV-Env-ΔG VLPs [14, 61]. However, our goal here was to assess the conformation and homogeneity of BG505 Env and determine the relative abundance of native and non-native BG505 Env. As evident by EM analysis the viral particles were relatively fragile and could not be concentrated or purified by "rough handling" techniques such as high-speed centrifugal concentration or spin filtration. Samples prepared for HDX-MS were concentrated by low speed centrifugation and assessed by ns-EM to ensure the particles were not disrupted. Sample quantity was limited and thus suboptimal concentrations of Env were used and exchanges were performed in duplicate with a limited timecourse. Under denaturing quench conditions Env was digested with soluble pepsin and the resulting peptic peptides were isolated from viral debris by high-speed centrifugation and flash frozen in liquid nitrogen. Side-by-side exchanges were performed with purified BG505 SOSIP trimers [59]. Samples were analyzed by LC-MS with ion mobility spectrometry (IMS) using a Waters Synapt G2-Si as previously described [59].

Peptide coverage of BG505 Env from VSV-Env-ΔG samples was exceptionally poor and confounded by high background signal and overlapping peptides from unidentified contaminating viral proteins. However, we were able to clearly monitor some key conformational reporter peptides in gp120 that are known indicators of Env conformation and homogeneity. Using binomial fitting and bimodal deconvolution we were able to assess the relative abundance of non-native Env present in these samples and obtain a limited dynamic profile of the native trimeric Env.

We determined that there was approximately 20-30% non-native Env present in these samples (Figure 2.3). The short N-terminal gp120 peptide WVTVY is commonly used as a reporter for Env conformation and should be highly protected from exchange in trimeric Env, as seen in the BG505 SOSIPs (Figure 2.3 B and 2.4 B). However, we observed bimodal isotopic distributions in the VSV-Env-ΔG BG505 sample indicative of non-native Env (Figure 2.3). Bimodal deconvolution of these spectra suggested that these two HDX states were distinct non-interconverting states and are likely due to

misfolded or non-native Env as the ratio of these two states does not change over time [14, 62, 63]. This same exchange profile was observed throughout the N-terminus of gp120 spanning residues 13-25 (Figure 2.3 B). In each of these three peptides bimodal deconvolution indicated that approximately 20-30% of Env was non-native indicated by the unchanging exposed population. Analysis of a peptide at the trimer apex in V2 suggests that BG505 Env trimers on VSV-Env-ΔG VLPs may be more dynamic than BG505 SOSIPs, however this data can be confounded by the high abundance of non-native Env (Figure 2.5). Peptides at the trimer apex, including this V2 peptide, are commonly used to characterize the conformation of Env trimers as this region undergoes significant reorganization between the closed (BG505 SOSIP-like) and open (CD4-bound state) [25, 27, 28, 31, 34, 35, 40-42]. The apparent EX1 like kinetics observed in the V2 peptide for BG505 on VSV-Env-ΔG VLPs cannot be definitively attributed to either conformational heterogeneity arising from non-native Env or interconversion between the open and closed states. Such definitive conclusions require more comprehensive sequence coverage with multiple peptides reporting on the same phenomenon or a more homogenous sample set with trimeric Env. While these data are unreliable for characterizing Env's conformational dynamics due to the high degree of heterogeneity they serve as a proof of concept for how HDX-MS can interrogate protein structure and dynamics *in situ*.

High Density Env VLPs Display an Abundance of Native Trimeric Env

The work presented here was performed in collaboration with Michael Zwick and Daniel Leaman at The Department of Immunology and Microbiology at The Scripps Research Institute, La Jolla, CA. Electron Cryo-Tomography was performed by Dr. Vidya Mangala Prasad.

As previously discussed, the low copy number of Env on HIV-1 virions presents a challenge for structural biologists and immunologists aiming to characterize Env structure *in situ* and develop an effective vaccine against HIV-1 [37, 39, 47, 50, 51, 55, 56]. The low surface density of Env on HIV-1 virions also impedes the humoral immune response and the efficiency of antibody mediated

neutralization that is greatly enhanced by multivalent interactions [47, 55-57]. Strategies to increase Env copy numbers on VLPs and other multivalent vaccine platforms have met limited success and, as outlined above, can result in significant conformational heterogeneity leading to elicitation of non-neutralizing antibodies [47]. Recently, researchers in Michael Zwicks lab at the Scripps Research Institute developed an HIV VLP platform that produces VLPs with high surface density of native trimeric Env (termed hVLPs) [47]. Using successive rounds of fluorescence-activated cell sorting (FACS) they were able to select for VLP producer cells that produce VLPs that are densely decorated with native Env trimers [47, 64]. The Env present on these hVLPs was engineered by the Zwick lab to be highly stable and homogenous [47, 64]. Biochemical characterization of this engineered "Comb-mut" Env trimer indicated that it is resistant to denaturants, heat, proteolysis, and degradation and is likely in the closed conformation [47, 64]. Thus, the hVLP platform and Comb-mut Env trimer are well suited for characterizing Env structure and conformational dynamics *in situ* using cryo-ET and HDX-MS.

In contrast to the VSV-Env-ΔG VLPs, the hVLPs appeared as uniform spherical virions with an abundance of Env trimers decorating the surface (Figure 2.6 A) [47]. Remarkably, even after successive freeze-thaw cycles we observed minimal soluble Env in the background indicating that the hVLP particles are relatively robust. Using cryo-ET and sub-tomogram averaging Dr. Vidya Mangala Prasad sought to characterize the conformation of Comb-mut Env trimers on the surface of hVLPs and obtain a high-resolution structural model of native Env [37, 65, 66]. Prior efforts to obtain a high-resolution structure of Env by sub-tomogram averaging have been limited due to available imaging and data processing technologies [37]. Recent technological advances have greatly expanded the capabilities of cryo-ET and sub-tomogram averaging enabling us to characterize the structure of native Env with high-resolution [65-68]. The dense array of conformationally homogenous Comb-mut Env trimers decorating the hVLP surface enabled Dr. Mangala Prasad to obtain a sub-tomogram averaged model of native Env at 12 Å (Figure 2.6 B). Current efforts are underway to further improve the model resolution; however,

even at 12 Å we can definitively say that native Comb-mut Env trimers exist in the closed conformation. This model enables us to resolve the membrane-proximal external region (MPER) which had eluded prior characterization at high resolution. At the current resolution we are unable to resolve distinguishing features in the MPER or identify secondary structure elements, but further optimization and model refinement may improve the local resolution at the MPER. When compared to the high-resolution crystal structure of the BG505 SOSIP trimer, the C-terminus of the gp41 fusion domain appears splayed outward in the sub-tomogram averaged model (Figure 2.6 B). However, further refinement is required to interrogate these structural differences.

Next we sought to characterize the structural and conformational dynamics of Comb-mut Env trimers on hVLPs by HDX-MS. Cryo-ET and HDX-MS have proven to be powerful complementary structural and biophysical approaches for studying protein structure *in situ* [22, 66, 69, 70]. As previously discussed, the Comb-mut Env trimer was engineered to be stable under denaturing conditions and resistant to proteolysis [64]. While these features are desirable for immunogen design and production of homogenous trimeric Env they present a significant challenge for analysis by HDX-MS. Using a Thermo Fisher Fusion Orbitrap equipped with nano flow LC we performed peptide mapping using samples prepared under HDX-MS conditions and digested with soluble pepsin. The increased sensitivity and resolution afforded by the Fusion Orbitrap and nano-LC provided us with a maximum potential sequence coverage of 47% (Figure 2.7). We carried out HDX-MS analysis on Comb-mut Env hVLPs and BG505 SOSIPs under identical conditions using a Waters Synapt G2-Si and a custom HDX LC handling system. We were able to monitor far fewer peptides for the Comb-mut hVLPs than anticipated based on the peptide mapping experiments resulting is 8% sequence coverage (Figure 2.7). However, the peptides we were able to monitor are common reporter peptides for Env conformation. Analysis of a gp120 inner domain peptide indicates that Comb-mut Env on hVLPs is homogenous and trimeric and displayed a nearly identical exchange profile compared to BG505 SOSIPs (Figure 2.8). Furthermore, analysis of a

peptide in V2 indicates that Comb-mut Env is in the closed conformation and displays a similar exchange profile as BG505 SOSIPs which is known to adopt a closed conformation [24, 35, 39, 59]. While these peptides alone cannot be used to definitively characterize the conformational dynamics of Env on hVLPs, they are in good agreement with our cryo-ET observations.

2.3 Outlook and Future Directions: HDX-MS of native Env *in situ*

HDX-MS of the Comb-mut hVLP data is still in progress, however high background signal, inefficient pepsin digestion, and instrumentation limitations resulting in low mass accuracy limit the extent to which the data can be analyzed with confidence. However, some recent developments in HDX-MS sample preparation techniques suggest the sequence coverage for Comb-mut Env could be greatly improved. Using non-ionic detergents such as n-Dodecyl-β-D-maltoside (DDM) to solubilize the viral membrane we can isolate the solubilized Comb-mut Env trimers under quench conditions, remove the lipids from solution, and perform online pepsin digestion using immobilized pepsin [71-74]. While this has the potential to increase the background signal from internal viral proteins such as HIV gag, the increased digestion efficiency of immobilized pepsin should enable us to track more Env peptides that are present in higher abundance. This approach has shown great promise for monitoring peptides in protease resistant regions of the influenza HA fusion domain that previously eluded characterization. Detergent solubilization of integral and peripheral membrane proteins is common practice in HDX-MS experiments [14, 21, 71-74]. However, these analyses are predominantly carried out with purified proteins in synthetic lipid vesicles or lipid nanodiscs [71-74]. Lipid depletion using zirconium oxide was also successfully used to study the Dengue Virus surface proteins by HDX-MS [75]. However, we anticipate the background signal from internal viral proteins, especially HIV-1 gag which is present in staggeringly high amounts relative to Env, to remain a significant limitation to our analysis.

While these studies demonstrate how HDX-MS, even with limited peptide coverage, can be used to assess protein conformation and homogeneity *in situ* we were unable to characterize the conformational dynamics of native Env to any meaningful degree. Future efforts using the hVLP platform are aimed at characterizing the conformational dynamics of native BG505 Env trimers of the viral surface by HDX-MS. The BG505 SOSIP trimer has long served as an invaluable tool for structural biologists and has become a standard conformational reference for our own HDX-MS studies of Env [28, 29, 31-34, 38-40, 53, 59]. Recent evidence suggests that the conformations sampled by SOSIP trimers are markedly different than those sampled by native Env trimers on the viral surface [25-36, 38, 48, 76]. Past structural studies of numerous highly diverse Env SOSIPs indicated that Env dynamically interconverts between a closed and open "CD4 bound" conformation, and that these conformational dynamics are critical for mediating interactions with cellular receptors and neutralizing antibodies [25, 26, 28-35, 48, 59, 76]. However, when monitored by sm-FRET native Env trimers were found to reversibly interconvert between at least three distinct conformations [29]. Furthermore, their data indicate that the ground state for native Env is distinct from the closed state observed in high resolution structures and by HDX-MS for SOSIPs [29]. While native Env samples conformations resembling the known open and closed states, the true ground state for native Env has yet to be characterized by any high-resolution technique. Thus, we aim to use cryo-ET and HDX-MS to characterize the structure and conformational dynamics of native BG505 Env trimers on the surface of hVLPs. The work presented here serves as a proof of concept for such future studies. Despite the challenges and limitations outlined here future developments in HDX-MS sample handling and methodology, combined with improved instrumentation should enable us to characterize the conformational dynamics of native Env trimers *in situ*.

2.4 Materials and Methods

HDX-MS of VSV-Env-ΔG BG505 VLPs

All VSV-Env-ΔG BG505 VLPs were provided by Joanne DeStefano at the IAVI AIDS Vaccine Design and Development Laboratory. VSV-Env-ΔG BG505 VLPs were prepared in HBSS buffer with 5% trehalose as a stabilizing additive. Env concentration was determined by western blotting using the BG505 SOSIP as a control and determined to be 0.07 mg/mL. Samples were concentrated for HDX-MS by low speed centrifugation to 0.2 mg/mL and resuspended in HDX PBS buffer ph 7.4 (10 mM Phosphate, 150 mM NaCl, 0.02% NaN_3). Each HDX-MS reaction was prepared to contain either 2 ug of BG505 Env in the VSV-Env-ΔG BG505 VLP samples or 6 ug BG505 SOSIPs. HDX-MS reactions were initiated by rapidly diluting 10 uL of protein containing sample into 90 uL deuteration buffer (10 mM Phosphate, 150 mM NaCl, 85% D_2O (Cambridge Isotope Laboratories)) to a final pH^* = 7.6. Samples were deuterated for either 60 seconds or 30 minutes before being diluted 1:1 with ice cold quench buffer (200 mM TCEP [tris(2-carboxyethyl) phosphine] and 0.2% formic acid (FA)) to a final pH of 2.5. Quenched samples were digested with 30 ug/mL of porcine pepsin (Worthington Labs) under quench conditions for 5 minutes on ice. Labeled peptides were purified by high speed centrifugation at 0°C (2 minutes at 25,000 rcf) and immediately flash frozen in liquid nitrogen. BG505 SOSIP samples were handled identically to ensure consistent labeling and back exchange. Frozen samples were stored at -80°C until analysis. All samples were prepared containing 0.25 ug/mL of each PPPI and PPPF tetrapeptides (AnaSpec) as internal exchange standards [77]. Totally deuterated samples were prepared by as previously described [59]. VSV-Env-ΔG BG505 VLP reactions were performed in duplicate, BG505 SOSIP exchanges were performed in singlicate due to sample handling errors during LC-MS analysis.

Reverse Phase Liquid Chromatography and Mass Spectrometry of VSV-Env-ΔG BG505 VLPs and BG505 SOSIPs

Samples were thawed for 5 minutes on ice and manually injected into a Waters HDX Manager kept at 1°C. Samples were trapped on a Waters ACQUITY UPLC CSH C18 VanGuard 130Å, 1.7 μm, 2.1 mm by 5 mm trap column for 3 minutes with a flow of solvent A [2% acetonitrile, 0.1% FA, 0.025% trifluoroacetic acid (TFA)] at a rate of 150 μL/min. Peptides were resolved over a Waters ACQUITY UPLC CSH C18 130Å, 1.7 μm, 1 x 100 mm column using a 10 minute linear gradient of 3% to 50% solvent B (Solvent B: 100% acetonitrile and 0.1% FA) and analyzed using a Waters Synapt G2-Si Q-TOF with ion mobility enabled. Source and desolvation temperatures were 70°C and 130°C respectively. The StepWave ion guide settings were tuned to prevent non-uniform gas phase proton exchange in the source [78]. A series of trap column wash steps were implemented between each injection to minimize carryover [62].

HDX-MS of Comb-mut Env V4 hVLPs

Comb-mut Env V4 hVLPs were provided by Michael Zwick and Daniel Leaman at The Department of Immunology and Microbiology at The Scripps Research Institute, La Jolla, CA and detailed methods for the production and purification of those samples are described here [47, 64]. Env on hVLPs was quantified by SDS-PAGE using BG505 SOSIPs as a standard. HDX-MS reactions were initiated by diluting 20 uL of either hVLPs or BG505 SOSIPs with 180 uL deuteration buffer (10 mM Phosphate, 150 mM NaCl, 85% D_2O (Cambridge Isotope Laboratories)) to a final $pH^* = 7.45$. Samples were deuterated for 5 seconds, 60 seconds, 30 minutes, or 3 hours before being diluted 1:1 with ice cold quench buffer (8 M urea, 200 mM TCEP [tris(2-carboxyethyl) phosphine] and 0.2% formic acid (FA)) to a final pH of 2.5. Quenched samples were digested with 30 ug/mL of porcine pepsin (Worthington Labs) under quench conditions for 5 minutes on ice. Labeled peptides were purified by high speed centrifugation at 0°C (2

minutes at 25,000 rcf) and immediately flash frozen in liquid nitrogen. BG505 SOSIP samples were handled identically to ensure consistent labeling and back exchange. Frozen samples were stored at -80°C until analysis. All samples were prepared containing 0.25 ug/mL of each PPPI and PPPF tetrapeptides (AnaSpec) as internal exchange standards [77]. Totally deuterated (TD) samples were prepared by collecting purified peptide eluent following reverse phase LC separation of a pepsin digested undeuterated sample [22]. Following evaporation of the LC elution buffer the peptides were resuspended in HDX PBS pH 7.50 Buffer, deuterated in Deuteration Buffer for 2 hours at 37°C, and quenched and frozen as described above. All reactions were performed in duplicate.

Reverse Phase Liquid Chromatography and Mass Spectrometry of Comb-mut Env V4 hVLPs and BG505 SOSIPs

Samples were thawed for 5 minutes on ice and manually injected into a custom built HDX LC system kept at 0°C using a 500 uL sample loop. Samples were trapped on a Waters ACQUITY UPLC CSH C18 VanGuard 130Å, 1.7 μm, 2.1 mm by 5 mm trap column for 7 minutes with a flow of solvent A [2% acetonitrile, 0.1% FA, 0.025% trifluoroacetic acid (TFA)] at a rate of 150 μL/min. Peptides were resolved over a Waters ACQUITY UPLC CSH C18 130Å, 1.7 μm, 1 x 100 mm column using a 20 minute linear gradient of 3% to 50% solvent B (Solvent B: 100% acetonitrile and 0.1% FA) and analyzed using a Waters Synapt G2-Si Q-TOF with ion mobility enabled. Source and desolvation temperatures were 70°C and 130°C respectively. The StepWave ion guide settings were tuned to prevent non-uniform gas phase proton exchange in the source [78]. A series of trap column wash steps were implemented between each injection to minimize carryover [62].

HDX-MS Data Analysis

Peptic BG505 Env peptides were identified previously and used as a reference list [59]. Ion mobility and LC retention time filtered spectra were extracted from the raw MS files using CDCReader [79]. Spectra were analyzed using HXExpress V2 with binomial fitting and bimodal deconvolution [63, 80]. Fitting with more than one binomial distribution was only performed when a single binomial was not sufficient to encompass the mass envelope and the two populations could be separated with confidence as previously described [22, 63, 80].

2.5 Figures

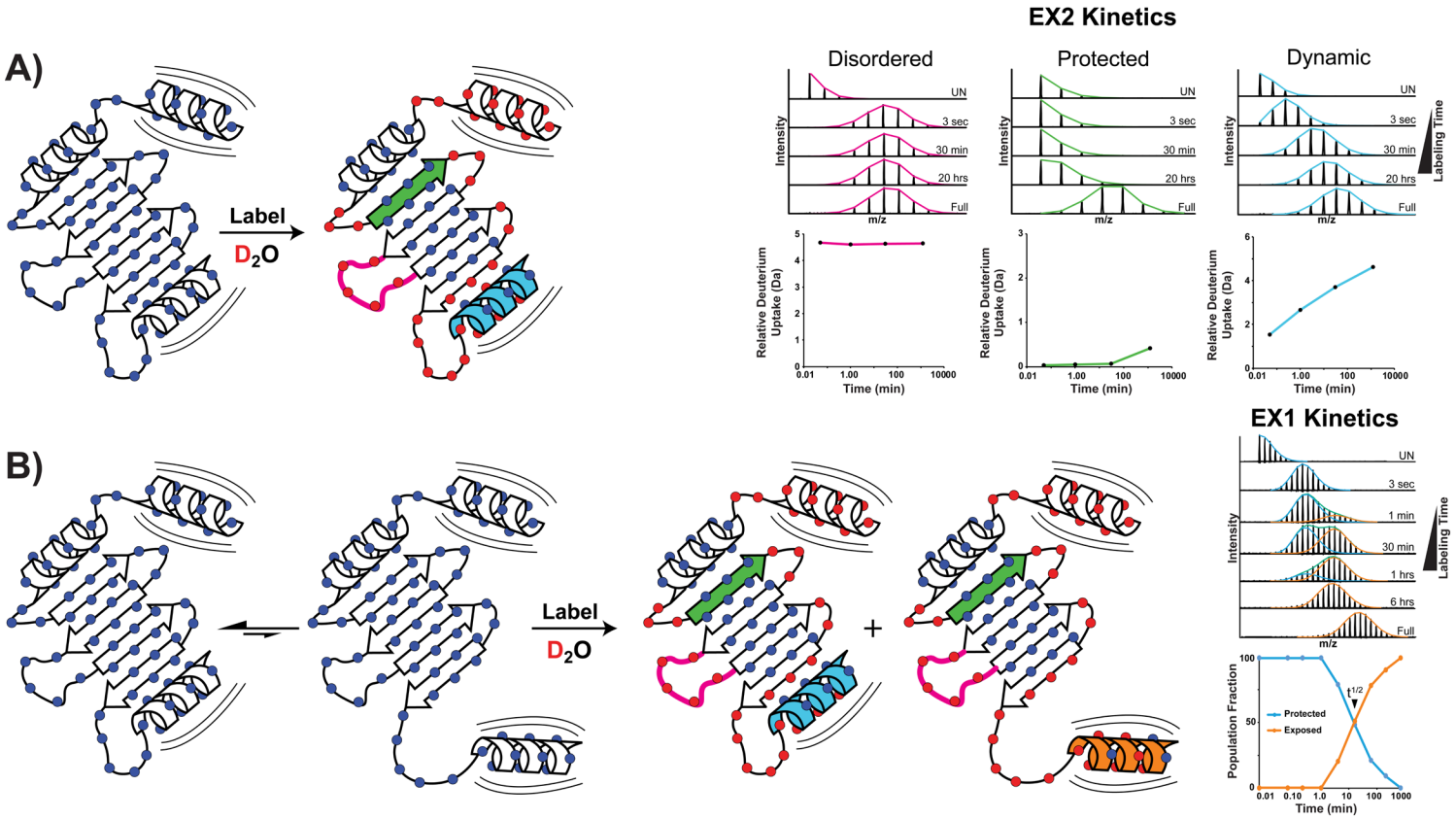

Figure 2.1 Protein structural dynamics and motion monitored by HDX-MS. Continuous labeling HDX-MS probes the accessibility of backbone amide hydrogens (blue circles) by their exchange with deuterium in solution. Under equilibrium conditions the majority of protein structural dynamics and motion manifests as "EX2 kinetics" (A) where deuterium is gradually incorporated across the protein backbone in a manner directly related to the local structural dynamics and changes in amide accessibility. Examples of peptide specific HDX-MS data with representative mass spectra show the gradual incorporation of deuterium over time. Peptide segments in highly structured regions with strong hydrogen bonding networks (green beta sheet) take up deuterium much slower than regions with exposed and accessible amides (pink loop) and those undergoing dynamic motions (blue helix) that occur faster than the labeling rate. (B) When these dynamic structural changes are slower than the labeling rate (e.g., a reversible interconversion or conformational change) they produce unique and resolvable HDX states that manifest as "EX1 kinetics." Here the protein reversibly interconverts between conformations with a protected (blue) or exposed (orange) helical domain. Analysis of the mass spectra reveals the equilibrium distribution of these two states and their respective half-lives. †

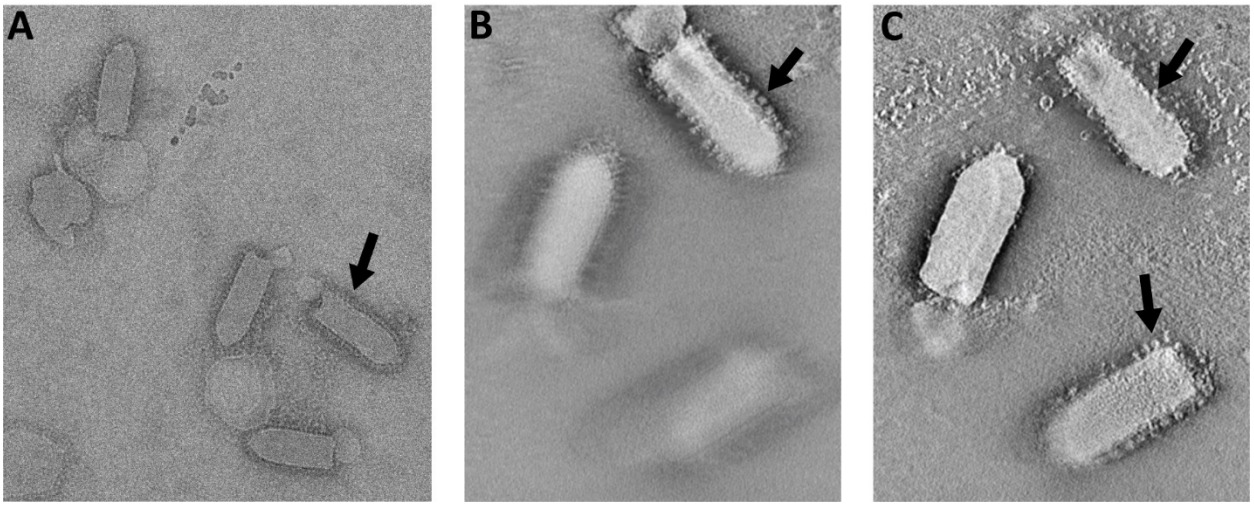

Figure 2.2 Analysis of VSV-Env-ΔG BG505 VLPs by ns-EM and ns-ET. VSV-Env-ΔG BG505 VLPs imaged by ns-EM (A) were found to be heterogenous and were often broken or without any membrane. Intact particles were densely coated with surface proteins (A black arrow). In negative stain tomographic Z-plane slices (B and C) of VSV-Env-ΔG BG505 VLPs side views of Env trimers can be clearly identified (B and C black arrows). Top views of Env were difficult to obtain on viral particles but could be clearly seen in free trimers. All images were taken by Dr. Long Gui and Dr. James Williams.

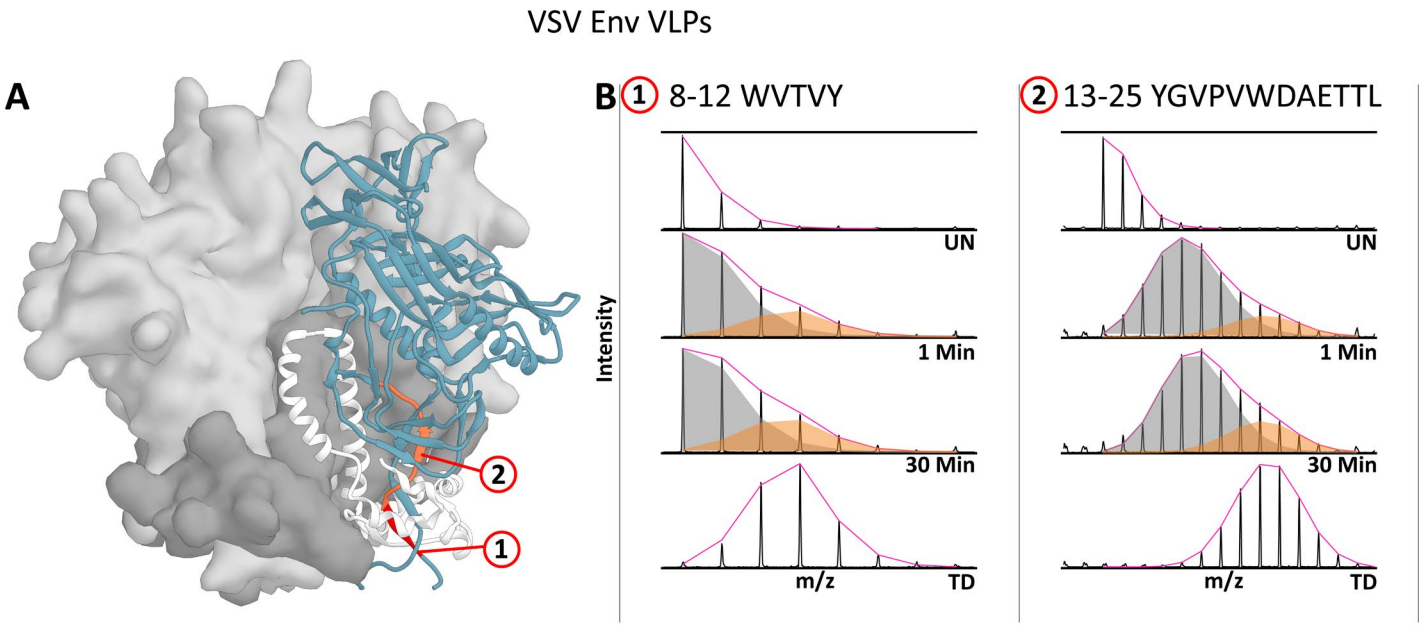

Figure 2.3 N-terminal gp120 Peptides Report on Env Quaternary Organization. Bimodal deconvolution of gp120 N-terminal peptides (B and C) indicates between 20-30% of total Env are non-native. Disruption of Env quaternary structure exposes the gp120-gp41 interface to solvent resulting in rapid deuterium exchange (B and C Orange Fit). In native Env trimers these regions are highly protected and resistant to deuterium exchange even at late time points (B and C Grey Fit). Conformational heterogeneity resulting from non-native Env can be readily distinguished from EX1 kinetics arising from conformational sampling as the ratio of each population does not change over time, as seen in these gp120 peptides. (A) Peptides mapped onto Env structure: Peptide 1 (Red) and Peptide 2 (Coral) (PDB 5fuu).

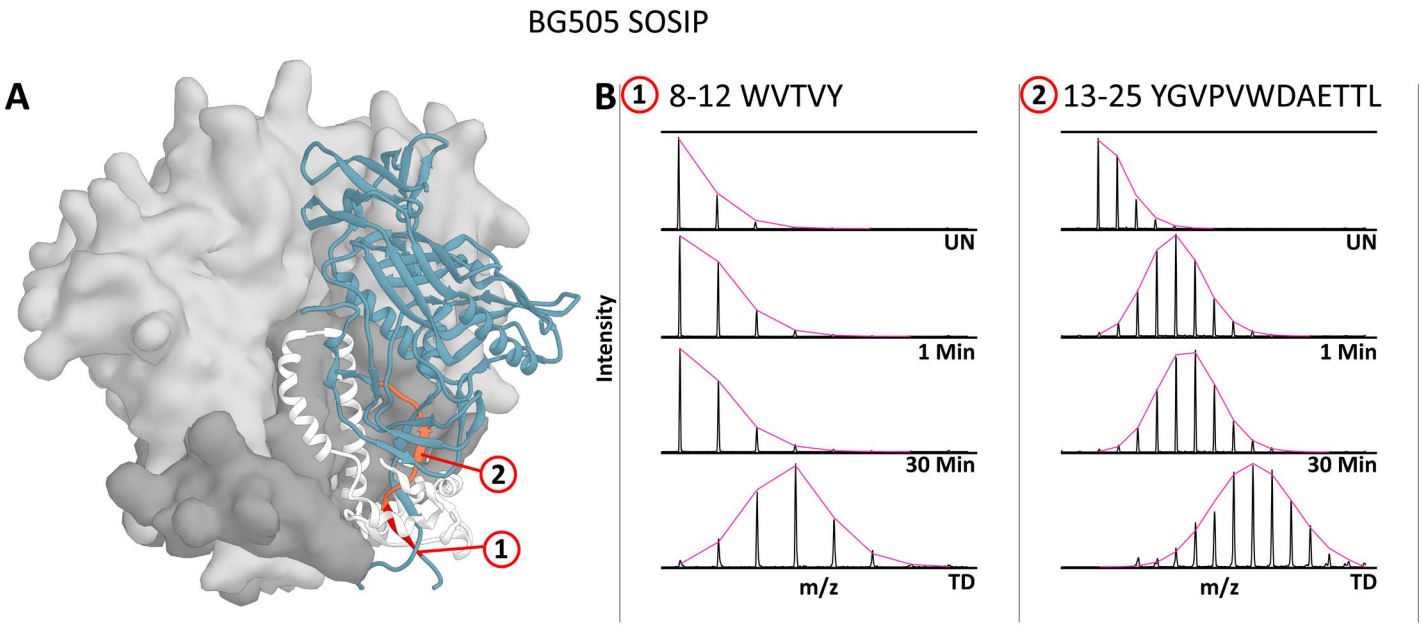

Figure 2.4 N-terminal gp120 Peptides in BG505 SOSIP Trimers are Protected and Unimodal. In homogenous trimeric Env gp-120 N-terminal peptides are protected from exchange and unimodal (B and C). (A) Peptides mapped onto Env structure: Peptide 1 (Red) and Peptide 2 (Coral) (PDB 5fuu).

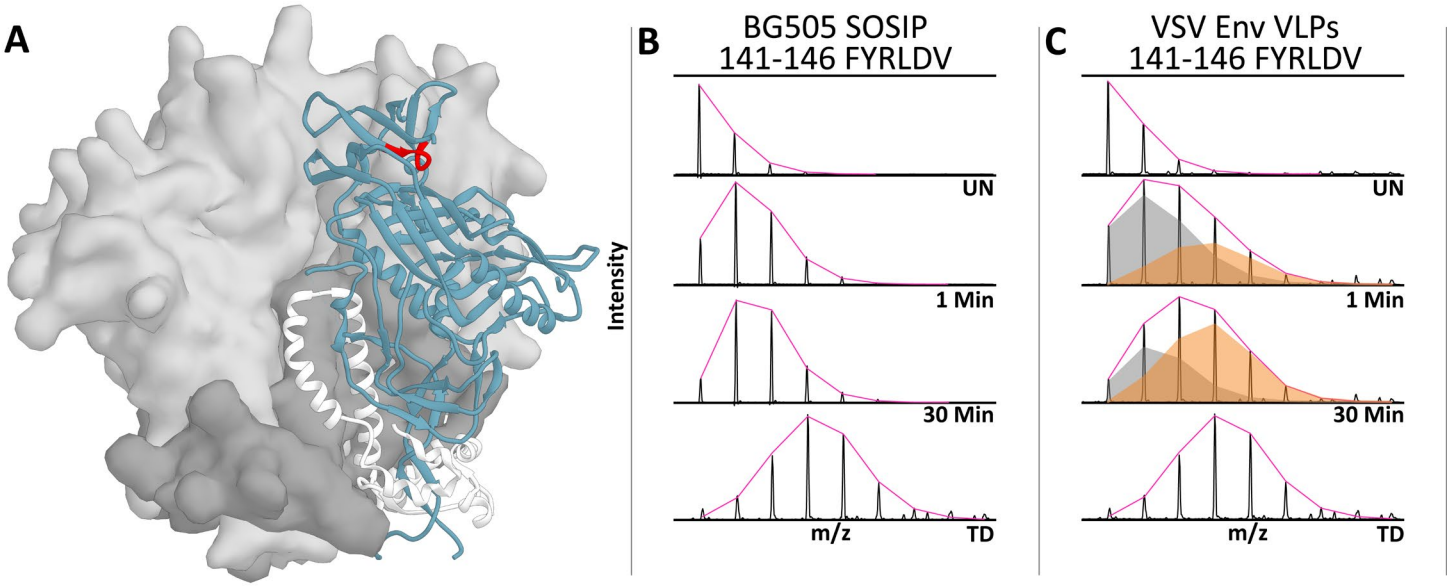

Figure 2.5 gp120 V2 Peptide Reports on Env Conformational Dynamics. In BG505 SOSIPs the gp120 V2 peptide (B) indicates Env is in the closed conformation and does not sample the open state. This same V2 peptide in VSV-Env-ΔG BG505 VLPs (C) is bimodal and displays EX1 kinetics. In conformationally dynamic Env variants similar EX1 kinetics profiles are observed, however the high degree of non-native Env present here likely contributes to the observed dynamics. (A) Peptide mapped onto Env structure in red (PDB 5fuu).

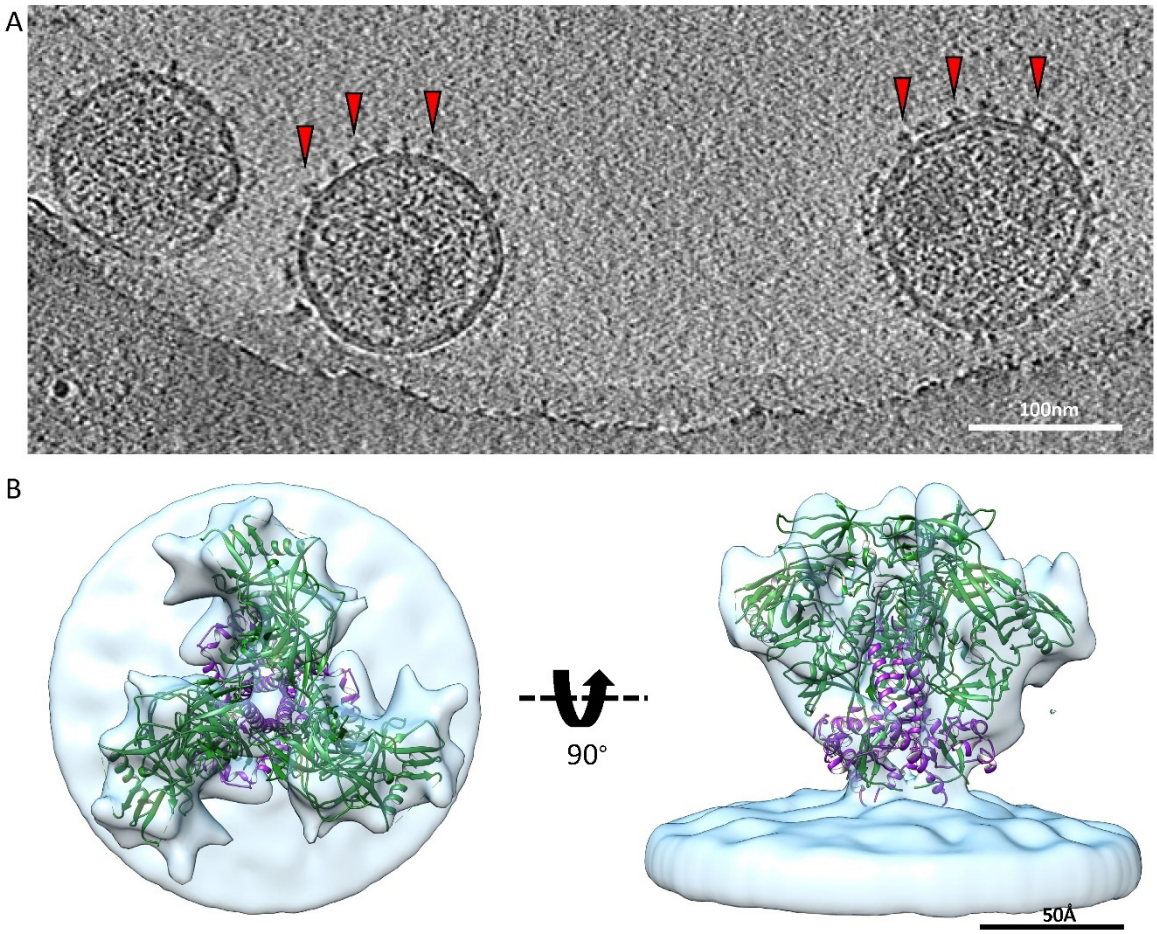

Figure 2.6 Cryo-ET and Sub-Tomogram Averaged Model of Comb-mut Env on hVLPs. (A) Representative cryo-EM micrograph of V4 hVLPs with Comb-mut Env trimers decorating the surface (Red Arrows). (B) Sub-tomogram averaged structure of Comb-mut Env trimers on the surface of V4 hVLPs at 12 Å resolution with atomic resolution model docked in (PDB 6mu6). Figure kindly provided by Dr. Vidya Mangala Prasad.

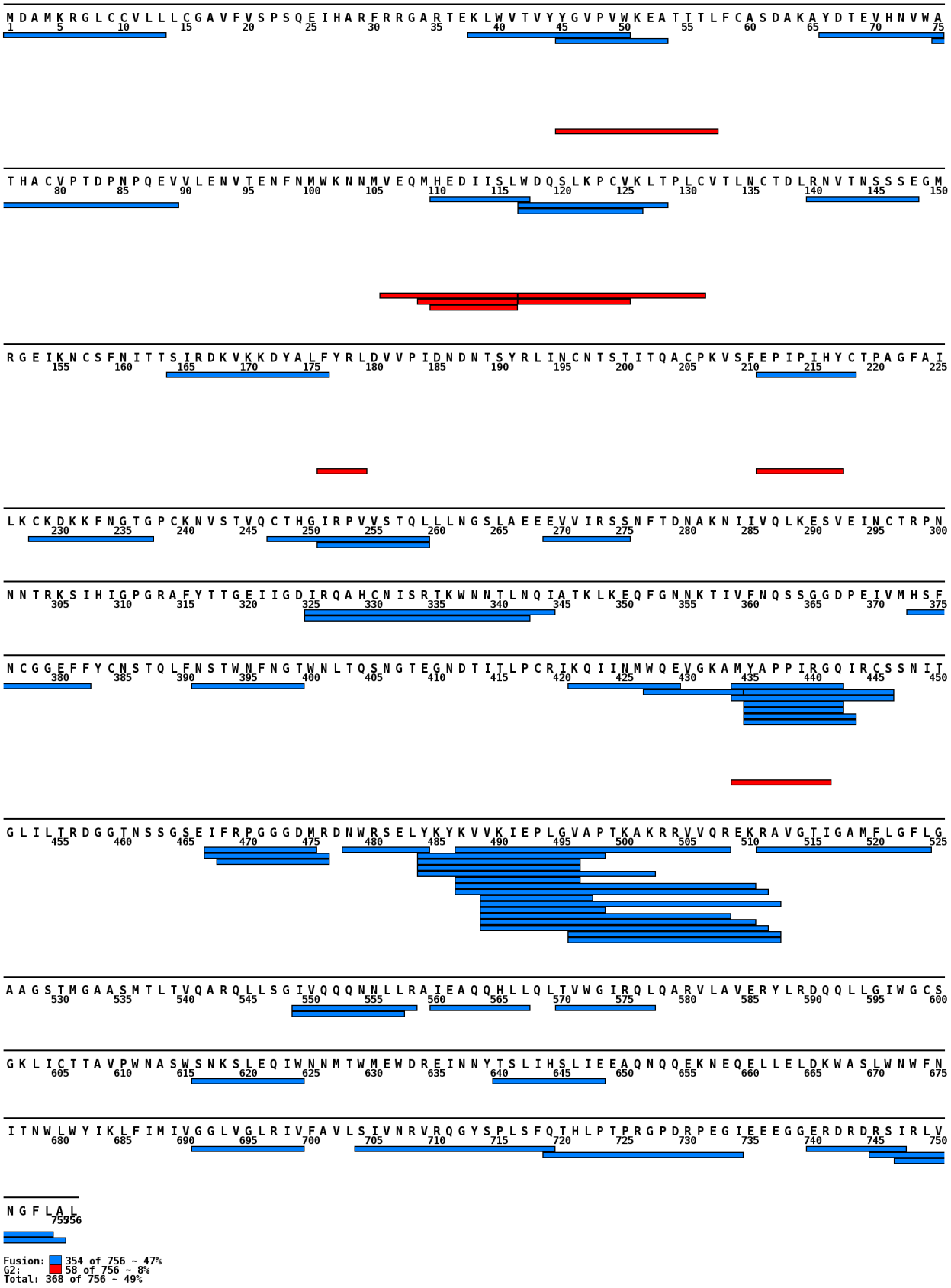

Fusion: 354 of 756 ~ 47%
G2: 58 of 756 ~ 8%
Total: 368 of 756 ~ 49%

Figure 2.7 Coverage Map of Comb-mut Env V4 hVLPs. Comparison of peptide coverage obtained using a Thermo Fisher Fusion Orbitrap with nano flow LC (Blue) and Waters Synapt G2-Si under HDX-MS conditions (Red). The majority of glycopeptides identified by the Fusion are not included as they could not be confirmed manually in the HDX-MS data. Coverage map generated using MSTools [81].

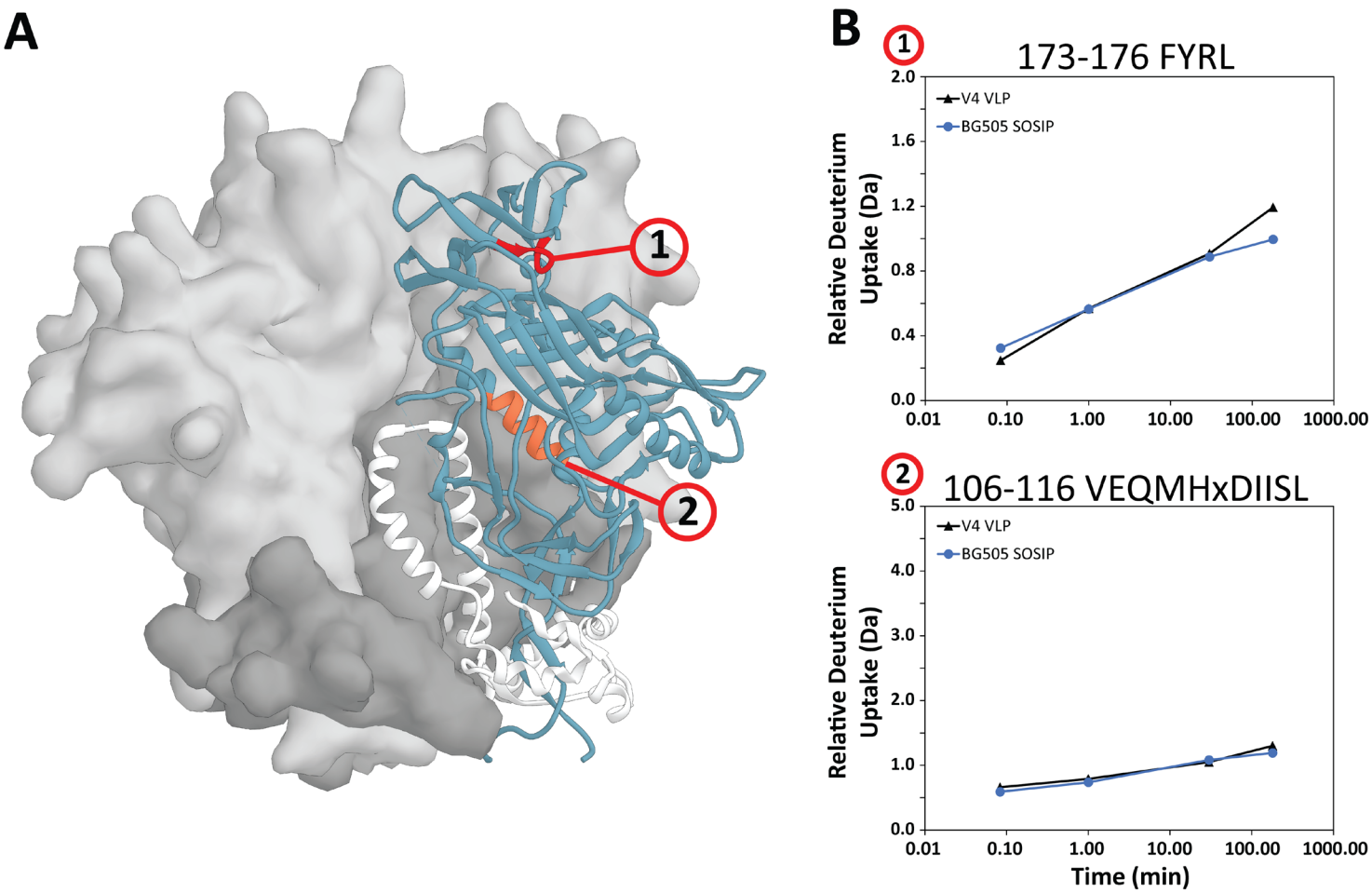

Figure 2.8 HDX-MS of V4 hVLPs and BG505 SOSIP. Comparison of the V2 loop (Peptide 1) and gp120 inner domain (Peptide 2) peptides by HDX-MS reveal similar dynamics. The V2 loop is a common indicator for conformational dynamics in Env trimers and appears unimodal in both trimers here suggesting Comb-mut Env trimers on v4 hVLPs exists in the closed conformation similar to BG505 SOSIPs. The gp120 inner domain peptide reports on quaternary organization and dynamics and appears protected and unimodal in both Comb-mut Env and BG505 SOSIP trimers. (A) Peptides mapped onto Env structure: Peptide 1 (Red) and Peptide 2 (Coral) (PDB 5fuu).

References

1. Benhaim, M., K.K. Lee, and M. Guttman, *Tracking Higher Order Protein Structure by Hydrogen-Deuterium Exchange Mass Spectrometry.* Protein and peptide letters, 2019. **26**(1): p. 16-26.
2. Englander, W.S., *Hydrogen exchange and mass spectrometry: A historical perspective.* Journal of The American Society for Mass Spectrometry, 2006. **17**(11): p. 1481-1489.
3. Bu, Z. and D. Callaway, *Chapter 5 Proteins MOVE! Protein dynamics and long-range allostery in cell signaling.* Advances in Protein Chemistry and Structural Biology, 2011. **83**: p. 163-221.
4. Percy, A.J., et al., *Probing protein interactions with hydrogen/deuterium exchange and mass spectrometry—A review.* Analytica Chimica Acta, 2012. **721**: p. 7-21.
5. Bai, Y., et al., *Primary structure effects on peptide group hydrogen exchange.* Proteins: Structure, Function, and Bioinformatics, 1993. **17**(1): p. 75-86.
6. Weis, D.D., *Hydrogen Exchange Mass Spectrometry of Proteins: Fundamentals, Methods, and Applications.* wiley, 2016: p. 295-321.
7. Zhang, Z. and D.L. Smith, *Determination of amide hydrogen exchange by mass spectrometry: A new tool for protein structure elucidation.* Protein Science, 1993. **2**(4): p. 522-531.
8. Deng, Y., Z. Zhang, and D.L. Smith, *Comparison of continuous and pulsed labeling amide hydrogen exchange/mass spectrometry for studies of protein dynamics.* Journal of the American Society for Mass Spectrometry, 1999. **10**(8): p. 675-684.
9. Marcsisin, S.R. and J.R. Engen, *Hydrogen exchange mass spectrometry: what is it and what can it tell us?* Analytical and bioanalytical chemistry, 2010. **397**(3): p. 967-972.
10. Hamuro, Y. and S.J. Coales, *Optimization of Feasibility Stage for Hydrogen/Deuterium Exchange Mass Spectrometry.* Journal of The American Society for Mass Spectrometry, 2018. **29**(3): p. 623-629.
11. Chalmers, M.J., et al., *Differential hydrogen/deuterium exchange mass spectrometry analysis of protein–ligand interactions.* Expert Review of Proteomics, 2014. **8**(1): p. 43-59.
12. Chamberlain, A.K., T.M. Handel, and S. Marqusee, *Detection of rare partially folded molecules in equilibrium with the native conformation of RNaseH.* Nature structural biology, 1996. **3**(9): p. 782-787.
13. Ferraro, D.M., N.D. Lazo, and A.D. Robertson, *EX1 hydrogen exchange and protein folding.* Biochemistry, 2004. **43**(3): p. 587-594.
14. Hodge, E.A., M.A. Benhaim, and K.K. Lee, *Bridging protein structure, dynamics, and function using hydrogen/deuterium-exchange mass spectrometry.* Protein Sci, 2019.
15. Weis, D.D., et al., *Identification and characterization of EX1 kinetics in H/D exchange mass spectrometry by peak width analysis.* Journal of The American Society for Mass Spectrometry, 2006. **17**(11): p. 1498-1509.
16. Smith, D.L., Y. Deng, and Z. Zhang, *Probing the Non-covalent Structure of Proteins by Amide Hydrogen Exchange and Mass Spectrometry.* Journal of Mass Spectrometry, 1997. **32**(2): p. 135-146.
17. Sivaraman, T. and A.D. Robertson, *Kinetics of conformational fluctuations by EX1 hydrogen exchange in native proteins.* Methods in molecular biology (Clifton, N.J.), 2001. **168**: p. 193-214.
18. Malhotra, P. and J.B. Udgaonkar, *Tuning Cooperativity on the Free Energy Landscape of Protein Folding.* Biochemistry, 2015. **54**(22): p. 3431-3441.
19. Hudgens, J.W., R. Huang, and E. D□Ambro, *Method validation and standards in hydrogen/deuterium exchange mass spectrometry.* Hydrogendeuterium exchange mass spectrometry: Fundamentals, techniques and applications, 2016: p. 40-50.

20. Wu, Y., S. Kaveti, and J.R. Engen, *Extensive deuterium back-exchange in certain immobilized pepsin columns used for H/D exchange mass spectrometry.* Analytical chemistry, 2006. **78**(5): p. 1719-1723.
21. Benhaim, M., K.K. Lee, and M. Guttman, *Tracking Higher Order Protein Structure by Hydrogen-Deuterium Exchange Mass Spectrometry.* Protein Pept Lett, 2019. **26**(1): p. 16-26.
22. Benhaim, M., et al., *Structural monitoring of a transient intermediate in the hemagglutinin fusion machinery on influenza virions.* Sci Adv, 2020.
23. Davenport, T.M., et al., *Isolate-specific differences in the conformational dynamics and antigenicity of HIV-1 gp120.* J Virol, 2013. **87**(19): p. 10855-73.
24. Guttman, M., et al., *Antibody potency relates to the ability to recognize the closed, pre-fusion form of HIV Env.* Nat Commun, 2015. **6**: p. 6144.
25. Guttman, M., et al., *CD4-induced activation in a soluble HIV-1 Env trimer.* Structure, 2014. **22**(7): p. 974-84.
26. Lee, J.H., G. Ozorowski, and A.B. Ward, *Cryo-EM structure of a native, fully glycosylated, cleaved HIV-1 envelope trimer.* Science, 2016. **351**(6277): p. 1043-8.
27. Liang, Y., et al., *Probing the Impact of Local Structural Dynamics of Conformational Epitopes on Antibody Recognition.* Biochemistry, 2016. **55**(15): p. 2197-213.
28. Liu, Y., et al., *Conformational States of a Soluble, Uncleaved HIV-1 Envelope Trimer.* J Virol, 2017. **91**(10).
29. Lu, M., et al., *Associating HIV-1 envelope glycoprotein structures with states on the virus observed by smFRET.* Nature, 2019. **568**(7752): p. 415-419.
30. Munro, J.B., et al., *Conformational dynamics of single HIV-1 envelope trimers on the surface of native virions.* Science, 2014. **346**(6210): p. 759-63.
31. Ozorowski, G., et al., *Open and closed structures reveal allostery and pliability in the HIV-1 envelope spike.* Nature, 2017. **547**(7663): p. 360-363.
32. Stadtmueller, B.M., et al., *DEER Spectroscopy Measurements Reveal Multiple Conformations of HIV-1 SOSIP Envelopes that Show Similarities with Envelopes on Native Virions.* Immunity, 2018. **49**(2): p. 235-246 e4.
33. Torrents de la Pena, A., et al., *Similarities and differences between native HIV-1 envelope glycoprotein trimers and stabilized soluble trimer mimetics.* PLoS Pathog, 2019. **15**(7): p. e1007920.
34. Wang, H., et al., *Partially Open HIV-1 Envelope Structures Exhibit Conformational Changes Relevant for Coreceptor Binding and Fusion.* Cell Host Microbe, 2018. **24**(4): p. 579-592 e4.
35. Wang, H., et al., *Cryo-EM structure of a CD4-bound open HIV-1 envelope trimer reveals structural rearrangements of the gp120 V1V2 loop.* Proc Natl Acad Sci U S A, 2016. **113**(46): p. E7151-E7158.
36. Ward, A.B. and I.A. Wilson, *Insights into the trimeric HIV-1 envelope glycoprotein structure.* Trends Biochem Sci, 2015. **40**(2): p. 101-7.
37. Zhu, P., et al., *Distribution and three-dimensional structure of AIDS virus envelope spikes.* Nature, 2006. **441**(7095): p. 847-52.
38. Alsahafi, N., et al., *SOSIP Changes Affect Human Immunodeficiency Virus Type 1 Envelope Glycoprotein Conformation and CD4 Engagement.* J Virol, 2018. **92**(19).
39. Torrents de la Pena, A., et al., *Improving the Immunogenicity of Native-like HIV-1 Envelope Trimers by Hyperstabilization.* Cell Rep, 2017. **20**(8): p. 1805-1817.
40. Klasse, P.J., et al., *Influences on trimerization and aggregation of soluble, cleaved HIV-1 SOSIP envelope glycoprotein.* J Virol, 2013. **87**(17): p. 9873-85.

41. Sanders, R.W., et al., *A next-generation cleaved, soluble HIV-1 Env trimer, BG505 SOSIP.664 gp140, expresses multiple epitopes for broadly neutralizing but not non-neutralizing antibodies.* PLoS Pathog, 2013. **9**(9): p. e1003618.
42. Binley, J.M., et al., *A recombinant human immunodeficiency virus type 1 envelope glycoprotein complex stabilized by an intermolecular disulfide bond between the gp120 and gp41 subunits is an antigenic mimic of the trimeric virion-associated structure.* J Virol, 2000. **74**(2): p. 627-43.
43. Calder, L.J., et al., *Structural organization of a filamentous influenza A virus.* Proc Natl Acad Sci U S A, 2010. **107**(23): p. 10685-90.
44. Harris, A., et al., *Influenza virus pleiomorphy characterized by cryoelectron tomography.* Proc Natl Acad Sci U S A, 2006. **103**(50): p. 19123-7.
45. Whitt, M.A., *Generation of VSV pseudotypes using recombinant DeltaG-VSV for studies on virus entry, identification of entry inhibitors, and immune responses to vaccines.* J Virol Methods, 2010. **169**(2): p. 365-74.
46. Rey, F.A. and S.M. Lok, *Common Features of Enveloped Viruses and Implications for Immunogen Design for Next-Generation Vaccines.* Cell, 2018. **172**(6): p. 1319-1334.
47. Stano, A., et al., *Dense Array of Spikes on HIV-1 Virion Particles.* J Virol, 2017. **91**(14).
48. Ma, X., et al., *HIV-1 Env trimer opens through an asymmetric intermediate in which individual protomers adopt distinct conformations.* Elife, 2018. **7**.
49. Bresk, C.A., et al., *Induction of Tier 1 HIV Neutralizing Antibodies by Envelope Trimers Incorporated into a Replication Competent Vesicular Stomatitis Virus Vector.* Viruses, 2019. **11**(2).
50. Racine, T., G.P. Kobinger, and E.J. Arts, *Development of an HIV vaccine using a vesicular stomatitis virus vector expressing designer HIV-1 envelope glycoproteins to enhance humoral responses.* AIDS Res Ther, 2017. **14**(1): p. 55.
51. Rabinovich, S., et al., *A novel, live-attenuated vesicular stomatitis virus vector displaying conformationally intact, functional HIV-1 envelope trimers that elicits potent cellular and humoral responses in mice.* PLoS One, 2014. **9**(9): p. e106597.
52. Ou, L., et al., *Preclinical Development of a Fusion Peptide Conjugate as an HIV Vaccine Immunogen.* Scientific Reports, 2020. **10**(1).
53. Sliepen, K., et al., *Structure and immunogenicity of a stabilized HIV-1 envelope trimer based on a group-M consensus sequence.* Nat Commun, 2019. **10**(1): p. 2355.
54. Xu, K., et al., *Epitope-based vaccine design yields fusion peptide-directed antibodies that neutralize diverse strains of HIV-1.* Nature Medicine, 2018. **24**(6): p. 857-867.
55. Burton, D.R., *Advancing an HIV vaccine; advancing vaccinology.* Nature Reviews Immunology, 2018. **19**(2): p. 77-78.
56. Murin, C.D., I.A. Wilson, and A.B. Ward, *Antibody responses to viral infections: a structural perspective across three different enveloped viruses.* Nat Microbiol, 2019. **4**(5): p. 734-747.
57. Pancera, M., A. Changela, and P.D. Kwong, *How HIV-1 entry mechanism and broadly neutralizing antibodies guide structure-based vaccine design.* Curr Opin HIV AIDS, 2017. **12**(3): p. 229-240.
58. Arslan, I., J.R. Tong, and P.A. Midgley, *Reducing the missing wedge: High-resolution dual axis tomography of inorganic materials.* Ultramicroscopy, 2006. **106**(11-12): p. 994-1000.
59. Verkerke, H.P., et al., *Epitope-Independent Purification of Native-Like Envelope Trimers from Diverse HIV-1 Isolates.* J Virol, 2016. **90**(20): p. 9471-82.
60. De Carlo, S. and J.R. Harris, *Negative staining and cryo-negative staining of macromolecules and viruses for TEM.* Micron, 2011. **42**(2): p. 117-31.
61. Guttman, M. and K.K. Lee, *Isotope Labeling of Biomolecules: Structural Analysis of Viruses by HDX-MS.* Methods Enzymol, 2016. **566**: p. 405-26.

62. Fang, J., et al., *False EX1 signatures caused by sample carryover during HX MS analyses.* Int J Mass Spectrom, 2011. **302**(1-3): p. 19-25.
63. Guttman, M., et al., *Analysis of overlapped and noisy hydrogen/deuterium exchange mass spectra.* J Am Soc Mass Spectrom, 2013. **24**(12): p. 1906-12.
64. Leaman, D.P. and M.B. Zwick, *Increased functional stability and homogeneity of viral envelope spikes through directed evolution.* PLoS Pathog, 2013. **9**(2): p. e1003184.
65. Caston, J.R., *Conventional electron microscopy, cryo-electron microscopy and cryo-electron tomography of viruses.* Subcell Biochem, 2013. **68**: p. 79-115.
66. Briggs, J.A., *Structural biology in situ--the potential of subtomogram averaging.* Curr Opin Struct Biol, 2013. **23**(2): p. 261-7.
67. Stass, R., S.L. Ilca, and J.T. Huiskonen, *Beyond structures of highly symmetric purified viral capsids by cryo-EM.* Curr Opin Struct Biol, 2018. **52**: p. 25-31.
68. Chang, J., et al., *Reconstructing virus structures from nanometer to near-atomic resolutions with cryo-electron microscopy and tomography.* Adv Exp Med Biol, 2012. **726**: p. 49-90.
69. Fontana, J., et al., *Structural changes in Influenza virus at low pH characterized by cryo-electron tomography.* J Virol, 2012. **86**(6): p. 2919-29.
70. Garcia, N.K. and K.K. Lee, *Dynamic Viral Glycoprotein Machines: Approaches for Probing Transient States That Drive Membrane Fusion.* Viruses, 2016. **8**(1).
71. Li, M., M. Guttman, and W.M. Atkins, *Conformational dynamics of P-glycoprotein in lipid nanodiscs and detergent micelles reveal complex motions on a wide time scale.* Journal of Biological Chemistry, 2018. **293**(17): p. 6297-6307.
72. Harrison, R.A. and J.R. Engen, *Conformational insight into multi-protein signaling assemblies by hydrogen-deuterium exchange mass spectrometry.* Curr Opin Struct Biol, 2016. **41**: p. 187-193.
73. Duc, N.M., et al., *Effective application of bicelles for conformational analysis of G protein-coupled receptors by hydrogen/deuterium exchange mass spectrometry.* J Am Soc Mass Spectrom, 2015. **26**(5): p. 808-17.
74. Rey, M., et al., *Effective removal of nonionic detergents in protein mass spectrometry, hydrogen/deuterium exchange, and proteomics.* Anal Chem, 2010. **82**(12): p. 5107-16.
75. Lim, X.X., et al., *Conformational changes in intact dengue virus reveal serotype-specific expansion.* Nat Commun, 2017. **8**: p. 14339.
76. Yang, Z., et al., *Asymmetric opening of HIV-1 Env bound to CD4 and a coreceptor-mimicking antibody.* Nat Struct Mol Biol, 2019. **26**(12): p. 1167-1175.
77. Zhang, Z., A. Zhang, and G. Xiao, *Improved protein hydrogen/deuterium exchange mass spectrometry platform with fully automated data processing.* Anal Chem, 2012. **84**(11): p. 4942-9.
78. Guttman, M., et al., *Tuning a High Transmission Ion Guide to Prevent Gas-Phase Proton Exchange During H/D Exchange MS Analysis.* J Am Soc Mass Spectrom, 2016. **27**(4): p. 662-8.
79. Marty, M.T., et al., *Bayesian deconvolution of mass and ion mobility spectra: from binary interactions to polydisperse ensembles.* Anal Chem, 2015. **87**(8): p. 4370-6.
80. Weis, D.D., J.R. Engen, and I.J. Kass, *Semi-automated data processing of hydrogen exchange mass spectra using HX-Express.* J Am Soc Mass Spectrom, 2006. **17**(12): p. 1700-3.
81. Kavan, D. and P. Man, *MSTools—Web based application for visualization and presentation of HXMS data.* International Journal of Mass Spectrometry, 2011. **302**(1-3): p. 53-58.

Chapter 3. Structural Monitoring of a Transient Intermediate in the Hemagglutinin Fusion Machinery on Influenza Virions

The work presented in this chapter has been reproduced in its entirety in accordance with copyright permissions from:
Benhaim MA, Mangala Prasad V, Garcia NK, Guttman M, Lee KK. Structural monitoring of a transient intermediate in the hemagglutinin fusion machinery on influenza virions. *Sci Adv*. 2020;6(18):eaaz8822. Published 2020 Apr 29. doi:10.1126/sciadv.aaz8822

3.1 Introduction

Infection by influenza virus, and all enveloped viruses, requires fusion of the viral and host membranes. Enveloped viruses have evolved specialized fusion protein machinery that undergoes major conformational changes in order to drive the membrane fusion reaction to completion [1]. For influenza virus, the hemagglutinin (HA) fusion glycoprotein trimer mediates entry into host cells by its receptor binding and membrane fusion activities [1, 2]. HA is first synthesized as an inactive, single chain polypeptide precursor (HA0) that trimerizes and is activated by proteolytic processing [3, 4]. The resulting functional HA assembly is a homotrimer of disulfide-linked heterodimers consisting of a receptor binding subunit, HA1, and a membrane fusion subunit, HA2 (Figure 3.1 A). The N-terminus of HA2 includes the hydrophobic fusion peptide, which in the pre-fusion configuration is sequestered away from membranes in a pocket that extends into the central core of the HA trimer, while the C-terminus of the HA2 subunit is anchored in the virus membrane by a transmembrane domain. Influenza virus infection begins when HA binds sialic acid on cell surface receptors through a low affinity, high avidity interaction that initiates internalization through receptor-mediated endocytosis. The HA fusion machinery is activated by low pH in the maturing endosome, triggering a cascade of large-scale conformational changes where the refolding of HA to the post-fusion state is coupled to overcoming the

activation energy barrier that separates pre- and post-fused membranes (Figure 3.1B)[5-8]. The formation of the resulting fusion pore enables transfer of the viral genome into the cell [9].

Crystal structures of the pre-fusion HA ectodomain and an HA2 fragment of the post-fusion state illustrate the beginning and end points of the membrane fusion process (Figure 3.1B). Comparison of the pre- and post-fusion structures reveals the dramatic structural reorganizations that occur in the fusion domain during membrane fusion, but they do not reveal the structural calisthenics occurring between these end points [5-8]. The mechanism by which a fusion protein activates and mediates membrane fusion remains poorly understood. The conventional mechanistic model for HA fusion activation and membrane fusion describes pre-fusion HA as a spring-loaded fusion machine [7, 10, 11]. The salient features of the spring-loaded model are that the pre-fusion structure represents a high-energy metastable configuration of the HA trimer, which upon exposure to acidic pH rapidly and irreversibly refolds to a new post-fusion hairpin conformation. In this post-fusion state, the fusion peptide is relocated ~100 Å towards the target membrane at the apex of an extended coiled coil, where it is colocalized with the relocated transmembrane anchor. Key interactions that maintain HA in the metastable state have been suggested to center on a “clamp” in HA1 that constrains a key HA2 loop and a “hook” formed by the fusion peptide that lashes two helices together in the pre-fusion trimer [7]. The “Uncaging” model for HA activation suggests that HA1 acts as a cage or clamp containing the spring-loaded HA2 fusion machine; whereupon low pH releases the HA1 cage, allowing rapid and irreversible activation of the spring-loaded HA2 fusion machine [7, 11-13]. By contrast, a “fusion peptide release” model suggests that low pH first stimulates release of the HA2 N-terminal fusion peptide “hook” from its sequestered pocket in the core of HA2 prior to HA1 head domains dissociating from each other [12, 14-21]. In this model, the exposed fusion peptide, tethered to a highly dynamic HA2 subunit, is deployed and available to engage with the target membrane prior to the large-scale refolding of HA2 into the post-fusion, hairpin conformation [22].

To date, only piecemeal biophysical evidence has been available to support one or the other of these models of HA activation. No detailed structural analysis describing how different regions of HA1 and HA2 respond to acidic pH once the fusion machinery is triggered has been available. HDX-MS analysis of the soluble Bromelain-released HA (BHA) ectodomain at pH values approaching the threshold of activation revealed dynamic structural changes throughout HA, suggesting that it is primed for fusion peptide release [12]. Increased dynamics were observed at and around the fusion peptide whereas the HA1 receptor binding domain interface became more protected prior to acid activation [12]. Crystal structures of BHA under similar conditions revealed a structural relaxation in the HA2 B-loop at the HA1-HA2 interface suggesting exposure to mildly acidic conditions loosens structural constraints around the fusion domain and primes HA for activation [23]. By cryo-electron tomography Fontana et al. observed morphological changes in HA at low resolution on the virus surface, which led them to infer that fusion peptide release precedes dissociation of the HA1 globular head and that both of these events are reversible [15]. Recently, single-molecule FRET imaging enabled the first observation of a dynamic HA intermediate state during membrane fusion [14]. To gain a mechanistic understanding of fusion protein activation and function, detailed resolution of structural reorganization throughout the fusion protein and sequencing of conformational events traversed by HA is needed.

Here we present a pulse labeling Hydrogen/Deuterium-exchange Mass Spectrometry (HDX-MS) method that enables us to capture snapshots of the HA fusion machinery undergoing its complex conformational changes during activation (Figure 3.1 C). Pulse labeling HDX-MS is sensitive to changes in a protein's local secondary structure, conformation, and global quaternary organization. It enables one to monitor accessibility of amide hydrogens across the protein backbone [24]. Changes in the local structure of a given peptide segment can be distinguished from the initial state by measuring changes in the extent of amide exchange. In our pulse deuteration approach using intact infectious virions, we trigger HA's activation then introduce a rapid deuteration pulse that labels the HA ensemble

immediately prior to quenching the exchange reaction. Using binomial fitting and bimodal deconvolution, we were able to resolve and characterize distinct, often co-existing structural states, measure their relative abundances, and monitor the transition between conformational states [24, 25]. The transitions observed throughout the protein reveal the nature and sequence of the local conformational changes that occur throughout HA during fusion activation on intact infectious virions. Our data provide new insight into the conformational changes traversed by HA and allow us to probe the on-pathway dynamic intermediate ensemble conformation populated by HA during its activation. This intermediate ensemble exhibits a structurally flexible fusion domain prior to formation of the post-fusion state. These changes coincide with reorganization of the N-terminal HA2 fusion domain, the HA1-HA2 interface, as well as between HA1 subunits; but are clearly distinguished from the transition to a stable post-fusion conformation. These data thus provide a detailed structural, dynamic, and temporal characterization of a type-I fusion protein's activation in the native context on the surface of infectious virions.

3.2 Results

HA Presented on Whole Influenza Virions Remains in the Pre-fusion Conformation at Neutral pH

The pre-fusion conformation of HA on intact X-31 H3N2 influenza virions was first examined under neutral pH (pre-activation) conditions (pH 7.5, 37°C) from our pulse deuteration series to assess the presence of any conformational heterogeneity amongst HA spikes prior to activation. Our experimental conditions allowed peptides spanning the majority of HA1 to be monitored including the F' domain, hinge region, receptor binding domain, and trimeric interface (Figure 3.1 A)(HA numbering follows Wilson, 1981)[5]. We obtained greater than 93% sequence coverage for HA1 on whole virus resulting from more than 30 unique peptides (Figure S3.1). The coverage throughout HA2 on whole virus was more limited (34% sequence coverage); however, we were able to monitor key peptides involved in

the structural reorganization from the pre- to post-fusion state including the N-terminal fusion peptide, A-helix, B-loop, and portions of the C-helix. Only those peptides present and trackable throughout the acidified reactions were included in analysis. Under neutral pH conditions, we observed unimodal HDX profiles for all identifiable HA peptides indicating that the HA on the virus surface was in a conformationally uniform state and that no detectable sub-populations (e.g. misfolded or unprocessed HA) were present. These pulse deuteration results are consistent with our previously reported continuous deuteration labeling HDX-MS studies of pre-fusion H3 Aichi/68 HA on intact virions [12]. Western blot analysis of HA on whole virions and BHA further confirms that no unprocessed HA is present (Figure S3.2). Correct HA processing was also confirmed by mass spectrometry as no peptides unique to HA0 were found. Analysis of the internal exchange standard PPPI showed consistent labeling times for each reaction (Figure S3.3).

The HA2 Fusion Machinery Becomes Highly Solvent Accessible and Dynamic in a Transient Intermediate State Following Low-pH Activation

In order to monitor the conformational pathway traversed by HA, we next activated influenza virions from the same stock as above by lowering the pH to 5.1. At time points ranging from 0 seconds to 360 minutes, the virus was exposed to a 5 second pulse of D_2O that transiently raised the pH* to 8.0 (Figure 3.1 C). Following this brief pulse deuteration, samples were rapidly quenched, digested, and frozen for subsequent analysis by mass spectrometry. Pulse labeling HDX-MS enables us to monitor structural changes as they occur during protein motion; however, we are limited to monitoring only those structural changes significant enough to produce a new, unique, and resolvable HDX state. It remains possible that early structural changes that are too subtle to alter amide protection, occur too quickly, are reversed by the brief elevated pH pulse (pH* = 8.0), or go undetected by this approach. For example, it has been suggested that some early acid-induced structural changes in HA are reversible

upon reneutralization; as recently demonstrated for fusion peptide release by Das et al. using SM-FRET [14, 15, 18]. We note however that under our pulse conditions (pH* = 8.0, 22°C), exposed amide hydrogens will exchange fully in 20 ms (5 half-lives for an exposed amide), meaning that in our approach, HA becomes labeled very rapidly in most cases prior to large-scale refolding events that can take place [26]. Our data show that the rate of exchange for exposed amides across HA is faster than the rate of refolding as the alternative scenarios would produce markedly different data. If the rate of refolding was greater than the rate of exchange, this would result in all peptides being in the refolded state before they become labeled [24, 27]. Similarly, if the rate of refolding was comparable to the rate of exchange, we would be able to detect a population with an intermediate level of deuteration as the peptide transitions to a more protected state and is simultaneously labeled [24, 27]. As we do not observe either of these phenomena in our data, we can assume with confidence that refolding does not have an appreciable effect on the structural transitions observed here. Hence we can monitor all but the fastest refolding events in HA.

Notably, in contrast to the ubiquitous unimodal spectra for all HA peptide segments that were observed prior to low pH-induced activation, once exposed to pH 5.1 conditions, bimodal spectra began to emerge for numerous peptides throughout the HA trimer. From the pool of peptides showing clear bimodal isotopic distributions throughout the acidification process, it was possible to apply bimodal deconvolution to quantify the contribution and relative abundance of each conformational state throughout the full time course [25]. Examples of peptide-specific population shift data are shown in Figures 3.2, 3.3, 3.5 and Supplemental Figures 3.5-7. The shift in the relative populations across the complete time course revealed two distinct, sequential conformational transitions occurring throughout HA1 and at least three conformational transitions in HA2. Below, we describe these changes sequentially as they appeared following acidification.

The first observable conformational changes following exposure of the virus to acidic conditions (pH 5.10) occurred rapidly after acidification. Analysis of key peptides in the HA2 fusion machinery subunit reveal the concurrent formation of a dynamic fusion peptide-released intermediate ensemble state that emerges as soon as 5 seconds after activation of HA on intact influenza virions (Figure 3.2 B). As seen in the mass spectra, a transient intermediate conformation reported by the A-helix is highly solvent accessible (red envelopes and traces in Figure 3.2 B Peptide 1) compared to the initial and final protected states. This exposed conformational population shows a clear increase and subsequent decrease in abundance over the course of HA's conformational change, peaking at 1 minute after acid-activation. As the exposed population is almost maximally deuterated, we infer that this segment is highly exposed and likely sampling relatively disordered conformations (Figure 3.2 B Peptide 1). At 1 minute, a highly protected conformational state, consistent with the proposed extended helical intermediate and known post-fusion helical bundle conformation that incorporate the A-helix into the bundle, also begins to appear, and grows monotonically over the course of the transition as the exposed, dynamic intermediate decreases in abundance (Figure 3.2 B Peptide 1).

Analysis of the A-helix required constraining the binomial fits for the exposed intermediate and post-fusion states (Figure 3.2 B Peptide 1- red and blue envelopes respectively), which were well defined and consistent throughout the time course. This revealed an additional transition where the pre-fusion neutral pH conformation shifts to a slightly more exposed state, emerging by 3.5 minutes post-acidification (Figure 3.2 B Peptide 1– see peak shift of orange envelopes relative to vertical green line). Described in more detail below, this likely reflects the structural relaxation of adjacent stem regions of HA1 that pack against the A-helix in pre-fusion HA. It is likely that this population is present at earlier time points, however we are unable to clearly resolve its presence as the pre-fusion, neutral pH like state is more abundant and we are limited to monitoring at most three states concurrently. If we tried instead to constrain the m/z centroid position of the initial pre-fusion, neutral pH conformation (grey

envelopes) throughout the time course, the deconvolution of the multimodal spectra produced a poorer overall fit for each state but did not change the overall kinetics of the population changes (Delta Chi Square = -4.3e7). This indicates that at some of the intermediate time points, there are at least four coexisting states sampled by the A-helix (Figure 3.2 B and C); the ordered and solvent protected helical pre-fusion neutral pH state (grey), a slightly more dynamic, exposed but structured fusion peptide released intermediate state (orange), a highly exposed unstructured fusion peptide released intermediate state (red), and the highly protected helical post-fusion state (blue). Together these two resolvable intermediate populations contribute to the dynamic intermediate ensemble state. It is highly likely that there exist a number of interconverting structures that contribute to these mass envelopes that we are unable to resolve. While quantitative analysis of the HA2 N-terminal fusion peptide itself was confounded by a significant loss of signal intensity over time, perhaps due to the significant hydrophobicity of this segment, peak width analysis revealed an increase in conformational heterogeneity and formation of an exposed state at 5 seconds post-acidification (Figure S3.4). The peptide's behavior was thus consistent with the formation of a fusion peptide released state as early as 5 seconds post-acidification.

We observed parallel behavior starting as early as 5 seconds post-acidification for formation of an intermediate state involving the HA2 B-loop (Figure 3.2 B Peptide 2). In this intermediate state, the B-loop is more exposed than the structured loop observed in the pre-fusion state. The pre-fusion B-loop is defined by ordered but exposed amides, whereas the intermediate state appears fully exposed (red envelopes and traces in Figure 3.2 B Peptide 2). As with the A-helix, the B-loop subsequently reports on the transition from the dynamic intermediate state to the ordered post-fusion helical bundle conformation [8]. Interestingly, we note that a small sub-population of highly protected B-helices (approximately 15%) began to appear starting at 5 seconds post-acidification. This minor fraction's behavior may be consistent with previous sm-FRET observations that some fraction of HA can transition

relatively directly to the post-fusion state without traversing the dynamic intermediate state that is observed [14]. Analysis of the B-loop required constraining the pre-fusion neutral pH state (grey) throughout the time course. It is possible that the broad multimodal distribution represented by the grey and red fits at intermediate time points contains more than two distinct structural states that are indistinguishable by HDX and cannot be resolved in our data.

Taken together, these data indicate that the dynamic intermediate ensemble state reported by the A-helix (HA2 39-52) and B-loop (HA2 53-69) segments appears rapidly, starting within 5 seconds after acidification. In this state, the critical fusion-peptide associated sub-domains of HA2 are structurally dynamic and distinct from the known pre- and post-fusion structures of HA2 (Figure 3.2 C). The intermediate ensemble becomes populated well-before formation of the post-fusion state, where these segments form highly protected, stable helices as part of the trimeric core helical bundle (Figure 3.2)[6, 8].

Concomitant with HA2 Activation, the HA1-HA2 and HA1-HA1 Interfaces Reorganize

The HA1 subunit has been described as serving as a clamp around the HA2 fusion machinery subunit, however as our data above reveal, key portions of HA2 become highly dynamic and exposed soon after activation conditions were introduced [7]. To understand how and on what timescale HA1 reorganizes, we examined peptide segments that first form contacts with HA2 in the pre-fusion state; these peptides include the HA1 F' domain which packs against the HA2 N-terminal fusion peptide proximal subdomain and A-helix (Figure 3.1 A). We then examined peptides involved in maintaining the trimerized HA1-HA1 head, which must eventually dissociate in order for HA2 to be able to adopt the post-fusion state.

In the same early time frame in which HA2 began to populate a dynamic intermediate state, we observe that within the HA1 subunit the fusion peptide proximal HA1 F' region (HA1 26-33 and 281-316)

began to transition to a more exposed state (Figure 3.3 A Peptides 1 and 2), and by 3.5 minutes post-acidification almost completely populated this new state (Figures S2.5 A and B, S2.6 A1 and A6, and Table S3.1). The increase in exposure is likely due to a loss of quaternary packing interactions between the F' domain and the N-terminal segment of HA2 that are present in pre-fusion HA. Indeed, in regions of HA1 that span the HA1-HA2 interface including the HA1 hinge and F' region (Figure 3.3 and Figures S3.5-6 and Table S3.1), peptides show a distinct initial increase in deuterium uptake and broadening of the mass envelope from 5 seconds up until 1 minute, where the mass envelope then narrows to a single more uniform population that reflects a conformational state with an intermediate level of exposure between the pre-fusion and fully exposed states (Figure 3.3 and Figure S3.5 A). These changes occur in concert with the early changes in HA2 in the fusion peptide-associated regions. Together these peptide segments cover nearly the entire HA1-HA2 quaternary interface and show the large-scale structural reorganization that occurs following fusion peptide release and the coinciding reorganization of the N-terminal HA2 fusion domain (Figures 3.2 and 3.3 and Figures S3.5 and S3.6).

In contrast, HA1 peptides that do not form quaternary contacts with HA2 or adjacent HA1 protomers do not show any increased deuterium uptake until 3.5 minutes post-acidification (Figures S3.5 D and S3.6). These peptides in a sense serve as internal standards that demonstrate that the changes we monitor in other sites are significant and a result of structural reorganization.

In the first, early conformational transition, we also observed reorganization of the protomeric interface between HA1 receptor binding domains that reveals a shift to a more exposed state (HA1 212-228) (Figure 3.3 A Peptide 3 and Figure S3.5 A). This shift takes place on the same timescale as fusion peptide release, occurring between 15 seconds and 1 minute. Reorganization of the HA1-HA1 interface thus coincides with changes that take place proximal to the fusion peptide subdomain in the HA stem region and across the HA1-HA2 interface.

A Large-scale Unfolding in HA1 is Seen at Late Timepoints Following Fusion Activation

In a late stage of structural reorganization within HA1, beginning at 3.5 minutes, we observed widespread unfolding of the HA1 globular head, marked by transitions to nearly fully deuterated states (Figure 3.3 A Peptide 2, and Figures S3.5 C-D and S3.6, and Table S3.1). Peptides spanning the C-terminal segment of the F' domain (HA1 281-316), which form quaternary contacts with the HA2 fusion domain, show an initial conformational change and increase in exposure associated with fusion peptide release (Figure 3.3 A Peptide 2 - grey to orange coloring) and subsequently a distinct shift to a maximally exposed state (Figure 3.3 A Peptide 2 – orange to purple coloring). HA1 peptides that do not form quaternary contacts with HA2 or adjacent HA1 protomers do not show any increased deuterium uptake until 3.5 minutes post-acidification where they transition to fully exposed state (Figures S3.5 D and S3.6). Certain HA1 peptides with strong secondary and tertiary structural elements, including portions of the 110-helix and peptides spanning the receptor binding site, do not fully unfold but nevertheless transition to a significantly more exposed state in concert with the unfolding event (HA1 109-119, 175-194, 234-243) (Figures S3.5 A and S3.6). These data suggest that that receptor binding HA1 head domain transitions to a molten globule-like state following extended exposure to endosomal pH conditions.

pH Dependence of HA Fusion Activation

To determine whether HA fusion activation follows a similar trajectory across a range of fusogenic pH conditions, we performed pulse labeling HDX-MS on HA acidified to pH 5.25 at 37°C exactly as described above. The overall nature and sequencing of events mirror the trajectory described at pH 5.10, however the onset of each conformational event was delayed (Figure 3.4). Both fusion subunit triggering and reorganization of the HA1 receptor binding domain (RBD) at the protomeric interface commenced between 15 seconds and 1 minute post-acidification and reached completion by 12 minutes (Figure 3.4 A-D orange coloring). The same form of dynamic intermediate state was

observed in both the A-helix and B-loop with HDX profiles; however, this state was slightly less abundant at each time point when compared to activation at pH 5.10 (Figures 3.2, 3.4, and S3.7). The late stage unfolding of the globular head was also observed with delayed onset and kinetics compared to the pH 5.10 condition (Figure 3.4 C-F purple coloring). These data suggest that shifting the pH of activation can accelerate or slow the onset and rate of change for each conformational event but does not change the structural or dynamic nature or sequence of those conformational changes.

Soluble BHA Ectodomain Follows a Two-state Transition from Pre- to Post-fusion Forms

The soluble bromelain-released HA ectodomain (BHA) or analogous trimeric ectodomain constructs are commonly used for the study of HA's structure and function in place of the native full-length membrane anchored HA. However, it has been suggested that significant differences exist between how BHA and full-length HA behave during fusion activation [28]. Detailed structural and functional analysis of HA activation for intact trimeric spikes versus soluble ectodomain has not been possible with previously employed methods. Here, we sought to use the pulse deuteration approach to characterize the conformational changes in BHA and to compare them with the behavior of intact HA on virions under identical fusion activation conditions at pH 5.25.

Pulse labeling HDX-MS demonstrated that fusion peptide release and head opening events occurred similarly between BHA and HA on virions both in terms of the structural changes that occur and the kinetics of each conformational change (Figures 3.5 A Peptides 1 and 2 and S3.8). Most notably, in contrast to what we observed for HA on intact virions, in soluble BHA the A-helix and B-loop display unambiguous two state behavior transitioning directly from the pre- to post-fusion states with no observable intermediate (Figure 3.5 A Peptides 3-4). Both the A-helix and B-loop transition to their respective protected post-fusion states in concert with the fusion peptide release and head opening events (Figures 3.5 A Peptides 3-4 and S3.8). The two coexisting populations in the A-helix data could

not be resolved by bimodal deconvolution as the centers of each population were too close. Analysis using a single binomial fit reveals an increase and subsequent decrease in the peak width over time. Most notably there are no changes in the mass envelope that indicate the presence of a more exposed state and the increase in width can be unambiguously attributed to the formation of the post-fusion state (Figure 3.5 A Peptide 3). BHA thus transitions from pre- to post-fusion conformations in a two-state fashion, whereas intact HA on whole virus particles exhibits the presence of a transient but highly populated, dynamic conformational intermediate state.

Visualization of Low pH-Induced HA Structures by Cryo-Electron Tomography

In order to obtain complementary structural characterization of HA under neutral pH and fusion activating conditions, cryo-electron tomography of virions treated identically to the HDX-MS experiments was performed. At neutral pH, the HA trimeric spikes are closely spaced and well-ordered on the virion surface, consistent with previous cryo-ET imaging of influenza virus (Figures S3.9 A-C and S3.10 A) [29, 30]. By contrast, influenza virion tomograms of the virus treated for 1 minute at pH 5.10 show a high degree of variability in the HA structure and organization (Figures S3.9 D-E and S3.10 B). Here, individual HA appear to populate a heterogenous mixture of low pH-induced configurations, and have, in part, lost the characteristic hour-glass shaped structure of neutral pH HA (Figure S3.9 A-B, D-E). Even HA spikes on the same virion have variability in their relative conformations. In these acid-triggered states, HA still maintains its overall trimeric nature as seen from closely clustered HA1 subunits in the top view cross-sections (Figure S3.9 F). From these types of images, the low pH HA appears to be sampling different conformation states, some of which show variable degrees of separation of the HA1 interface or overall thinning of HA (Figure S3.9), but there does not seems to be a singular dominant, discrete intermediate state.

3.3 Discussion

Viral fusion proteins face a unique challenge in terms of staying poised in a pre-fusion state on the surface of the virus until exposed to the necessary triggering events that activate them into a fusogenic state. Once activated they undergo structural calisthenics that are required to draw two opposing membranes together and induce them to fuse. This refolding process is believed to be critical to driving fusion forward. To date however, we have had a very limited view into how these dynamic fusion machines carry out their function, and the structural, dynamic nature of the activated, fusogenic forms of the machinery.

HA populates an ensemble of highly dynamic intermediate states during activation

The influenza HA membrane fusion protein has been viewed as a "spring-loaded" fusion machine that rapidly and irreversibly activates upon exposure to the low pH environment of the maturing endosome [7, 10, 11, 13, 31]. This view was proposed based upon experiments that indicated that the pre-fusion state is in a trapped, high-energy metastable state, which can be induced to transition irreversibly to the stable, low-energy post-fusion state through a range of destabilizing conditions [7, 8, 11]. Recent methodological advances have made it possible to study the transitions between viral fusion protein conformational states under native activation conditions [14, 15]. For example, a single-molecule FRET (sm-FRET) imaging of HA displayed on engineered lentivirus particles enabled the conformational change of the HA2 subunit to be monitored during fusion activation and membrane fusion [14]. Using HA with two fluorescent dyes that served as FRET pairs engineered into HA2, Das et al. show that acid-activated HA reversibly samples multiple intermediate conformations and proceeds through a highly flexible obligate intermediate state during activation and membrane fusion. While sm-FRET provides a powerful means to probe the relative disposition of the two fluorescent probe

molecules that were covalently attached to HA, the behavior of most of the trimer remained uncharacterized. No information has been available for sites such as HA1 receptor binding subunits, which have been hypothesized to cage the HA2 fusion subunit modulating its activation, as well as regions of HA2 that undergo dramatic refolding that is key to the fusion protein's ability to deploy the fusion peptide and draw the two membranes together.

Using HDX-MS and cryo-ET, we investigated the nature and sequence of the conformational changes that occur throughout the HA fusion machinery during activation on intact virions and in soluble isolated ectodomain forms. Our data reveal concurrent reorganization of the HA1-HA2 interface centered around the HA2 N-terminal fusion peptide proximal subdomain (segments spanning from the B-loop to the fusion peptide) and HA1 protomeric interface (Figures 3.2-3.4, and S3.4-3.7). The loss of quaternary contacts between HA1 and HA2 is also seen across the HA1-HA2 interface at the HA2 apex. As a result of the loosening of these key restraints, the HA2 A-helix and B-loop are freed to populate at least two structurally distinct states in the intermediate ensemble (Figure 3.2). We propose that in this intermediate state, the A-helix and B-loop flexibility enables the released fusion peptide to sample space and grapple to a membrane (Figure 3.6). Furthermore, the A-helix clearly adopts two structurally distinct states in the intermediate ensemble corresponding to a slightly more dynamic, exposed but structured fusion peptide released intermediate state and a highly exposed, unstructured fusion peptide released intermediate state (Figures 3.2 and 3.6). The structural dynamics monitored by HDX-MS are consistent with recent molecular dynamics simulations that indicated that during the transition to the post-fusion helical bundle, the A-helix and B-loop are capable of sampling diverse secondary structure elements and can become relatively unstructured [20]. The sm-FRET studies by Das et al., likewise support the conclusion that a high degree of conformational dynamics contribute to the observed intermediate states.

Previously reported low-resolution cryo-ET images of HA on influenza particles at acidic pH, were interpreted in terms of two intermediate conformations including one in which the HA stalk was narrowed due to HA2 fusion peptide release and another in which the globular head domains had dissociated from each other [15]. It was not clear in the past study whether the sub-tomogram averaged states reflected the behavior of the majority of HA or a subset that was most amenable to classification in those tomograms. Based upon cryo-ET data we gathered under conditions identical to those used for HDX-MS, we found the HA spikes to be considerably more conformationally heterogeneous than one might expect for two discrete states (Figures S3.9-3.10). We conclude that this is most likely due to the flexibility and dynamic nature of key regions in the fusion machinery in HA1 as well as HA2. Subtomogram averaging attempts to isolate different states and obtain a high-resolution model were not successful; the small fraction of particles that could be averaged gave a low-resolution map similar to that of Fontana et.al, but this could not be improved, again most likely due to heterogeneity amongst the HA spikes.

The apparent structural heterogeneity of HA supports the idea that HA populates a structurally dynamic intermediate ensemble during activation rather than one or two discrete, well-ordered intermediate conformations. The highly dynamic nature throughout the HA spike has important implications for efforts that might seek to target the fusion-active intermediate with inhibitors [32], and may suggest that stabilization of the pre-fusion state or pre-fusion structural elements [33] is a more fruitful aim than attempting to target intermediate conformations directly.

Our findings as well as the recent sm-FRET results reframe our understanding of how HA functions as a biomechanical fusion machine. The data does not necessarily challenge the characterization of pre-fusion HA as existing in a metastable state or the fact that in the course of mediating fusion it transitions irreversibly to the true low-energy post-fusion state. Rather, the data now clearly indicate that the activated forms of these fusion machines transiently populate highly dynamic ensembles of

intermediate states that can persist for minutes prior to completing the final irreversible transition to the stable post-fusion state.

Presentation on virions yields a more sequential HA activation pathway than in isolated HA ectodomain

These data provide the most detailed portrait to date of a viral fusion protein intermediate state and the traversal of fusion active HA trimers across the conformational pathway. While the conventional view of type I fusion proteins as "mouse traps" would suggest that once triggered or destabilized, the fusion protein will snap to the post-fusion conformation, our data demonstrate that HA on the surface of intact virions populates an ensemble of highly dynamic intermediate states that are not observed for soluble ectodomain. Indeed, a dramatic, two-state change is exhibited by soluble BHA ectodomain, which does not appear to populate any discernable intermediate states, instead transitioning directly between the pre-fusion and highly stable post-fusion state (Figures 3.4 and 3.5). This comparison of full length HA and BHA during fusion activation underscores the significant differences in functional behavior that result from excising the HA ectodomain from the context of the intact virion [28]. Stabilizing interactions present in full length HA in virus particles appear to encourage the formation of the transiently populated intermediate state [9, 12, 14, 15, 34, 35]. Additional interactions include those involving the viral membrane, HA transmembrane domain, HA cytoplasmic tail, and internal viral components such as the M1 matrix protein are absent with soluble BHA [34, 36]. We note that by cryo-ET, it is clear that the M1 matrix layer remains assembled and membrane-associated under the pH 5.1 conditions used in the HDX-MS pulse labeling experiments (Figure 39). Past studies have suggested an interaction between the HA cytoplasmic tail and the matrix layer [9, 34, 35, 37-40]. These data indicate that those interactions with an intact matrix layer could persist during activation. In addition, trimerization of the transmembrane domain or presentation on the membrane serve as brakes on the

HA2 C-terminal reorganization [34] These interactions borne by HA2 on the surface of influenza virions likely regulate that sub-domain's ability to reorganize, allowing the fusion peptides to be released and insert into a target membrane prior to complete refolding to the post-fusion state.

Additionally, studies have suggested that there exists a long-range connection between the HA1 RBD and the HA2 fusion peptide proximal subdomain. Mutations in and around the HA2 fusion peptide were found to significantly alter the dynamic behavior of the HA1 RBD and protomeric interface [41]. Recent studies have shown that "breathing" motions in the HA1 RBD and protomeric interface are linked to flexibility of the HA2 fusion peptide [42, 43]. Das et al. demonstrated that receptor binding dramatically increased dynamics in HA2 and promoted formation of a fusion peptide released state at neutral pH [14]. We previously demonstrated that while a neutralizing antibody that binds to the HA1 subunit stabilized the pre-fusion or pre-fusion-like configuration for the trimerized HA head, its binding did not prevent fusion peptides from being released such that they could disrupt liposomal membranes [33]. In some circumstances, it appears that the various structural elements of the HA spike respond to acidic pH in relatively independent rather than concerted fashion meaning HA does not function as one cooperative unit but rather each domain does appear to be linked in some manner. While the present data does not directly probe the allosteric linkage between spike apex and fusion peptide associated regions, the reorganizations observed throughout the HA2 fusion peptide proximal subdomain and the HA1 RBD indicate a concurrent if not necessarily concerted reorganization of distal regions.

Mechanistic differences between influenza subtypes

Our observations are based upon an H3N2 influenza virus strain. Different influenza virus strains vary widely in their acid stabilities and fusion kinetics, and may exhibit different mechanisms of fusion activation [44-47]. In the sm-FRET study, H5 HA was examined. In one notable difference, substantial sampling of conformational states reported by the fluorescent probes in HA2 was reported even under

neutral pH, pre-fusion conditions. The HDX-MS data for H3 HA examined here and in past continuous deuterium labeling experiments [12] did not show signatures of conformational sampling prior to triggering. We do not yet understand the structural basis for these functional variations. It is not clear how different HA's, with varying acid stabilities, would influence or alter the mechanism of fusion activation [44]. Our results show that, in the absence of a target membrane, the early conformational changes in HA that produce the fusion active intermediate ensemble occur rapidly upon acidification and that refolding to the post-fusion state is relatively slow. When a target membrane is present the rate of formation for the intermediate is unperturbed while the transition to the post-fusion state is rapidly accelerated, meaning formation of the fusion active intermediate is the rate limiting step for fusion [14]. It is possible that by modulating the acid stability of its HA a virus can control when, and how quickly fusion will occur during infection ensuring the virus does not prematurely and spontaneously inactivate before reaching the correct subcellular location. *In vitro* membrane fusion experiments, including our own, initiate fusion by rapid acidification to a single fusogenic pH [12, 14, 15, 17-19, 35, 44]. Evidence suggests that during infection, the modified endosomal acidification pathway proceeds through distinct pH stages with varying rates of acidification between them [37, 48]. This staged acidification pathway may have an effect on HA fusion activation or other viral components involved in the membrane fusion process, including acidification of the viral interior by the matrix M2 proton channel and reorganization of the matrix M1 layer [16, 35, 37, 48, 49]. It is also possible that this stepwise acidic priming might accelerate the formation of the fusion active intermediate ensemble by gradually increasing the dynamics across HA as the pH approaches the activation threshold.

Powerful, new complementary biophysical and structural techniques enable us to develop a more complete mechanistic model for protein-membrane fusion in an enveloped virus. Future experiments examining pathways of activation in other membrane fusion systems will enable us to test the universality of fusion protein activation and function. Indeed, the time-resolved, pulse deuteration

HDX-MS approach we employed opens the door to analysis of highly complex biological assemblies, enabling one to probe intact functional complexes, including whole virions. As the data with influenza virus demonstrates, investigating the complete functional system provides key insights into its behavior that are lost when components are examined in isolation. This approach thus provides a step towards realizing a long-standing goal of performing structural analysis of intact biological systems as they carry out their functions.

3.4 Materials and Methods

Influenza Virus and Bromelain Released HA Purification

Purified influenza virus A X-31 A/Aichi/68 (H3N2) was purchased from Charles River Laboratories and stored at -80°C prior to use. Virus was purified by centrifugation concentrated in HDX HBS buffer (150 mM NaCl, 10 mM HEPES pH 7.50, and 0.02% NaN_3). Whole virus HA concentration was determined by western blotting as previously described (Figure S3.2)[33]. The soluble Bromelain released HA ectodomain (BHA) was produced and purified from influenza virus as previously described and concentrated in HDX HBS pH 7.50 buffer [12].

Pulse Labeling HDX of Whole Influenza Virus

For each reaction, a stock of purified influenza virus containing 4.0 μg of HA in HDX HBS pH 7.50 buffer was rapidly diluted 1:1 with HDX HBS Acidification buffer (150 mM NaCl, 10 mM HEPES, 80 mM Citrate, and 0.02% NaN_3) to a final pH of either 5.10 or 5.25 at 37°C. Virus was acidified for 5 seconds, 15 seconds, 1 minute, 3.50 minutes, 12 minutes, 40 minutes, 2 hours, and 6 hours. Following acidification, each reaction was rapidly pulse labeled with deuterium for 5 seconds at room temperature (22°C) by dilution into Pulse Deuteration Buffer (25 mM Phosphate, 150 mM NaCl, 0.02% NaN_3, and 85% D_2O (Cambridge Isotope Laboratories)) to a final pH* 8.0. The pulse labeling reactions were then rapidly

quenched by dilution 1:1 with ice-cold quench buffer (200 mM TCEP [tris(2-carboxyethyl) phosphine] and 0.2% formic acid (FA)) with 30 μg/mL of porcine pepsin (Worthington Labs) to a final pH of 2.50 and digested on ice for 5 minutes. The labeled HA peptides were separated from intact virions by high speed centrifugation at 25,000 rcf and 0°C for 2 minutes. The supernatant was collected and immediately flash frozen in liquid nitrogen then stored at -80°C until analysis. Undeuterated samples were prepared identically to the deuterated samples with water in place of D_2O. A no acidification or "0 second" control was also prepared where the acidification buffer was included with the Pulse Deuteration Buffer and was otherwise treated identically to acidified reactions. All samples were prepared containing 0.25 μg/mL of each PPPI and PPPF tetrapeptides (AnaSpec) as internal exchange standards [50]. Pulse labeling reactions were performed in triplicate by manual pipetting with the assistance of a metronome to ensure consistent labeling times. Labeling consistency was verified by analyzing the PPPI and PPPF internal exchange standards (Figure S3.3). All HDX buffers were prepared with LC-MS grade Optima Water (Fischer Scientific). Totally deuterated (TD) samples were prepared by collecting purified peptide eluent following reverse phase LC separation of a pepsin digested undeuterated sample. Following evaporation of the LC elution buffer the peptides were resuspended in HDX HBS pH 7.50 Buffer, deuterated in Pulse Deuteration Buffer for 2 hours at 37°C, and quenched and frozen as described above.

Pulse Labeling HDX of BHA

Pulse labeling HDX of the soluble BHA ectodomain was performed identically to the whole influenza virus reactions at pH 5.25. Samples containing 2.5 μg of BHA each were acidified to pH 5.25 at 37°C and pulse labeled with deuterium at pH 8.0 and 22°C following the same time-course outlined above. The pulse labeled reactions were quenched by dilution 1:1 with ice-cold quench buffer (200 mM TCEP and 0.2% FA) and immediately flash frozen in liquid nitrogen and stored at -80°C until analysis. The

"0 second", TD, and undeuterated samples were prepared as stated above and all reactions contained the PPPI and PPPF tetrapeptides (AnaSpec) as internal exchange standards.

Reverse Phase Liquid Chromatography and Mass Spectrometry

Samples were thawed for 5 minutes on ice and manually injected into a Waters HDX Manager kept at 1°C. Whole virus HA samples were trapped on a Waters ACQUITY UPLC CSH C18 VanGuard 130Å, 1.7 μm, 2.1 mm by 5 mm trap column for 3 minutes with a flow of solvent A [2% acetonitrile, 0.1% FA, 0.025% trifluoroacetic acid (TFA)] at a rate of 150 μL/min. BHA samples were digested online with immobilized pepsin for 5 minutes and trapped as described previously [51]. Peptides were resolved over a Waters ACQUITY UPLC CSH C18 130Å, 1.7 μm, 1 x 100 mm column using a 10 minute linear gradient of 3% to 50% solvent B (Solvent B: 100% acetonitrile and 0.1% FA) and analyzed using a Waters Synapt G2-Si Q-TOF with ion mobility enabled. Source and desolvation temperatures were 70°C and 130°C respectively. The StepWave ion guide settings were tuned to prevent non-uniform gas phase proton exchange in the source [52]. A series of trap column wash steps were implemented between each injection to minimize carryover [53].

HDX-MS Data Analysis

Peptic HA peptides were identified previously [12]. For glycopeptides only the most abundant glycoforms were examined. Ion mobility and LC retention time filtered spectra were extracted from the raw MS files using CDCReader [54]. Spectra were analyzed using HXExpress V2 with binomial fitting and bimodal deconvolution [25, 55]. Fitting with more than one binomial distribution was only performed when a single binomial was not sufficient to encompass the mass envelope and the two populations could be separated with confidence. The relative areas of each population were plotted as a function of time in acidification buffer to track the kinetics of each structural transition. When necessary, the "0

second" neutral pH, or Pre-Fusion, control HDX population was used as a fitting constraint for bimodal deconvolution. In cases where a bimodal distribution is indicated by broadened isotopic distributions, but cannot be deconvoluted with confidence, peak width analysis was used to support the population analysis [56]. Peptides showing more than 10% chromatographic carryover were not used for bimodal deconvolution. Peptides whose signal intensity dropped significantly over the course of the acidification reaction, presumably due to the formation of the proteolytically resistant post fusion HA2 structure, were also excluded from bimodal analysis. HDX quality data can be found in Table S3.2.

Cryo-Electron Tomography

Purified influenza virus in HBS pH 7.50 buffer was rapidly diluted 1:1 with HBS acidification buffer (150 mM NaCl, 10 mM HEPES, 80 mM Citrate, and 0.02% NaN_3) to a final pH of 5.10 at 37°C and incubated for 1 minute. BSA gold beads (10nm) were then added to sample. Using a Vitrobot Mark IV (FEI Co.), 3µl of this sample was applied to C-flat 2/2 200mesh grid, blotted and plunge frozen in liquid ethane. Frozen grids were imaged using a 300kV Titan Krios with a Gatan K2 direct electron detector. Tilt series were collected from -48º to +48º with a 3º step size at a magnification of 53000X which corresponds to 2.58 Å/pixel. The total dose per tilt-series was ~64 electrons/ $Å^2$. Thirty tilt-series were collected and further processed.

Tilt-series image frames were corrected for electron beam-induced motion using motioncor2 [57]. These were then processed for tomogram generation using batch tomography in IMOD using standard procedures [58]. Briefly, the tilt-series images were aligned using the gold bead markers. The aligned images were then reconstructed to give a 3D volume using weighted back-projection. The final tomograms were rotated, binned and low pass-filtered for visualization using IMOD and ImageJ [59, 60].

Statistical Analysis

Whole virus HDX-MS experiments were performed in triplicate. The mean and standard deviations of these replicates were used to determine the significance of changes in a peptides deuteration level or population fractions when bimodal distributions were present. When bimodal distributions were present but could not be resolved into clear isotopic distributions the peak width and deuterium uptake values of the beginning and end points of the reaction were used to calculate the population shift.

3.5 Figures and Tables

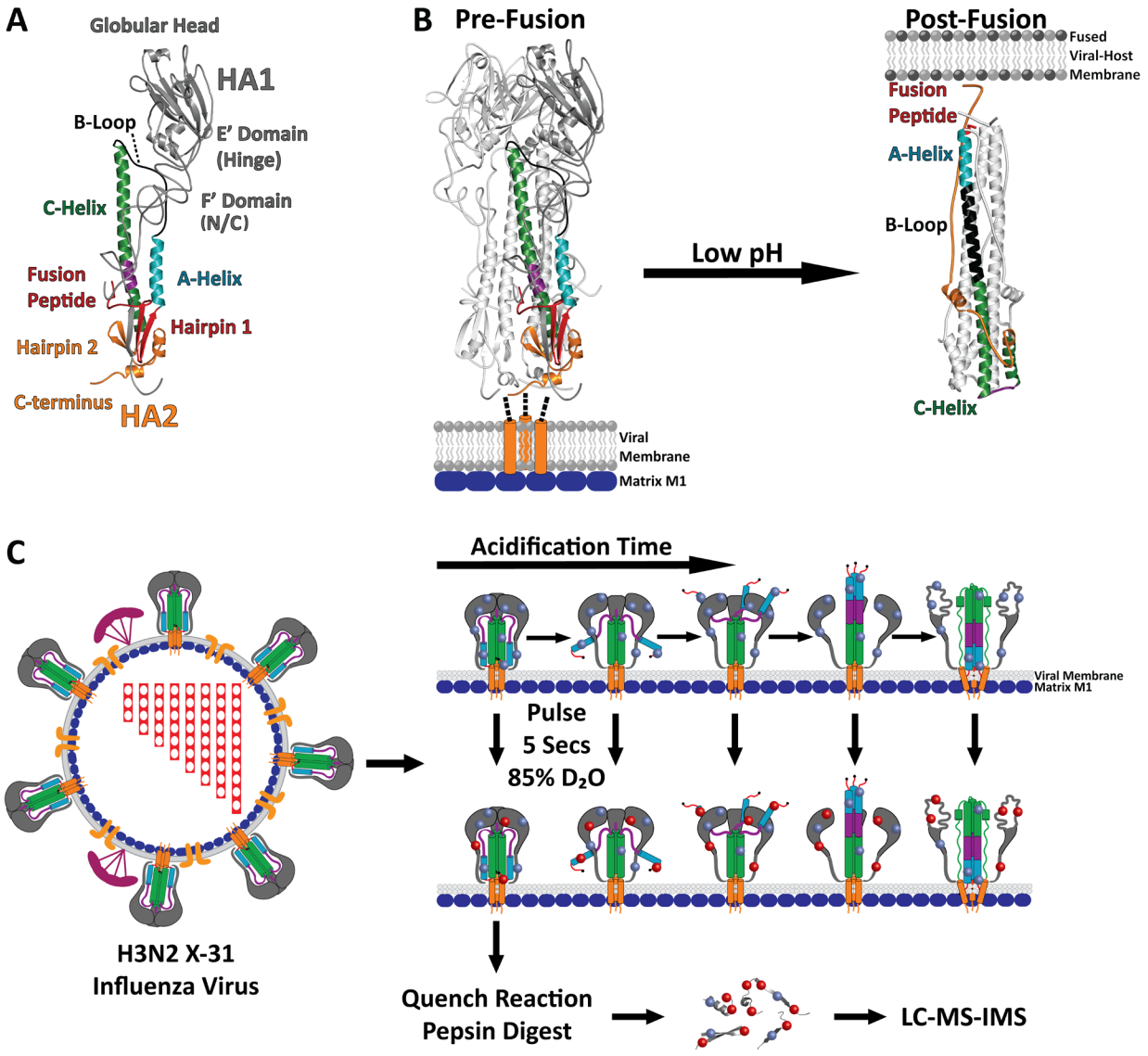

Figure 3.1. Monitoring HA's Structure and the Low pH Induced Reorganization by Pulse Labeling HDX-MS.

(A) Core HA structural features and regions colored and mapped onto a single HA heterodimer protomer (A)(HA numbering according to Wilson, 1981)(PDB: 2HMG)[5]. **(B)** Comparison of the pre- and post-fusion crystal structures for the HA ectodomain reveals the dramatic structural reorganization that occurs in HA2 following activation by low pH, currently the structure of HA1 in the post-fusion state is unknown (PDB: 2HMG and 1QU1). **(C)** Schematic depicting pulse labeling HDX-MS of whole infectious H3N2 X-31 virions. Cartoon model of HA fusion activation during pulse labeling with amide hydrogens (blue spheres) exchanging with deuterium (red spheres).

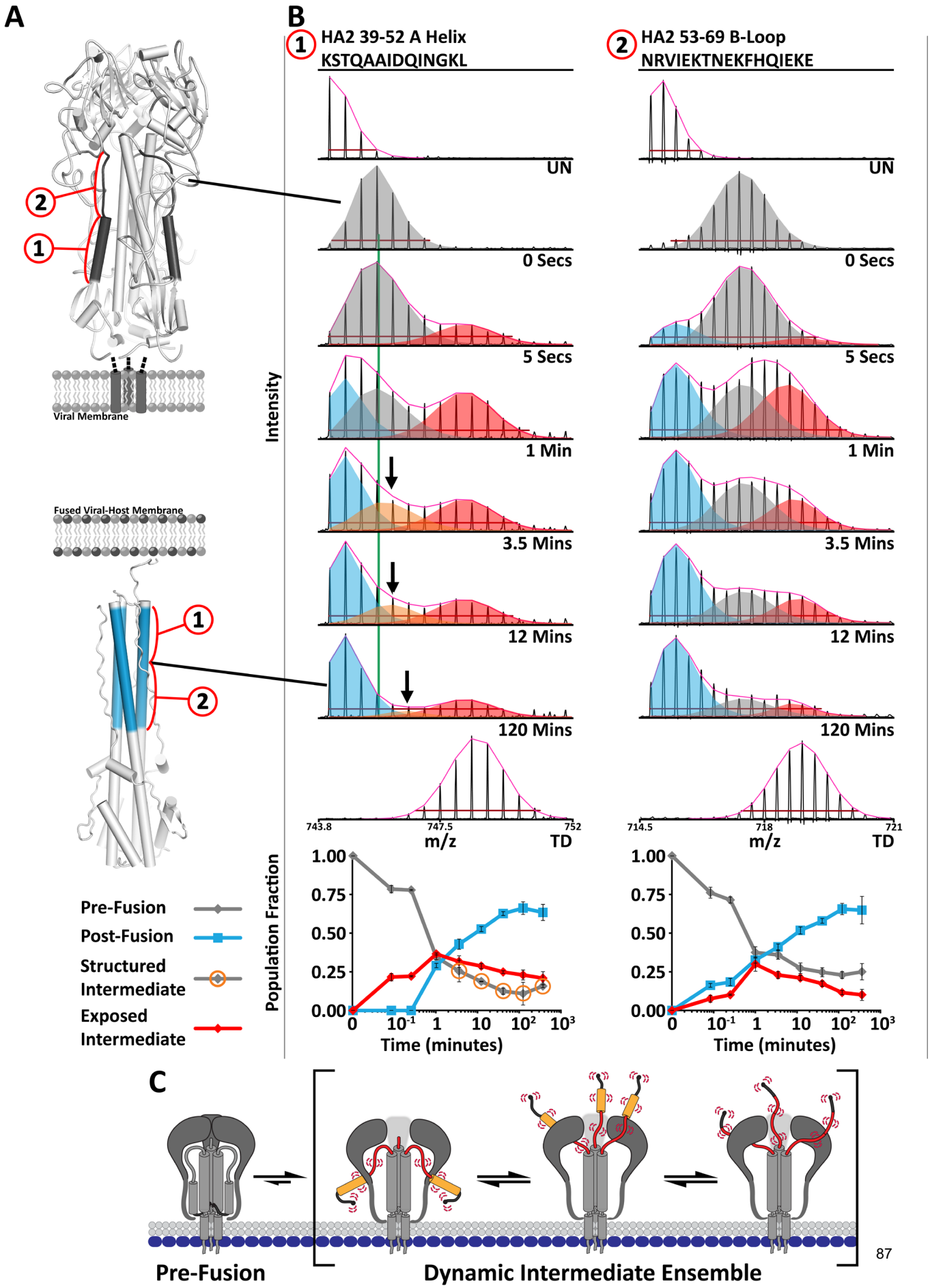
A
B
C
1
2
HA2 39-52 A Helix
KSTQAAIDQINGKL
HA2 53-69 B-Loop
NRVIEKTNEKFHQIEKE
UN
0 Secs
5 Secs
1 Min
3.5 Mins
12 Mins
120 Mins
Intensity
743.8
747.5
752
714.5
718
721
m/z
TD
Population Fraction
1.00
0.75
0.50
0.25
0.00
0
10-1
1
10
102
103
Time (minutes)
Viral Membrane
Fused Viral-Host Membrane
Pre-Fusion
Post-Fusion
Structured Intermediate
Exposed Intermediate
Pre-Fusion
Dynamic Intermediate Ensemble

Figure 3.2. Formation of a Dynamic Intermediate Ensemble in Full Length HA.

Fusion subunit triggering and reorganization of the HA1 RBD interface directly result in formation of a dynamic fusion active intermediate state in HA2. **(A)** The HA2 A-helix and B-loop segments are highlighted on ribbon diagrams for the pre-fusion (top PDB:3HMG) and post-fusion (bottom PDB:1QU1) crystal structures. **(B)** The HA2 A-helix (segment 1) adopts a relatively unstructured intermediate state (red spectral envelope) following acid activation that is distinct from the pre-fusion (grey) and post-fusion (light blue) helical states. The neutral pH pre-fusion conformation is tracked by the centroid (green vertical line). The presence of a fourth coexisting state by 3.5 min that is slightly more exposed than the neutral pH pre-fusion state is denoted by the orange envelopes. Formation of the post-fusion helical bundle is indicated by the formation of the low m/z, minimally deuterated population that increases in relative abundance over time (light blue). The HA2 B-loop (segment 2) likewise reveals the formation of a highly exposed, dynamic intermediate state (red envelopes) on the same timescale as the A-helix. Undeuterated (UN) and totally deuterated (TD) controls are shown for each peptide. The red horizontal bar in each spectra corresponds to the distribution width and the magenta curve above each spectra displays the summation of each binomial fit. **(C)** Schematic illustrating the nature of the dynamic intermediate ensemble.

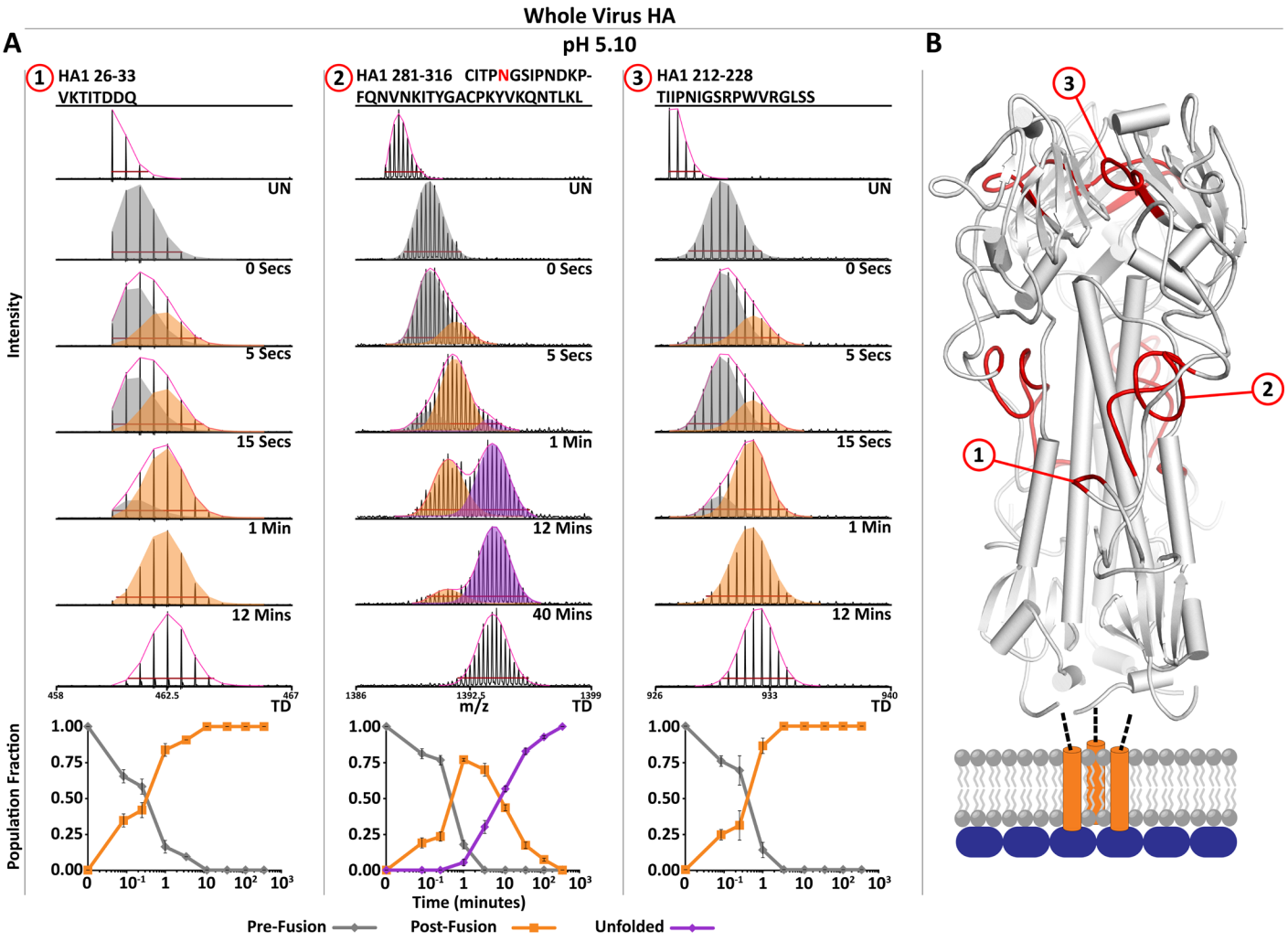

Figure 3.3. Concurrent fusion subunit triggering and HA1 RBD interface reorganization in full length HA.

(A) N-terminal HA1 peptides between HA1 and the HA2 fusion domain (Peptide 1 – F' region) display a transition to a more exposed state (orange envelope and traces) soon after acidification indicative of a loss of quaternary contacts. The HA1 hinge region (Peptide 2 – hinge and F' region), which forms quaternary contacts with the HA2 fusion domain, displays two distinct structural changes with the first corresponding to a loosening of the HA1-HA2 quaternary contacts (orange) and the second to unfolding of the HA1 globular head (purple). The HA1 RBD interface (Peptide 3 – HA1-HA1 trimeric interface) transitions to a more exposed state on the same time scale as the fusion peptide release event. Undeuterated (UN) and totally deuterated (TD) controls are shown for each peptide. The red horizontal bar in each spectra corresponds to the distribution width and the magenta curve above each spectra displays the summation of each binomial fit. **(B)** Peptide segments highlighted in 1-3 mapped onto ribbon diagram (PDB: 3HMG). Error bars indicate standard deviations from triplicate measurements.

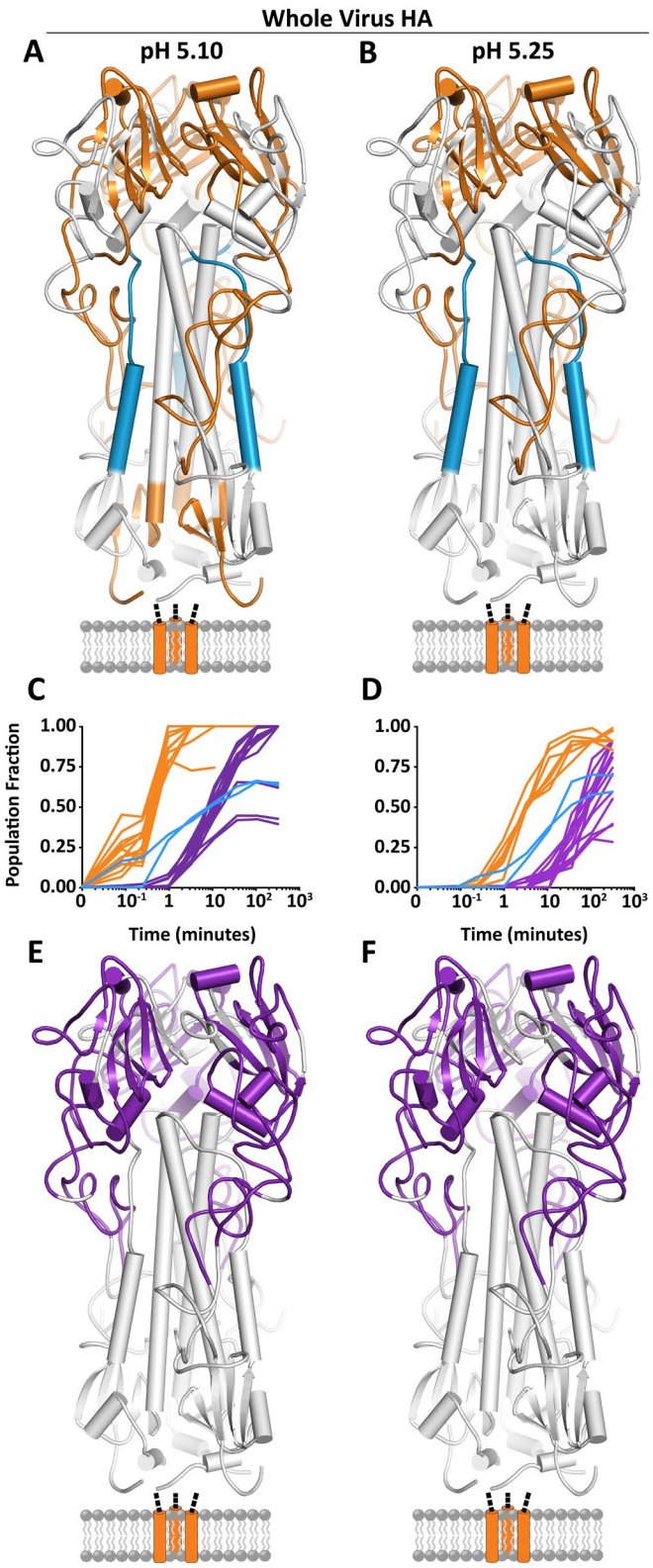
Whole Virus HA
A
pH 5.10
B
pH 5.25
C
D
Population Fraction
1.00
0.75
0.50
0.25
0.00
0
10-1
1
10
102
103
Time (minutes)
E
F

Figure 3.4. Global kinetic comparison and pH dependence of HA fusion activation for full length HA.

The specific pH of activation did not alter the nature **(A,B)** or sequence of any observed structural changes in full length HA but simply accelerated the onset and rate of change of each conformational event **(C,D)**. Conformational transitions that take place before 3.5 minutes are colored in orange. The last transition reported by HA1 peptides is to a largely unfolded, highly flexible state which begins at 3.5 minutes (purple; C,D and E,F). Formation of the post-fusion helical bundle in full-length HA is delayed due to formation of the intermediate state (A-D blue peptides and traces).

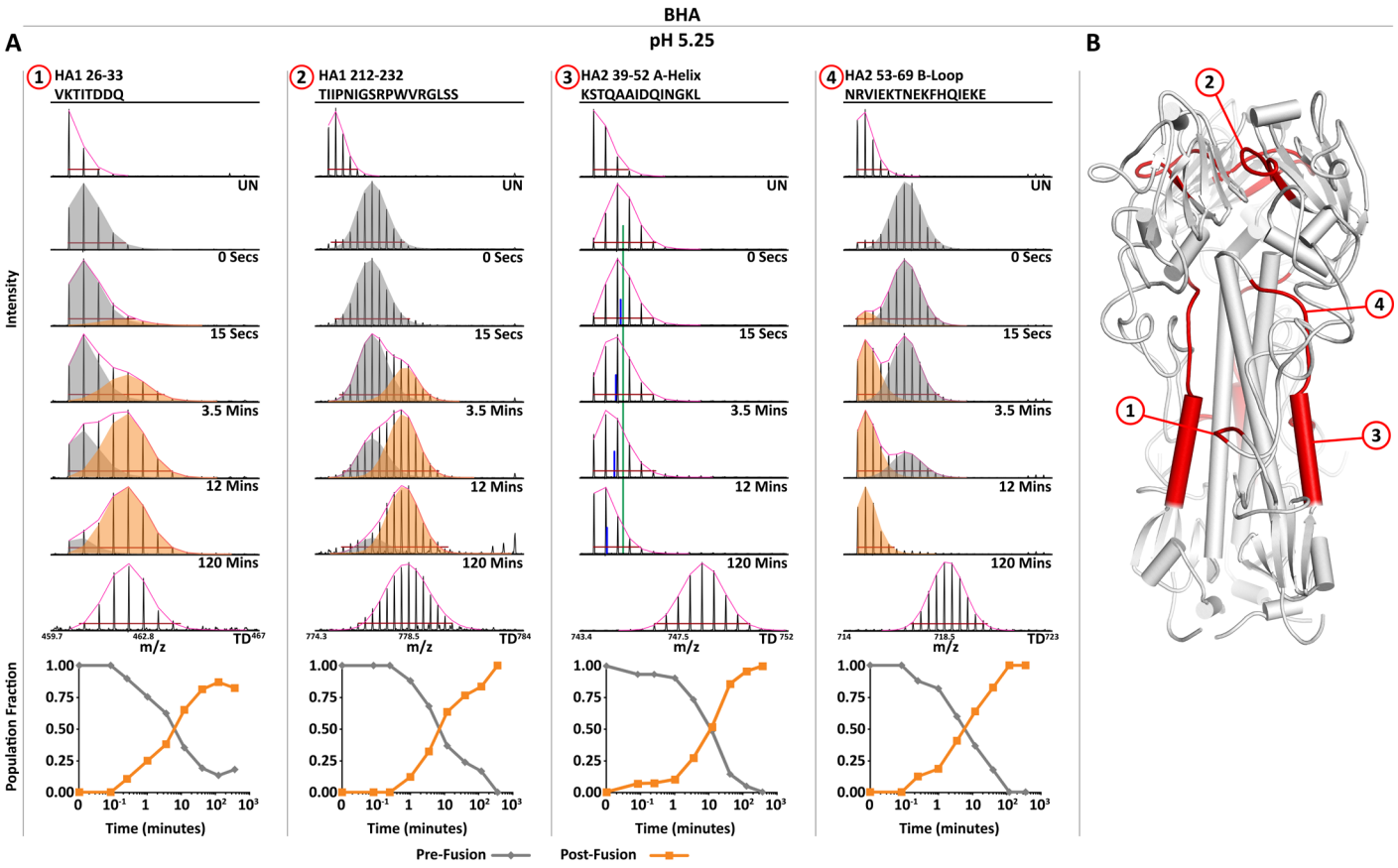

Figure 3.5. The soluble BHA ectodomain transitions directly to the post-fusion state following acid activation.

(A) Activation of the soluble BHA ectodomain at pH 5.25 reveals that fusion peptide release (segment 1) and reorganization of the HA1 RBD interface (segment 2) occur similarly to full length HA. However, both the HA2 A-Helix and B-Loop display a rapid transition from the pre-fusion state directly to the post-fusion state upon acid activation with no observable intermediate state (A-Helix segment 3 and B-Loop segment 4). The A-Helix is fit with a single binomial and the centroid of the 0 Second Pre-Fusion state (green line) is plotted for comparison with the centroid of each time point (blue line). Undeuterated (UN) and totally deuterated (TD) controls are shown for each peptide. The red horizontal bar in each spectra corresponds to the distribution width and the magenta curve above each spectra displays the summation of each binomial fit. **(B)** Peptide segments highlighted in 1-4 mapped onto ribbon diagram (PDB: 3HMG).

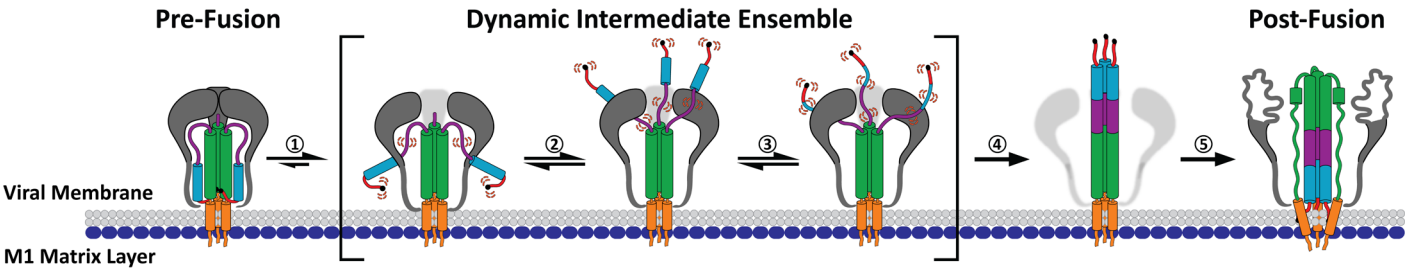

Figure 3.6. Proposed model for HA fusion activation.

Full length HA on whole influenza activates in response to low pH conditions with **(1)** concurrent reorganization of the HA2 fusion domain and HA1 RBD interface resulting in formation of a dynamic, fusion peptide released, intermediate state. This intermediate state is not a single discrete or static state, but rather a dynamic intermediate ensemble where the exposed fusion peptide is sampling conformational space in search of the target membrane **(2-3)**. In the dynamic intermediate ensemble, the HA2 fusion peptide proximal subdomain is structurally dynamic. Formation of the extended helical intermediate **(4)** and the subsequent refolding to the post-fusion state **(5)** in the absence of a target membrane is a relatively slow process for the majority of HA's. Finally, HA1 unfolds after extended exposure to low pH.

References

1. White, J.M., et al., *Structures and mechanisms of viral membrane fusion proteins: multiple variations on a common theme.* Crit Rev Biochem Mol Biol, 2008. **43**(3): p. 189-219.
2. Skehel, J.J. and D.C. Wiley, *Receptor binding and membrane fusion in virus entry: the influenza hemagglutinin.* Annu Rev Biochem, 2000. **69**: p. 531-69.
3. Chen, J., et al., *Structure of the hemagglutinin precursor cleavage site, a determinant of influenza pathogenicity and the origin of the labile conformation.* Cell, 1998. **95**(3): p. 409-17.
4. Lazarowitz, S.G. and P.W. Choppin, *Enhancement of the infectivity of influenza A and B viruses by proteolytic cleavage of the hemagglutinin polypeptide.* Virology, 1975. **68**(2): p. 440-54.
5. Wilson, I.A., J.J. Skehel, and D.C. Wiley, *Structure of the haemagglutinin membrane glycoprotein of influenza virus at 3 A resolution.* Nature, 1981. **289**(5796): p. 366-73.
6. Chen, J., J.J. Skehel, and D.C. Wiley, *N- and C-terminal residues combine in the fusion-pH influenza hemagglutinin HA(2) subunit to form an N cap that terminates the triple-stranded coiled coil.* Proc Natl Acad Sci U S A, 1999. **96**(16): p. 8967-72.
7. Carr, C.M. and P.S. Kim, *A spring-loaded mechanism for the conformational change of influenza hemagglutinin.* Cell, 1993. **73**(4): p. 823-32.
8. Bullough, P.A., et al., *Structure of influenza haemagglutinin at the pH of membrane fusion.* Nature, 1994. **371**(6492): p. 37-43.
9. Lee, K.K., *Architecture of a nascent viral fusion pore.* EMBO J, 2010. **29**(7): p. 1299-311.
10. Boonstra, S., et al., *Hemagglutinin-Mediated Membrane Fusion: A Biophysical Perspective.* Annu Rev Biophys, 2018. **47**: p. 153-173.
11. Carr, C.M., C. Chaudhry, and P.S. Kim, *Influenza hemagglutinin is spring-loaded by a metastable native conformation.* Proc Natl Acad Sci U S A, 1997. **94**(26): p. 14306-13.
12. Garcia, N.K., et al., *Dynamic changes during acid-induced activation of influenza hemagglutinin.* Structure, 2015. **23**(4): p. 665-76.
13. Kemble, G.W., et al., *Intermonomer disulfide bonds impair the fusion activity of influenza virus hemagglutinin.* J Virol, 1992. **66**(8): p. 4940-50.
14. Das, D.K., et al., *Direct Visualization of the Conformational Dynamics of Single Influenza Hemagglutinin Trimers.* Cell, 2018. **174**(4): p. 926-937 e12.
15. Fontana, J., et al., *Structural changes in Influenza virus at low pH characterized by cryo-electron tomography.* J Virol, 2012. **86**(6): p. 2919-29.
16. Fontana, J. and A.C. Steven, *Influenza virus-mediated membrane fusion: Structural insights from electron microscopy.* Arch Biochem Biophys, 2015. **581**: p. 86-97.
17. Huang, Q., et al., *Early steps of the conformational change of influenza virus hemagglutinin to a fusion active state: stability and energetics of the hemagglutinin.* Biochim Biophys Acta, 2003. **1614**(1): p. 3-13.
18. Leikina, E., et al., *Reversible stages of the low-pH-triggered conformational change in influenza virus hemagglutinin.* EMBO J, 2002. **21**(21): p. 5701-10.
19. Lin, X., et al., *Lowered pH Leads to Fusion Peptide Release and a Highly Dynamic Intermediate of Influenza Hemagglutinin.* J Phys Chem B, 2016. **120**(36): p. 9654-60.
20. Lin, X., et al., *Atomistic simulations indicate the functional loop-to-coiled-coil transition in influenza hemagglutinin is not downhill.* Proc Natl Acad Sci U S A, 2018. **115**(34): p. E7905-E7913.
21. Mair, C.M., et al., *A histidine residue of the influenza virus hemagglutinin controls the pH dependence of the conformational change mediating membrane fusion.* J Virol, 2014. **88**(22): p. 13189-200.

22. Park, H.E., J.A. Gruenke, and J.M. White, *Leash in the groove mechanism of membrane fusion.* Nat Struct Biol, 2003. **10**(12): p. 1048-53.
23. Xu, R. and I.A. Wilson, *Structural characterization of an early fusion intermediate of influenza virus hemagglutinin.* J Virol, 2011. **85**(10): p. 5172-82.
24. Walters, B.T., et al., *Folding of a large protein at high structural resolution.* Proc Natl Acad Sci U S A, 2013. **110**(47): p. 18898-903.
25. Guttman, M., et al., *Analysis of overlapped and noisy hydrogen/deuterium exchange mass spectra.* J Am Soc Mass Spectrom, 2013. **24**(12): p. 1906-12.
26. Bai, Y., et al., *Primary structure effects on peptide group hydrogen exchange.* Proteins, 1993. **17**(1): p. 75-86.
27. Malhotra, P., P.N. Jethva, and J.B. Udgaonkar, *Chemical Denaturants Smoothen Ruggedness on the Free Energy Landscape of Protein Folding.* Biochemistry, 2017. **56**(31): p. 4053-4063.
28. White, J.M. and I.A. Wilson, *Anti-peptide antibodies detect steps in a protein conformational change: low-pH activation of the influenza virus hemagglutinin.* J Cell Biol, 1987. **105**(6 Pt 2): p. 2887-96.
29. Harris, A., et al., *Influenza virus pleiomorphy characterized by cryoelectron tomography.* Proc Natl Acad Sci U S A, 2006. **103**(50): p. 19123-7.
30. Calder, L.J., et al., *Structural organization of a filamentous influenza A virus.* Proc Natl Acad Sci U S A, 2010. **107**(23): p. 10685-90.
31. Godley, L., et al., *Introduction of intersubunit disulfide bonds in the membrane-distal region of the influenza hemagglutinin abolishes membrane fusion activity.* Cell, 1992. **68**(4): p. 635-45.
32. Kilby, J.M., et al., *Potent suppression of HIV-1 replication in humans by T-20, a peptide inhibitor of gp41-mediated virus entry.* Nat Med, 1998. **4**(11): p. 1302-7.
33. Williams, J.A., et al., *Dissection of epitope-specific mechanisms of neutralization of influenza virus by intact IgG and Fab fragments.* J Virol, 2017.
34. Benton, D.J., et al., *Influenza hemagglutinin membrane anchor.* Proc Natl Acad Sci U S A, 2018. **115**(40): p. 10112-10117.
35. Gui, L., et al., *Visualization and Sequencing of Membrane Remodeling Leading to Influenza Virus Fusion.* J Virol, 2016. **90**(15): p. 6948-62.
36. Ruigrok, R.W., et al., *Membrane interaction of influenza virus M1 protein.* Virology, 2000. **267**(2): p. 289-98.
37. Stauffer, S., et al., *Stepwise priming by acidic pH and a high K+ concentration is required for efficient uncoating of influenza A virus cores after penetration.* J Virol, 2014. **88**(22): p. 13029-46.
38. Ali, A., et al., *Influenza virus assembly: effect of influenza virus glycoproteins on the membrane association of M1 protein.* J Virol, 2000. **74**(18): p. 8709-19.
39. Jin, H., et al., *Influenza virus hemagglutinin and neuraminidase cytoplasmic tails control particle shape.* EMBO J, 1997. **16**(6): p. 1236-47.
40. Enami, M. and K. Enami, *Influenza virus hemagglutinin and neuraminidase glycoproteins stimulate the membrane association of the matrix protein.* J Virol, 1996. **70**(10): p. 6653-7.
41. Yewdell, J.W., et al., *Mutations in or near the fusion peptide of the influenza virus hemagglutinin affect an antigenic site in the globular region.* J Virol, 1993. **67**(2): p. 933-42.
42. Bangaru, S., et al., *A Site of Vulnerability on the Influenza Virus Hemagglutinin Head Domain Trimer Interface.* Cell, 2019. **177**(5): p. 1136-1152 e18.
43. Turner, H.L., et al., *Potent anti-influenza H7 human monoclonal antibody induces separation of hemagglutinin receptor-binding head domains.* PLoS Biol, 2019. **17**(2): p. e3000139.
44. Costello, D.A., G.R. Whittaker, and S. Daniel, *Variations in pH sensitivity, acid stability, and fusogenicity of three influenza virus H3 subtypes.* J Virol, 2015. **89**(1): p. 350-60.

45. Di Lella, S., A. Herrmann, and C.M. Mair, *Modulation of the pH Stability of Influenza Virus Hemagglutinin: A Host Cell Adaptation Strategy.* Biophys J, 2016. **110**(11): p. 2293-2301.
46. Mair, C.M., et al., *Receptor binding and pH stability - how influenza A virus hemagglutinin affects host-specific virus infection.* Biochim Biophys Acta, 2014. **1838**(4): p. 1153-68.
47. Schrauwen, E.J., et al., *Amino Acid Substitutions That Affect Receptor Binding and Stability of the Hemagglutinin of Influenza A/H7N9 Virus.* J Virol, 2016. **90**(7): p. 3794-9.
48. Lakadamyali, M., et al., *Visualizing infection of individual influenza viruses.* Proc Natl Acad Sci U S A, 2003. **100**(16): p. 9280-5.
49. Puri, A., et al., *Conformational changes and fusion activity of influenza virus hemagglutinin of the H2 and H3 subtypes: effects of acid pretreatment.* J Virol, 1990. **64**(8): p. 3824-32.
50. Zhang, Z., A. Zhang, and G. Xiao, *Improved protein hydrogen/deuterium exchange mass spectrometry platform with fully automated data processing.* Anal Chem, 2012. **84**(11): p. 4942-9.
51. Verkerke, H.P., et al., *Epitope-Independent Purification of Native-Like Envelope Trimers from Diverse HIV-1 Isolates.* J Virol, 2016. **90**(20): p. 9471-82.
52. Guttman, M., et al., *Tuning a High Transmission Ion Guide to Prevent Gas-Phase Proton Exchange During H/D Exchange MS Analysis.* J Am Soc Mass Spectrom, 2016. **27**(4): p. 662-8.
53. Fang, J., et al., *False EX1 signatures caused by sample carryover during HX MS analyses.* Int J Mass Spectrom, 2011. **302**(1-3): p. 19-25.
54. Marty, M.T., et al., *Bayesian deconvolution of mass and ion mobility spectra: from binary interactions to polydisperse ensembles.* Anal Chem, 2015. **87**(8): p. 4370-6.
55. Weis, D.D., J.R. Engen, and I.J. Kass, *Semi-automated data processing of hydrogen exchange mass spectra using HX-Express.* J Am Soc Mass Spectrom, 2006. **17**(12): p. 1700-3.
56. Weis, D.D., et al., *Identification and characterization of EX1 kinetics in H/D exchange mass spectrometry by peak width analysis.* J Am Soc Mass Spectrom, 2006. **17**(11): p. 1498-1509.
57. Zheng, S.Q., et al., *MotionCor2: anisotropic correction of beam-induced motion for improved cryo-electron microscopy.* Nat Methods, 2017. **14**(4): p. 331-332.
58. Mastronarde, D.N. and S.R. Held, *Automated tilt series alignment and tomographic reconstruction in IMOD.* J Struct Biol, 2017. **197**(2): p. 102-113.
59. Kremer, J.R., D.N. Mastronarde, and J.R. McIntosh, *Computer visualization of three-dimensional image data using IMOD.* J Struct Biol, 1996. **116**(1): p. 71-6.
60. Schneider, C.A., W.S. Rasband, and K.W. Eliceiri, *NIH Image to ImageJ: 25 years of image analysis.* Nat Methods, 2012. **9**(7): p. 671-5.

Supplemental Figures

Table of Contents:

X-31 Influenza Virus H3 HA Peptide Coverage For HDX-MS

HA1

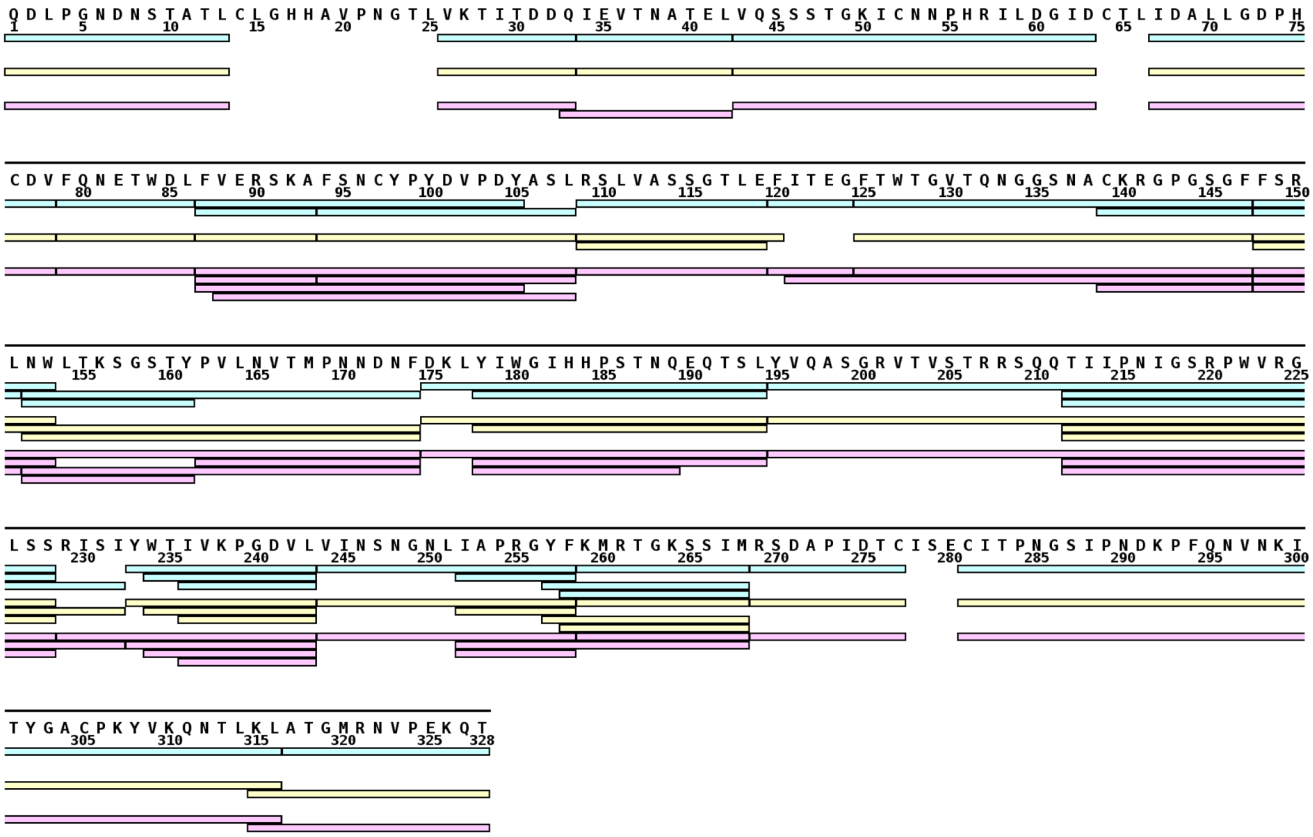

5.1: 310 of 328 ~ 95%
5.25: 306 of 328 ~ 93%
BHA: 310 of 328 ~ 95%
Total: 310 of 328 ~ 95%

HA2

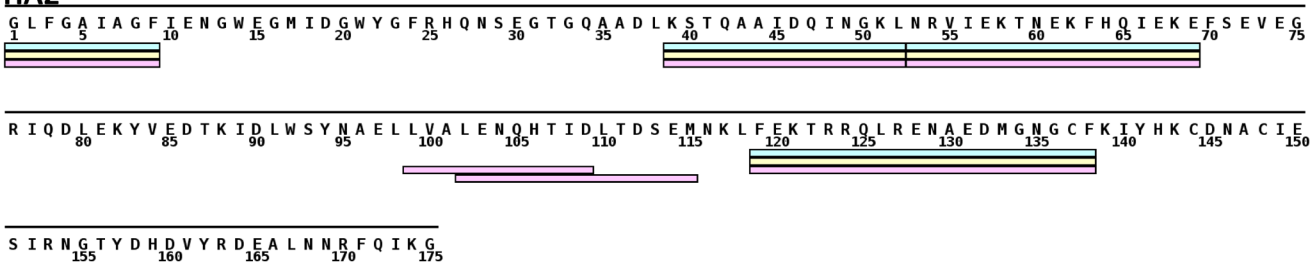

5.1: 60 of 175 ~ 34%
5.25: 60 of 175 ~ 34%
BHA: 77 of 175 ~ 44%
Total: 77 of 175 ~ 44%

Figure S3.1. HDX-MS Peptide Coverage Map Displaying Unique Peptides.
Nearly complete coverage of HA1 was obtained for all conditions. Only unique peptides where HDX-MS data was monitored in acidic conditions are shown here, an abundance of overlapping non-unique peptides were also identified and analyzed to confirm changes observed throughout HA1. Coverage of HA2 was limited, however we were able to monitor the most critical conformationally relevant peptides throughout the time course. The limited coverage throughout HA2 is attributed to protease resistance and steric occlusion from high HA density on virions. Peptide coverage shown here corresponds to Whole Virus samples at pH 5.10 and 5.25 as well as BHA at pH 5.25. Coverage map made using MSTools (*61*).

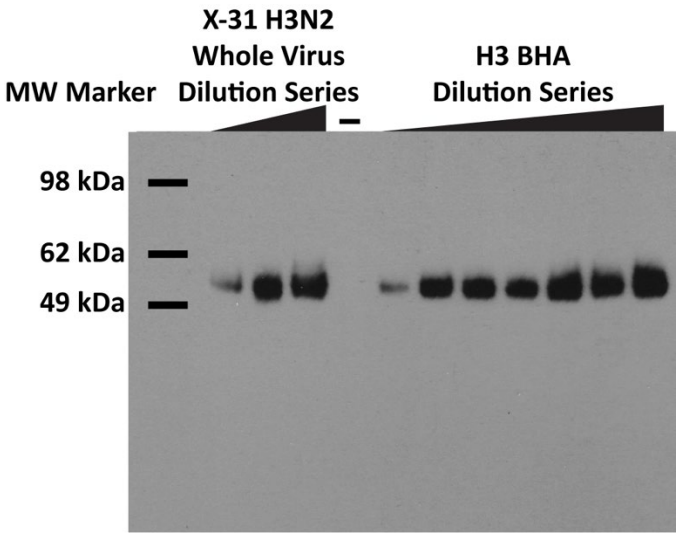

Figure S3.2. Western Blot Analysis of Whole Virus HA and BHA.
A concentration series of BHA and Whole X-31 H3N2 virions was analyzed by western blotting. The concentration of HA in whole virus samples was determined using the BHA concentration series. All HA present in whole virus and BHA samples was determined to be correctly cleaved into HA1 and HA0.

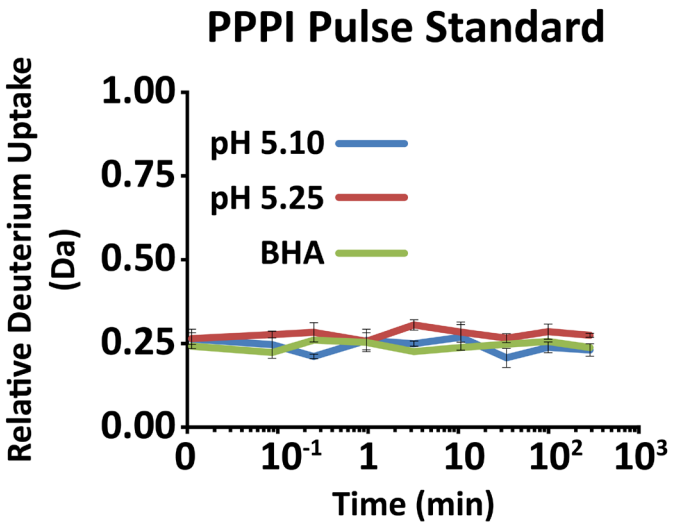

Figure S3.3. Internal PPPI Pulse Standard.
Internal pulse standard peptide PPPI relative deuterium uptake.

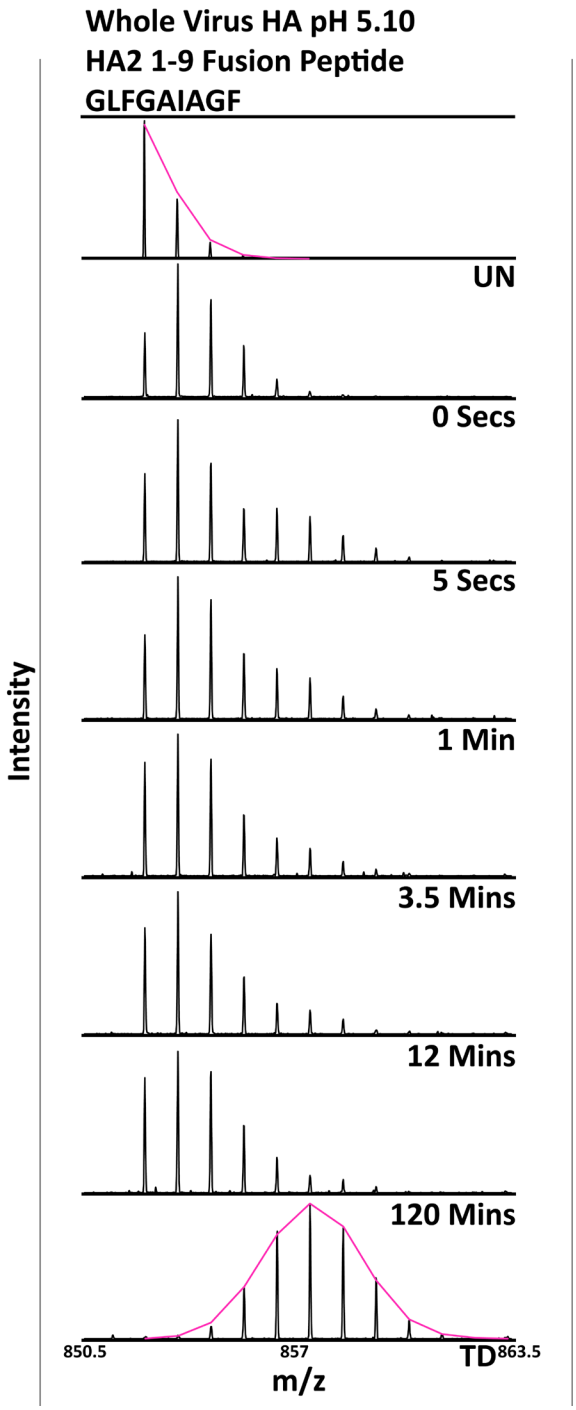

Figure S3.4. Peak Width Analysis of Whole Virus HA Fusion Peptide at pH 5.10.
The HA2 N-terminal fusion peptide displays complex multimodal behavior and precludes analysis by binomial fitting and bimodal deconvolution. Using peak width analysis the fusion peptide displays a clear increase and subsequent decrease in peak width in line with reorganization of the HA2 N-terminal fusion domain and the formation of the post fusion state. The fusion peptide appears protected at neutral pH, as previously observed, and becomes more exposed rapidly following acid activation (*12*). Aggregation at the fusion peptide and insertion into the membrane is known to occur and likely contributes to the data analysis limitations. Undeuterated (UN) and totally deuterated (TD) controls are shown.

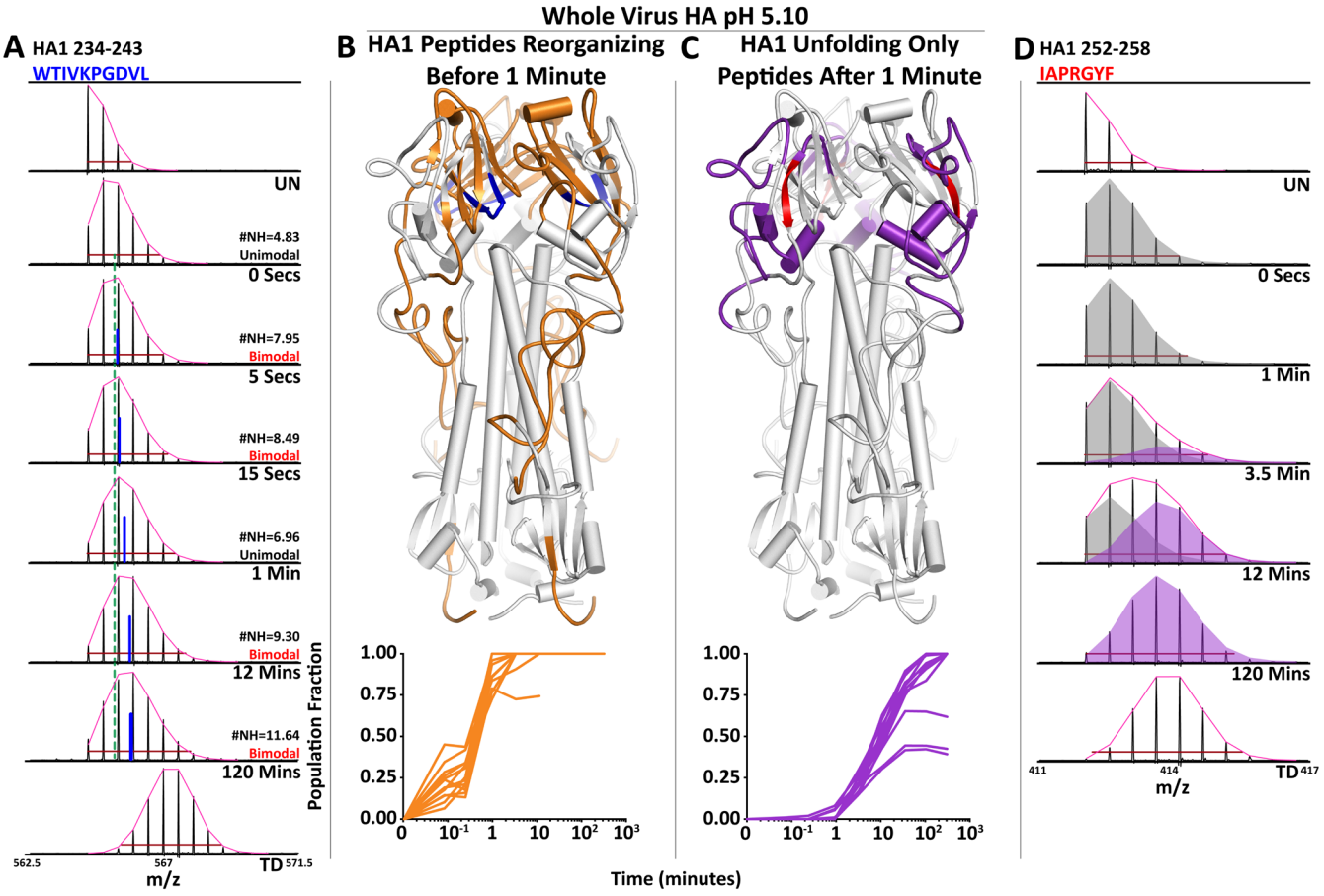

Figure S3.5. Reorganization along the HA1-HA2 Quaternary Interface and HA1-HA1 Protomeric Interface Precedes Late Stage Unfolding of HA1 RBD Subunit.

Peptide segments spanning the HA1-HA2 quaternary interface and HA1-HA1 protomeric interface transition to a uniform more exposed state by 1 minute at pH 5.1 **(A and B - orange)**. The HA1 peptide in **(A – peptide highlighted in blue in B)** is fit with a single binomial equation; the changes in deuterium uptake and envelope width correspond to the two structural transitions experienced by these quaternary interface peptides (distribution width as number of amides reported for each time point along with indication of a unimodal or bimodal distribution). Between 15 seconds and 1 minute these peptides display both an increase in deuterium uptake and a narrowing of the mass envelope indicating a transition to a more uniform more exposed state. Comparing the centroid of the neutral pH pre-fusion control (green dashed line) to that in each time point (blue line) highlights the change in structure that occurs at 1 minute. Subsequently, starting at 3.5 minutes these peptides begin to transition to an unfolded state, as shown by the increase in deuterium uptake and further shift in the centroid. All HA1 peptides where conformational transitions are observed between 5 seconds and 1 minute post acidification are colored in orange **(B)** to highlight that these peptides span nearly the entire HA1-HA2 and HA1-HA1 quaternary interface. The HA1 peptides that have no quaternary contacts with HA2 only experience late stage unfolding **(C - purple)** as indicated by a transition to a totally deuterated state (TD)**(D - peptide highlighted in red in C)**. Undeuterated (UN) and totally deuterated (TD) controls are shown for each peptide. The red horizontal bar in each spectra corresponds to the distribution width and the magenta curve above each spectra displays the summation of each binomial fit.

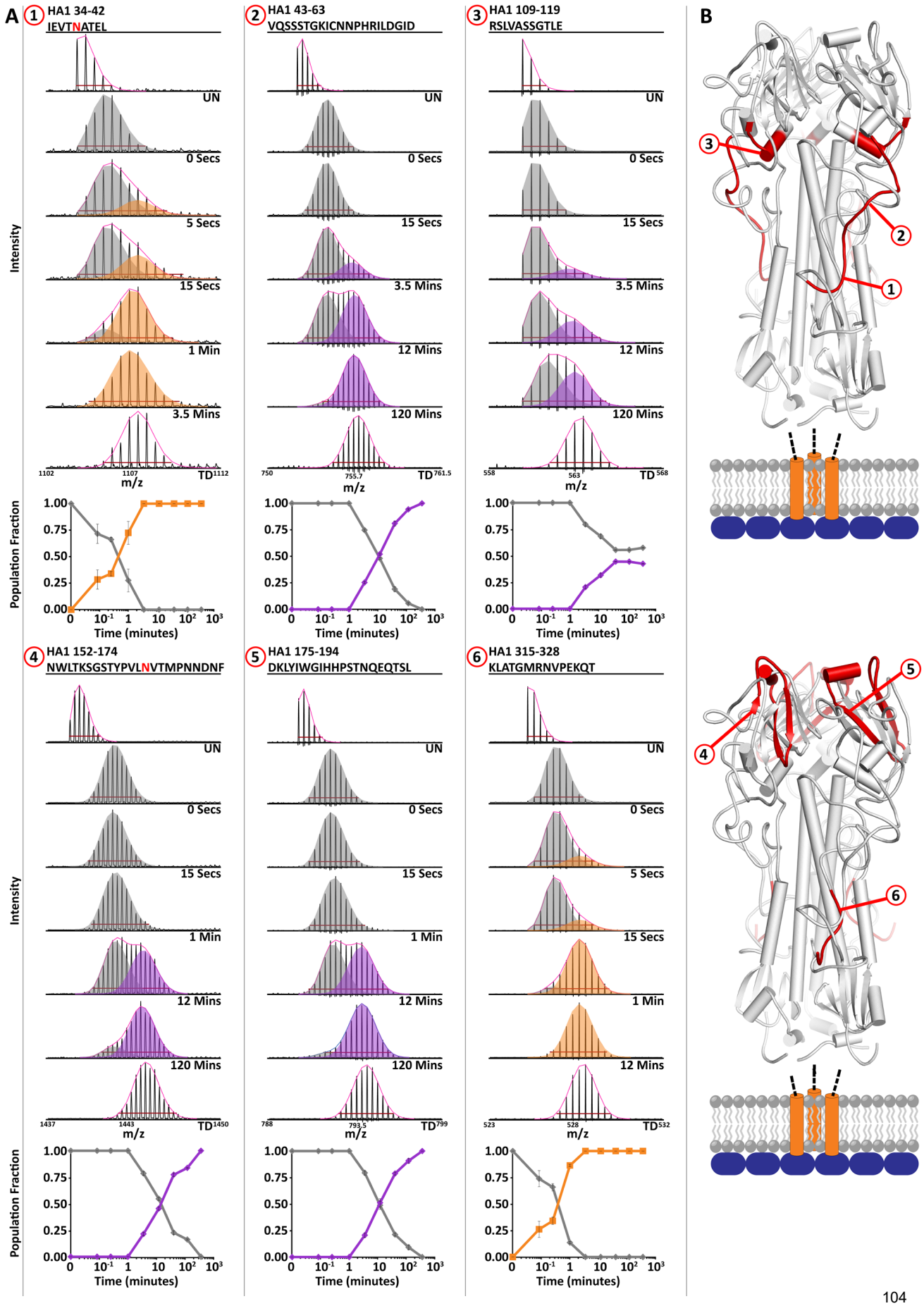
A
1 HA1 34-42
IEVTNATEL
2 HA1 43-63
VQSSSTGKICNNPHRILDGID
3 HA1 109-119
RSLVASSGTLE
4 HA1 152-174
NWLTKSGSTYPVLNVTMPNNDNF
5 HA1 175-194
DKLYIWGIHHPSTNQEQTSL
6 HA1 315-328
KLATGMRNVPEKQT
UN
0 Secs
5 Secs
15 Secs
1 Min
3.5 Mins
12 Mins
120 Mins
TD
m/z
Intensity
Population Fraction
Time (minutes)
B

Figure S3.6. Peptides Throughout HA Report Similar Structural Changes at pH 5.1.
(A) Peptides throughout HA1 display structural changes predominantly corresponding to the late stage unfolding event (segments 2-5). Peptides with strong secondary structure often do not fully transition to an unfolded state (segment 3). Peptides along the HA1-HA2 quaternary interface with little initial secondary structure only report on the early structural reorganizations associated with fusion peptide release (segments 1 and 6). The pre-fusion state is shown in grey for each peptide and the terminal (post-fusion) state is shown as either orange (completed by 3.5 minutes) or purple (beginning at 3.5 minutes). Undeuterated (UN) and totally deuterated (TD) controls are shown for each peptide. The red horizontal bar in each spectra corresponds to the distribution width and the magenta curve above each spectra displays the summation of each binomial fit. Red highlights in peptide sequences indicate glycosylation site where most abundant glycoform was used for analysis. **(B)** Peptide segments mapped onto ribbon diagrams (1-3 top, 4-6 bottom)(PDB: 3HMG).

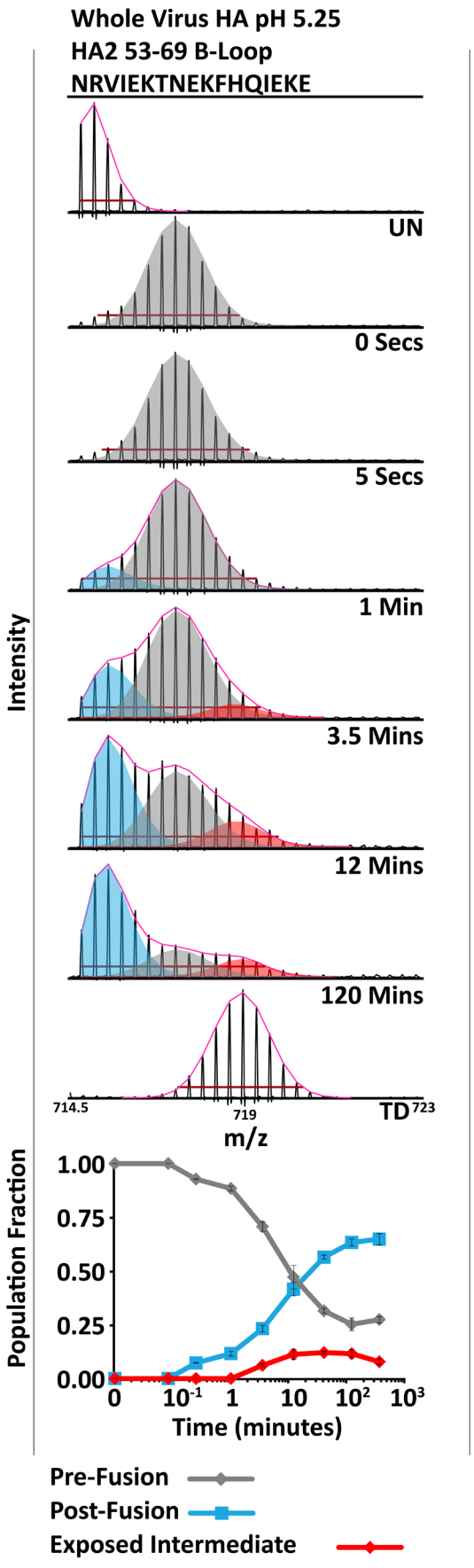
Whole Virus HA pH 5.25
HA2 53-69 B-Loop
NRVIEKTNEKFHQIEKE
UN
0 Secs
5 Secs
1 Min
3.5 Mins
12 Mins
120 Mins
Intensity
714.5
719
TD723
m/z
Population Fraction
1.00
0.75
0.50
0.25
0.00
0
10-1
1
10
102
103
Time (minutes)
Pre-Fusion
Post-Fusion
Exposed Intermediate

Figure S3.7. Formation of a Dynamic Intermediate at pH 5.25.
Analysis of the HA2 B-loop at pH 5.25 reveals the formation of a dynamic intermediate state, as observed at pH 5.1. A higher pH of activation resulted in decreased abundance of the intermediate state but had no effect on the nature of the structural changes. Undeuterated (UN) and totally deuterated (TD) controls are shown. The red horizontal bar in each spectra corresponds to the distribution width and the magenta curve above each spectra displays the summation of each binomial fit.

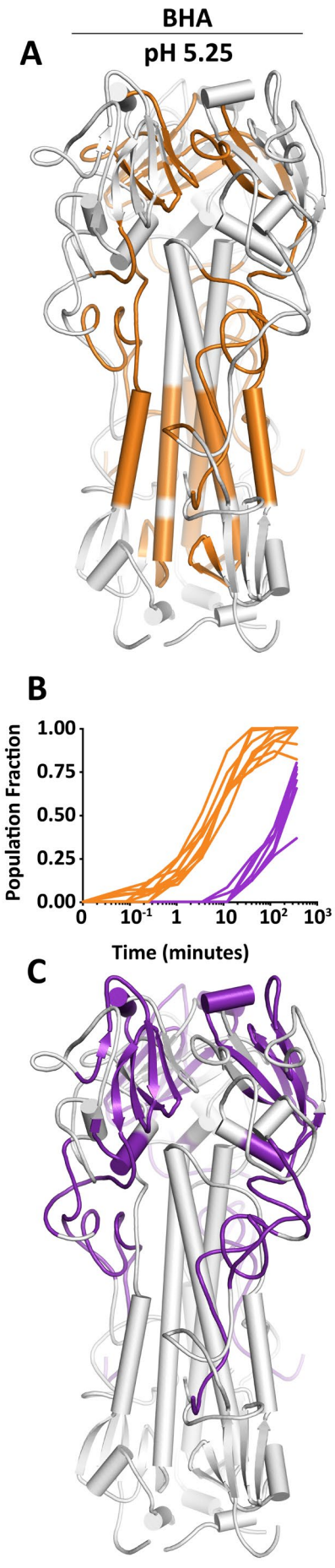
BHA
A
pH 5.25
B
Population Fraction
1.00
0.75
0.50
0.25
0.00
0
10-1
1
10
102
103
Time (minutes)
C

Figure S3.8. Global kinetic analysis of BHA peptides.
Global kinetic analysis of all BHA peptides revealed a rapid and direct transition from the pre- to post-fusion state with no observable intermediate state **(A and B)** (orange highlights and traces). The onset and kinetics of fusion subunit triggering **(A)** and globular head unfolding (purple highlights and traces) **(C)** were similar for BHA and full-length HA at pH 5.25, however BHA transitioned directly to the post-fusion state.

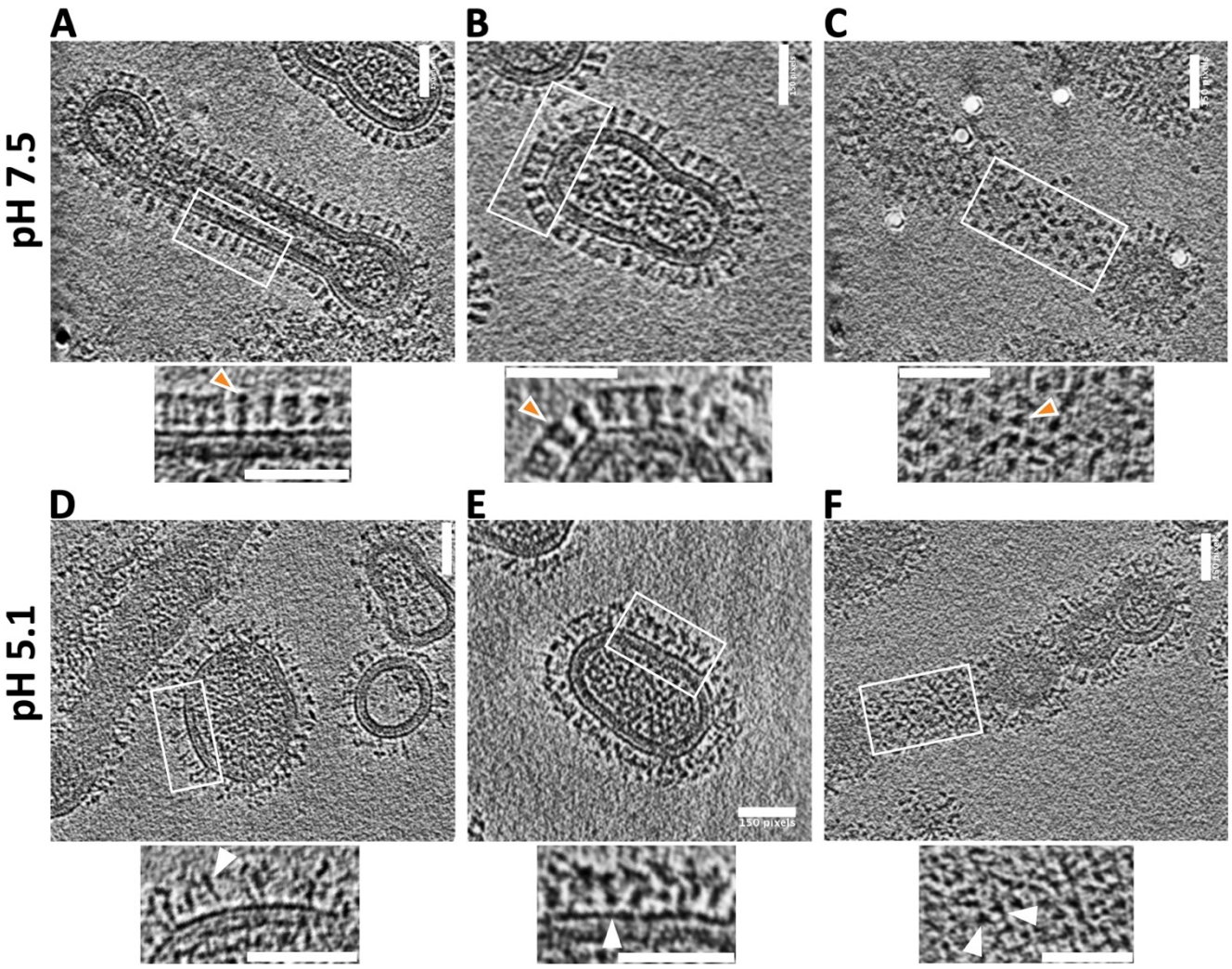

Figure S3.9. Cryo-Electron tomography reveals fusion active HA's conformational heterogeneity.
Direct visualization of influenza virions at pH 7.5 **(top A-C)** and pH 5.1 **(bottom D-F)** by cryo-ET reveals how limited exposure to low pH conditions (1 minute) results in widespread conformational heterogeneity in HA. Pre-fusion HA (orange arrows) are well resolved throughout all imaged virions (Enlarged selections beneath each image). **(D-F)** Acid-activated HA (white arrows) adopts a range of conformations as seen through side and top views. Although there is considerable heterogeneity, elongated 'post-fusion like' and well-resolved 'pre-fusion like' HA spikes can be identified at pH 5.1 (white arrows D,E). Comparing top down views of HA at neutral and acidic pH **(C and F)** reveal a loss of homogeneity and symmetry in the head. (Scale bar = 150 pixels or 38.7 nm).

A

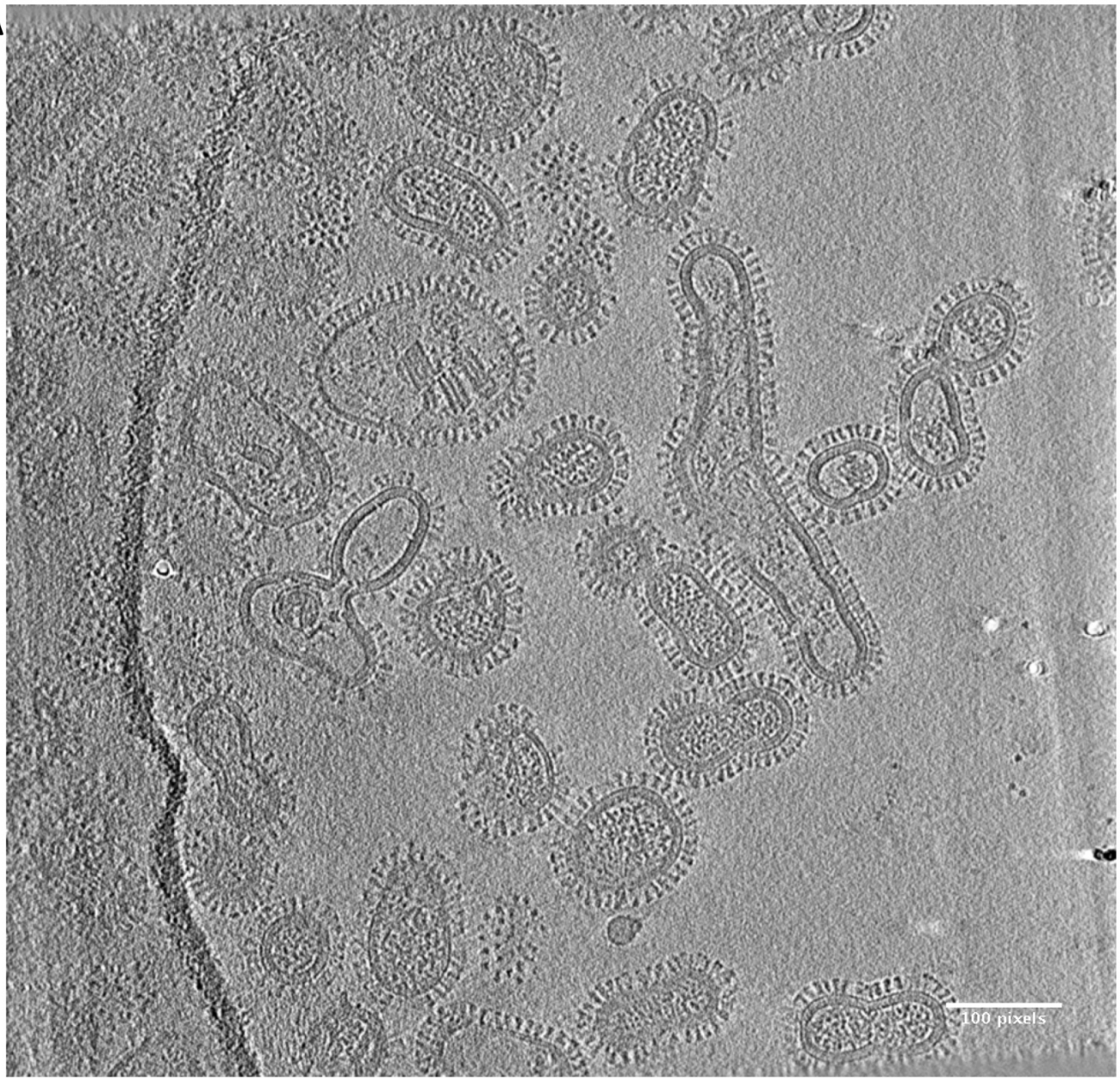

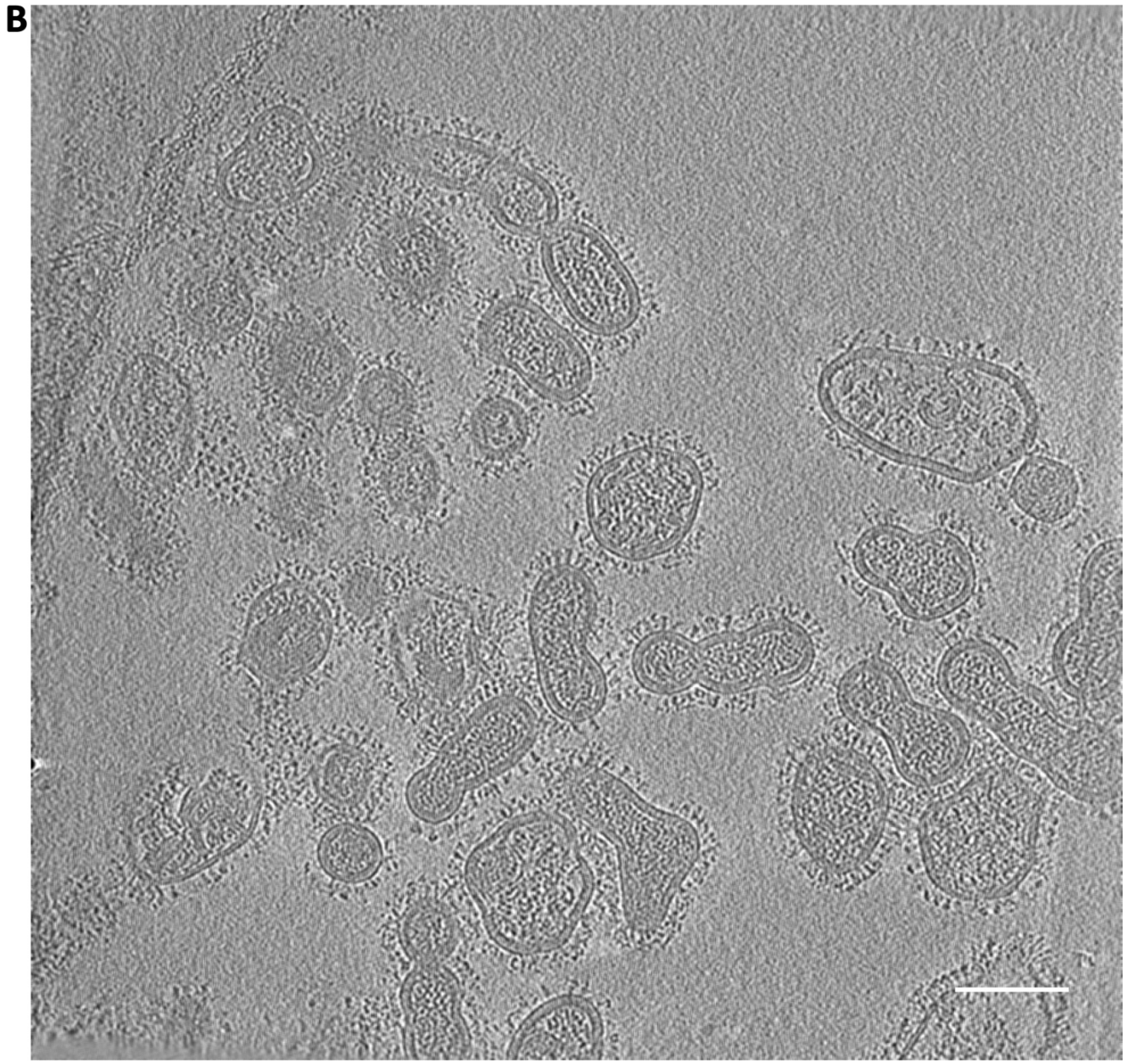

Figure S3.10. Whole field cryo-electron tomograms of influenza virus at pH 7.5 and 5.1.
HA in the pre-fusion conformation decorates the surface of influenza virus at pH 7.5 **(A)**. At pH 5.1 **(B)** after 1 minute HA is seen as conformationally heterogenous, with some HA resembling the pre-fusion state while others appear wholly disordered. (Scale bar = 100 pixels or 28.7 nm).

	Early Changing (5 Seconds – 3.5 Minutes)	Late Unfolding (3.5 Minutes – 6 Hours)	Fusion Subunit Triggering	HA1-HA2 Quaternary Contact	HA1 Interface	Unfolding Only
HA1						
F' Domain N-terminal						
1 13	x		x	x		
26-33	x		x	x		
34-42	x		x	x		
E' Domain (Hinge)						
43-63	x	x	x	x		
67-78		x				x
79-86		x				x
87-93	x	x		x		
94-108	x	x		x		
109-120		x		x		x
Globular Head						
125-147 (RBS)		x				x
148-153		x				x
152-174	x	x		x	x	
175-194 (RBS)	x	x		x	x	
HA1-HA1 Interface						
212-228	x				x	
212-232 (RBS)	x				x	
Globular Head						
233-243	x	x		x		
244-258		x				x
252-258		x				x
257-268	x	x		x		
F' Domain C-terminal						
269-277		x				x
281-316	x	x	x	x		
315-328	x		x	x		

Table S3.1. HA1 peptide conformational changes.
All unique HA1 peptides organized by structural region and their respective conformational changes. Peptides where structural transitions were observed between 5 seconds and 3.5 minutes post-acidification (timing relative to pH 5.10 condition) are marked as “Early Changing” and colored orange to correspond to Figure 4 coloring. Peptides where late stage unfolding was observed are colored purple to correspond to Figure 4 coloring.

						Whole Virus pH 5.10 0 Second		Whole Virus pH 5.25 0 Second			
	m/z	Start	End	Peptide Sequence	Length	Average Deuterium Uptake	Standard Deviation	Average Deuterium Uptake	Standard Deviation	BHA pH 5.25 0 Second Average Deuterium Uptake	Back Exchange (%)
HA1	1549.13	1	13	QDLPGNDNSTATL	12	5.72	0.15	5.67	0.14	5.38	8.68
	919.47	26	33	VKTITDDQ	7	1.48	0.02	1.45	0.06	Not Found	26.06
	460.24	26	33	VKTITDDQ	7	1.40	0.07	1.51	0.04	0.77	28.97
	1167.50	33	42	QIEVTNATEL	9	Not Found	Not Found	Not Found	Not Found	1.94	14.54
	1103.47	34	42	IEVTNATEL	8	2.44	0.03	2.37	0.17	1.66	2.01
	1127.56	43	63	VQSSSTGKICNNPHRILDGID	20	Not Found	Not Found	Not Found	Not Found	2.98	37.34
	752.04	43	63	VQSSSTGKICNNPHRILDGID	20	4.74	0.08	4.71	0.15	3.01	31.07
	564.28	43	63	VQSSSTGKICNNPHRILDGID	20	4.64	0.07	4.71	0.26	2.98	30.57
	634.30	67	78	IDALLGDPHCDV	11	1.70	0.04	1.73	0.02	1.22	46.65
	855.37	71	78	LGDPHCDV	7	1.50	0.08	1.63	0.07	Not Found	54.85
	1008.73	79	86	FQNETWDL	7	2.83	0.02	2.89	0.04	Not Found	7.53
	418.73	87	93	FVERSKA	6	1.83	0.11	1.87	0.00	1.35	21.54
	836.46	87	93	FVERSKA	6	1.75	0.05	1.74	0.05	1.29	23.30
	767.34	87	105	FVERSKAFSNCYPYDVPDY	18	4.48	0.09	4.53	0.27	3.14	38.63
	808.71	88	108	VERSKAFSNCYPYDVPDYASL	20	Not Found	Not Found	Not Found	Not Found	4.29	30.78
	877.37	94	108	FSNCYPYDVPDYASL	14	3.48	0.07	3.49	0.16	Not Found	31.05
	741.79	94	105	FSNCYPYDVPDY	11	2.03	0.04	Not Found	Not Found	Not Found	38.68
	560.30	109	119	RSLVASSGTLE	10	1.28	0.02	1.22	0.01	0.33	21.16
	1119.60	109	119	RSLVASSGTLE	10	1.27	0.05	1.20	0.01		21.35
	633.83	109	120	RSLVASSGTLEF	11	1.20	0.02	1.17	0.01		15.40
	566.28	120	124	FITEG	4	1.10	0.03	1.16	0.08	0.99	28.31
	1165.04	125	147	FTWTGVTQNGGSNACKRGPGSGF	22	9.48	0.10	9.55	0.21	8.92	25.34
	454.72	139	147	CKRGPGSGF	8	3.49	0.04	3.54	0.01	3.47	25.68

	522.30	148	151	FSRL	3	0.38	0.00	0.41	0.01	0.13	9.25
	411.71	148	153	FSRLNW	5	0.76	0.04	0.75	0.02	0.24	18.21
	830.42	148	161	FSRLNWLTKSGSTY	13	3.58	0.03	Not Found	Not Found	Not Found	No TD
	1205.28	148	174	FSRLNWLTKSGSTYPVLNVTMPNNDNF	26	7.92	0.05	7.87	0.06	6.56	No TD
	578.78	152	161	NWLTKSGSTY	9	2.90	0.06	2.89	0.03	2.51	23.53
	1438.94	152	174	NWLTKSGSTYPVLNVTMPNNDNF	22	7.28	0.14	7.39	0.26	6.47	15.09
	1589.14	162	174	PVLNVTMPNNDNF	12	4.24	0.09	4.30	0.09	Not Found	5.10
	789.72	175	194	DKLYIWGIHHPSTNQEQTSL	19	5.03	0.07	5.03	0.14	1.76	20.54
	670.99	178	194	YIWGIHHPSTNQEQTSL	16	3.10	0.06	3.12	0.07	1.87	34.03
	1005.98	178	194	YIWGIHHPSTNQEQTSL	16	3.04	0.06	3.03	0.08	1.78	33.69
	927.02	212	228	TIIPNIGSRPWVRGLSS	16	5.50	0.14	Not Found	Not Found	Not Found	14.31
	618.35	212	228	TIIPNIGSRPWVRGLSS	16	5.45	0.13	5.54	0.29	4.75	13.77
	774.78	212	232	TIIPNIGSRPWVRGLSSRISI	20	5.81	0.17	5.60	0.08	4.80	34.72
	645.85	233	243	YWTIVKPGDVL	10	1.25	0.10	1.38	0.19	0.61	19.43
	564.32	234	243	WTIVKPGDVL	9	1.26	0.10	1.35	0.18	Not Found	18.91
	840.52	236	243	IVKPGDVL	7	0.83	0.12	0.92	0.15	Not Found	21.97
	420.76	236	243	IVKPGDVL	7	0.84	0.05	0.88	0.09	0.29	22.74
	830.44	244	251	VINSNGNL	7	1.11	0.04	1.16	0.05	Not Found	30.02
	817.93	244	258	VINSNGNLIAPRGYF	14	1.93	0.05	1.91	0.06	0.54	28.61
	412.22	252	258	IAPRGYF	6	0.87	0.02	0.84	0.02	Not Found	9.96
	823.45	252	258	IAPRGYF	6	0.79	0.02	0.73	0.04	0.19	11.00
	648.35	252	268	IAPRGYFKMRTGKSSIM	16	Not Found	Not Found	Not Found	Not Found	2.06	No TD
	483.58	257	268	YFKMRTGKSSIM	11	2.65	0.05	2.57	0.04	Not Found	26.39
	724.87	257	268	YFKMRTGKSSIM	11	2.53	0.03	2.51	0.04	Not Found	26.33
	643.34	258	268	FKMRTGKSSIM	10	2.60	0.01	2.57	0.02	Not Found	25.99
	380.20	259	268	KMRTGKSSIM	9	2.62	0.14	2.53	0.01	Not Found	26.85

	569.80	259	268	KMRTGKSSIM	9	2.20	0.17	2.55	0.03	1.87	26.71
	977.44	269	277	RSDAPIDTC	8	1.34	0.00	1.36	0.07	0.74	36.09
	1387.65	281	316	CITPNGSIPNDKP FQNVNKITYGAC PKYVKQNTLKL	35	6.79	0.07	7.03	0.52	Not Found	17.94
	1372.85	281	328	CITPNGSIPNDKP FQNVNKITYGAC PKYVKQNTLKLA TGMRNVPEKQT	47	Not Found	Not Found	Not Found	Not Found	8.30	No TD
	524.95	315	328	KLATGMRNVPEK QT	13	3.98	0.25	3.72	0.00	2.88	17.88
	666.34	317	328	ATGMRNVPEKQ T	11	3.76	0.24	3.53	0.07		18.70
	m/z	Start	End	Peptide Sequence	Length	Average Deuterium Uptake	Standard Deviation	Average Deuterium Uptake	Standard Deviation	BHA pH 5.25 0 Second Average Deuterium Uptake	Back Exchange (%)
HA2	852.46	1	9	GLFGAIAGF	8	0.97	0.03	1.01	0.07	0.25	23.55
	617.61	22	38	YGFRHQNSEGT GQAADL	16	5.20	0.12	5.16	0.11	3.64	37.29
	743.91	39	52	KSTQAAIDQINGK L	13	2.18	0.02	2.16	0.06	1.54	17.24
	714.71	53	69	NRVIEKTNEKFH QIEKE	16	6.20	0.12	6.35	0.32	5.14	16.68
	681.88	119	128	FEKTRRQLRE	9	0.99	0.07	0.94	0.03	0.22	23.41
	516.61	119	130	FEKTRRQLRENA	11	1.33	0.03	1.29	0.05	Not Found	21.68
	801.04	119	138	FEKTRRQLRENA EDMGNGCF	19	1.94	0.03	1.93	0.02	Not Found	24.20
	597.77	139	148	KIYHKCDNAC	9	2.28	0.03	2.55	0.10	1.78	50.12
					Average Length		Redundancy		Average Back Exchange (%)		
					12.83		1.76		24.26		

Table S3.2. HDX Data Quality.

HDX data quality for all analyzed peptides. Peptides where multiple charge states were analyzed are included in the table as individual entries. The average deuterium uptake values and standard deviations for the 0 Second time points are included for all conditions. Peptides marked “Not Found” indicate where the corresponding ion was found but displayed weak intensity, overlapping ions, or significant signal loss in one or more time points.

Chapter 4: Strain Specific Mechanisms of HA Fusion Activation and an Improved Pulse Labeling HDX-MS Workflow

4.1 Introduction

Influenza HA serves as an invaluable model system for studying the mechanism of fusion activation and protein mediated membrane fusion. It is unclear, however, whether the mechanistic models derived from the study of the HA described in the previous chapters (a subtype H3 HA in the pulse labeling HDX-MS study and H5 in the sm-FRET study presented by Das et al.) are directly generalizable across all HA subtypes that exhibit different pH sensitivities and overall stability, or to other class I fusion proteins that are triggered by different signals [1-4]. Different influenza virus strains vary widely in their acid stabilities and fusion kinetics, and may exhibit different mechanisms of fusion activation [5-13]. Evidence suggests that even in the pre-fusion neutral pH conformation, different HAs can vary in their conformational and structural dynamics [1, 2, 14]. For example, in all of our HDX-MS experiments (both pulse and continuous labeling) with an H3 and H1 subtype HA we found no evidence of multiple conformations in the pre-fusion state at neutral pH [1, 2, 14] (Garcia et al. Unpublished Data). However, by sm-FRET Das et al. were able to detect multiple interconverting populations at neutral pH [1]. While the location and size of the fluorescent tag may have contributed to these conformational dynamics, our HDX-MS data suggests that the pre-fusion dynamics can vary significantly for different HAs. Currently we do not fully understand the structural basis for these, and other, functional variations and how they manifest mechanistically during fusion activation. We aim to further optimize our pulse labeling HDX-MS workflow to serve as a broadly applicable method for studying strain specific differences in HA's mechanism of fusion activation and monitoring the complete series of fusogenic conformational changes in HA during fusion with a target membrane.

Modulating HAs Acid Stability is an Adaptive Mechanism

Once activated by low pH, HA mediated membrane fusion occurs rapidly [1, 3, 6, 15]. Evidence suggests that the low pH induced activation of HA, and formation of a fusion active intermediate state capable of engaging the target membrane, is the rate limiting step in the fusion reaction [1, 2, 16]. Once HA engages the target membrane, the reorganization to the post-fusion state and fusion of the viral and host membranes occurs rapidly [1]. Thus, HA's acid stability is a primary factor in controlling when fusion, and the transfer of the viral genome and replication machinery into the cytosol, occurs during an infection [3, 5-13, 15, 17, 18]. The timing of the genome transfer is important for maximizing the chances of a successful infection; delivery of the genome too early or too late during endosomal trafficking can limit the likelihood that the genome will be transferred to the nucleus without incident [6-10, 13, 18-22].

Differences in HA's acid stability, along with receptor binding specificity, are strongly linked to virulence and host tropism [5-13, 18, 20, 23-25]. For example, HAs from highly pathogenic avian influenza viruses (HPAIs) are less acid stable and activate at higher pHs (pH 5.3 – 5.9) compared to the seasonal human pathogenic circulating strains (pH 5.0) [5-13, 20, 24, 25]. Zoonotic transmission events are often associated with changes, resulting from antigenic shift and antigenic drift, in HA's receptor binding specificity and acid stability [5-11, 13, 18, 20, 23-28]. For example, the 2009 pandemic H1N1 (A/California/7/2009 – H1N1pdm) strain becomes activated at pH 5.4 whereas a later strain (A/Brisbane/10/2010) that evolved from H1N1pdm is more acid stable and fuses at pH 5.0 [7, 11, 12, 26]. The difference in acid stability was attributed to a single amino acid mutation in HA2, E47K, which forms a stabilizing salt bridge with a highly conserved residue in HA1 (E21) [7, 11]. When this mutation was introduced in H1N1pdm Cal/09 HA the virus became more infectious and virulent in ferrets [7]. Mutations that affect HA's acid stability have been associated with increased virulence in mouse models for H1, H3, and H7 influenza viruses [8, 13, 18]. Similarly, mutations that lowered the pH activation threshold for a HPAI H5N1 strain below pH 5.6 were associated with decreased infectivity and virulence;

further supporting the idea that HA's acid stability is directly linked to host-tropism and virulence [8, 10, 13, 25, 27-30]. When clinical isolates of a human pathogenic H3N2 influenza virus (Brisbane/07) were compared to lab adapted H3N2 strains (H3N2 X-31 and Udorn) it was found that HA from the clinical isolate was more acid stable than its lab adapted counterparts [6]. Typically, a virus' fusion efficiency is highly dependent on pH, increasing in efficiency from the pH where fusion is first observed, peaking at an optimal pH, and then sharply decreasing as fusion is outcompeted by the rapid acid inactivation of HA [8, 31]. However, the Brisbane/07 H3N2 isolate displayed no such dependence and was equally fusion efficient at the first pH where fusion was observed (pH 5.5) as the lowest pH conditions tested (pH 4.5) [6]. The authors concluded that strains such as Brisbane/07 have adapted to fuse under an extended pH range with constant, albeit low, efficiency so that infection may occur under broader conditions; whereas, the lab adapted strains have evolved to infect and fuse with high efficiency under limited and specific conditions [6, 9, 17, 32]. Similar adaptations have been seen in the H1N1 PR8 strain that has been adapted for laboratory growth [17]. While the structural basis for how mutations such as E47K in H1N1pdm Cal/09 and Brisbane/10 can be easily rationalized from high-resolution structural information, we do not yet understand how these stabilizing or destabilizing mutations impact the mechanism of fusion activation [7, 11, 12, 26, 28, 30, 33, 34]. It is possible that mutations in and around the fusion peptide pocket in the core of HA2 destabilize the sequestered fusion peptide resulting in fusion peptide release at elevated pHs [25, 27-30, 33-36]. Similarly, mutations in and around ionizable residues throughout HA1 may function to destabilize the globular head interface or HA1-HA2 interface [27-30, 33-35, 37]. These critical, and often highly conserved, residues are thought to function as pH sensors throughout HA and regulate HA's fusion activation [28-30, 33, 36]. Changes in the residues themselves, or local environment, can dramatically alter the acid stability of HA [30, 33]. However, it is not clear whether mutations that destabilize the fusion peptide or globular head interface shift the mechanism of fusion activation towards either a HA1 uncaging or fusion peptide release mechanism.

We seek to understand how HAs mechanism of fusion activation differs amongst diverse strains of influenza A virus. Furthermore, optimization of the previously described pulse labeling HDX-MS workflow should enable us to monitor all stages of HA's conformational changes including HA2s C-terminal reorganization and asymmetric fold-back that occurs as HA reorganizes from the extended helical intermediate to the six-helix bundle post-fusion state [4, 38].

4.2 Results and Discussion

Strain Specific Mechanisms of HA Fusion Activation

Our previous studies have focused on characterizing the mechanism of HA fusion activation using the X-31 H3N2 strain which has been heavily adapted for laboratory use and extensively studied. As previously discussed, X-31 influenza membrane fusion efficiency is strongly dependent on pH and has adapted its fusogenic properties for growth in chicken eggs and tissue culture [6, 9, 14]. It is well known that HAs from different subtypes or groups have markedly different acid stabilities [1, 5-11, 13, 14, 17, 18, 20, 24, 25, 27-30, 33-36]. Preliminary HDX-MS data indicates H3 HA from X-31 and H1 HA from H1N1 PR8 respond to acidic conditions approaching fusion activation differently [14] (Garcia et al. Unpublished Data). Garcia et al. showed that under mildly acidic pHs approaching fusion activation H3 HA displayed polarized dynamic changes across the globular head and fusion peptide proximal subdomain. This data suggested that as you approach fusion activation the HA1-HA1 protomeric interface becomes bolstered whereas the fusion peptide and fusion peptide proximal subdomain become more dynamic. The authors concluded that these dynamic changes suggest X-31 HA is primed for activation through a fusion peptide release mechanism [14]. Using the same approach, Garcia et al. observed increased dynamics throughout HA in H1 HA from H1N1 PR8 (Garcia et al. Unpublished Data). These strain specific dynamic changes suggest that HAs from different strains may activate in different ways. Thus, we sought to characterize the mechanism of fusion activation for H1N1 PR8 influenza virus.

In order to characterize the mechanism of fusion activation by pulse labeling HDX-MS we first had to characterize the membrane fusion efficiency and pH dependence of H1N1 PR8 so that the conditions used during activation are analogous to those used for X-31 [2, 14]. Using a fluorescence dequenching membrane fusion assay we can monitor fusion peptide release and membrane fusion as previously described [14, 39-42]. When the HA fusion peptide is released from sequestration it induces leakage in synthetic liposomes containing a hydrophilic fluorescent dye, SRB, under self-quenching concentrations. As the fusion peptide disrupts the target membrane SRB is released and becomes de-quenched (Figure 4.1 A and B) [14, 39-41]. As the membrane fusion reaction proceeds and the viral and liposomal membranes begin to merge, the hydrophobic dye contained within the viral membrane diffuses into the newly merged membranes and becomes de-quenched thus reporting on membrane fusion (Figure 4.1 C and D) [14, 39-41].

We found that H1N1 PR8 was overall less fusogenic than H3N2 X-31 and becomes activated at a higher pH [14]. Previous experiments suggested that H1N1 PR8 HA is prone to rapid acid inactivation at low pH conditions approaching pH 5.0 (Unpublished Data). Compared to X-31, we did not observe as strong a dependence on pH for H1N1 PR8's fusion efficiency likely related to PR8's overall low fusion efficiency [14]. From pH 5.6 to pH 5.4 there was a relatively constant increase in the rate and extent of liposomal disruption and membrane fusion (Figure 4.1). At pH 5.3 and below we observed a comparatively sharp increase in the rate and extent of membrane fusion (Figure 4.1 C and D). At pH 5.0 both the rate and extent of liposome disruption and membrane fusion increased dramatically compared to any other condition (Figure 4.1). Based on these results we carried out preliminary pulse labeling HDX-MS experiments using H1N1 PR8 influenza virus at pH 5.10 at 37°C in order to assess the kinetics of HA fusion activation and determine the optimal time course and pH conditions to use in future experiments.

Pulse labeling HDX-MS of H1N1 PR8 influenza virus was performed exactly as described in Chapter 3 [2]. The relative concentration of HA on the viral surface was determined by SDS-PAGE using a soluble HA ectodomain construct expressed in and purified from mammalian cells. We focused our analysis on key reporter peptides in HA1 and HA2 including the HA1 F' domain and "30-loop", HA1-HA1 protomeric interface, and HA2 A-helix and B-loop. Based on the fluorescence data we expected HA from H1N1 PR8 to activate earlier and transition to the post-fusion state faster than H3 HA from X-31. Surprisingly, in our initial pulse labeling HDX-MS experiments at pH 5.10 we failed to capture any of the fusogenic conformational changes in H1N1 PR8 HA. N- and C-terminal HA1 peptides in the F' domain remained largely unchanged in the early time points and displayed a partial transition to an unfolded state in late time points, suggesting that our conditions may have triggered HA too quickly. Our fluorescence data indicated that at 37°C PR8 HA can spontaneously trigger at neutral pH resulting in release of the HA2 fusion peptide and disruption of the liposomal membrane (data not shown). Based on these results, we aim to perform future pulse labeling HDX-MS experiments on PR8 influenza virus at pH 5.4 and room temperature so that the conformational changes occur on a tractable timescale. Furthermore, the overall signal intensity from peptides throughout HA in the preliminary pulse labeling HDX-MS experiments was lower compared to X-31 HA for samples containing the same amount of HA. Future experiments will be performed using a newly optimized detergent solubilization step during the HDX-MS workflow that increases pepsin digestion efficiency for all conformational states of HA (described in detail below).

Detergent Solubilization of HA Enables Complete Monitoring of HA's Conformational Changes

Thus far our pulse labeling HDX-MS approach has enabled us to monitor conformational changes throughout HA for the fusion peptide release and HA1 head opening events, formation of the dynamic intermediate state, and the transition to the protected post-fusion like state [2]. However,

currently we are unable to definitively assign the highly protected terminal state we see in the HA2 A-helix and B-loop to the extended helical intermediate or true post-fusion six-helix bundle state [1, 2, 4]. Our peptide coverage throughout HA2 was limited, preventing us from observing conformational changes in the C-terminal domain of HA2 including the C-terminal helix-to-loop reorganization and the "leash in the groove" fold back that occurs as HA2 reorganizes from the extended helical intermediate to the six-helix bundle post-fusion state [1, 2, 4, 38, 43-45]. Recently, single particle cryo-EM analysis of the acid activated HA ectodomain indicated that the C-terminal reorganization of HA2 occurs after the extended helical intermediate is formed [4]. However, the exact nature and timing of this conformational change remains unresolved in their data due to experimental limitations [4]. In contrast, molecular dynamics simulations performed by Eddy et al. indicate that, when the N- and C-termini of HA2 are anchored in opposing membranes, the coiled-coil structure in HA2 does not fully form until the C-terminal domain of HA2 has zippered up and along the helical axis [45]. To date no study has been able to monitor this final stage of HAs fusogenic conformational change in high resolution. Furthermore, it is not well understood how this conformational change occurs during membrane fusion. In order for HA to reorganize from the extended helical intermediate bridging the viral and target membranes to the post-fusion six-helix bundle state with the N- and C-termini of HA2 recombined in the newly merged membrane HA must break its 3-fold symmetry [2, 4, 37, 38, 40, 41, 45-47]. Characterizing these final conformational changes in HA2 by pulse labeling HDX-MS should provide valuable insight into how HA reorganizes into the post-fusion state and how this reorganization effects the membranes during fusion.

As previously described, in our pule labeling HDX-MS workflow HA on the viral surface was proteolyzed under quench conditions using soluble porcine pepsin [2]. Together steric access to HA on the viral surface by pepsin and HAs conformation dependent protease resistance contributed to our severely limited sequence coverage in HA2. In solution digestion with pepsin is also inhibited by the high concentration of denaturant present in the quench buffer and is prone to autoproteolysis. Recently,

online digestion with immobilized pepsin has replaced in solution digestion for most HDX-MS workflows and affords significantly higher digestion efficiency even in the presence of non-ionic detergents [48-53]. HDX-MS of peripheral and integral membrane proteins has become increasingly common and accessible with advances in sample handling procedures [54-63]. Membrane proteins, including viral surface proteins, can be solubilized from membranes using MS-friendly non-ionic detergents and the phospholipids can be readily removed from solution under quench conditions before analysis [56, 61, 63-67].

Thus, we modified our pulse labeling HDX-MS workflow to incorporate a detergent solubilization and lipid depletion step (Figure 4.2). Quench buffer was prepared as previously described with the addition of 0.2% DDM (w/v) and pulse labeled samples were incubated under quench conditions with DDM for 30 seconds and vortexed to ensure efficient solubilization of the viral membrane and HA. Phospholipids from the viral membrane were removed from solution by addition of zirconium oxide resin. Solubilized HA was purified from the viral core and zirconium resin by centrifugal filtration at 0°C and immediately flash frozen in liquid nitrogen prior to analysis. Samples were digested online using immobilized pepsin and analyzed by LC-MS-IMS as previously described [2]. Peptide coverage was determined using a 0-second neutral pH undeuterated control and a 10-minute acidified undeuterated control (pH 5.10 37°C) to ensure peptide coverage was maintained throughout HAs conformational changes. Solubilization with DDM and online digestion with immobilized pepsin improved sequence coverage in HA2 from 39% to 79% (Figure 4.3). Furthermore, signal intensities for all peptides throughout HA1 and HA2 were dramatically improved compared to previous experiments. We did not observe any appreciable impact on signal intensity or quality due to ion suppression resulting from ionized detergent or lipids. Sequence coverage can be further improved through identification of the abundant glycoform for the single N-linked glycan present in HA2 which is currently absent in our analysis. Under these conditions we anticipate being able to monitor all HA2 peptides throughout the

complete series of conformational change with no significant reduction in signal intensity resulting from inconsistent digestion or conformation specific protease resistance. Furthermore, we believe this approach is broadly applicable for HDX-MS analysis all viral surface proteins including influenza NA and HIV-1 Env by continuous or pulse labeling. Under quench condition the influenza virus core collapses on itself and dissociates upon return to neutral pH making purification of HA and NA from solution relatively easy [19, 22]. For other enveloped viruses however, the abundance of internal proteins will likely result in higher background signal and overlapping peptides from contaminating proteins and will require further optimization.

Preliminary pulse labeling HDX-MS experiments using the improved detergent solubilization workflow are currently underway for X-31 influenza virus. These experiments aim to characterize the conformational changes in the C-terminal domain of HA2. Future work aims to use the improved workflow to monitor HAs conformational change during fusion with synthetic liposomes and characterize strain specific mechanisms of fusion activation.

4.3 Materials and Methods

Purification and DiD Labeling of H1N1 PR8 Influenza Virus

H1N1 PR8 influenza virus grown in embryonated chicken eggs was purchased from Charles River Laboratories. Virus was spin purified and labeled with 1,1'-Dioctadecyl-3,3,3',3'-tetramethylindodicarbocyanine (DiD) as previously described for fluorescence monitored membrane fusion experiments or purified without labeling for HDX-MS [2, 40, 41]. Labeled virus was resuspended in HBS buffer pH 7.4 (10 mM HEPES, 150 mM NaCl, and 50 mM sodium citrate) at 10 mg/mL total protein. For HDX-MS virus was resuspended in HDX HBS pH 7.4 (10 mM HEPES and 150 mM NaCl) at 10 mg/mL total protein.

Liposome Preparation and Characterization

Liposomes composed of 1,2-dioleoyl-*sn*-glycero-3phophocholine (DOPC) lipid, 25% cholesterol, and 5% ganglioside GD1a as a sialic acid receptor for HA were prepared by lipid extrusion as previously described [40, 41]. Briefly, DOPC, cholesterol, and GD1a stocks were combined in chloroform and dried under nitrogen gas and stored under vacuum for at least two hours and up to 12 hours. The lipid film was resuspended in HBS+SRB buffer pH 7.4 (10 mM HEPES, 150 mM NaCl, 50 mM sodium citrate, and 25 mM sulforhodamine B (SRB)). Following 6 freeze-thaw cycles using liquid nitrogen the liposomes were extruded 21 times using a 100 nm polycarbonate membrane and purified using a PD-10 desalting column (GE Healthcare) into HBS buffer pH 7.4. Liposomes were characterized for size and homogeneity by dynamic light scattering using a DynaPro NanoStar analyzer (Wyatt Technologies) and stored in the dark at 4°C for up to 7 days.

Fluorescence Monitored Membrane Fusion

Fluorescence monitored membrane fusion experiments were performed as previously described [40, 41]. DiD labeled H1N1 PR8 virus and SRB containing liposomes were combined, brought to 60 µL final volume, and incubated at pH 7.4 and 37°C for 10 minutes in a quartz cuvette to allow virus and liposomes to equilibrate and associate. Liposomes were in high excess to virus in all experiments. After equilibration 40 µL of acidification buffer (empirically determined ratios of HBS pH 7.4 and HBS pH 3.0 buffers were used to achieve the target pH at 100 µL total volume) was added and rapidly mixed with the virus and liposomes. Fluorescence dequenching was monitored using a Varian Cary Eclipse spectrophotometer using excitation and emission pairings of 644/665 nm for DiD and 565/586 nm for SRB with 2.5 nm slit widths. Membrane fusion was monitored for 30 minutes before addition of Triton X-100 to a final concentration of 1% to fully disrupt all liposomal and viral membranes resulting in maximum dequenching. The fluorescence dequenching data was normalized using the initial fully quenched (F_0) and final fully dequenched (F_{max}) signals as follows: $[(F_T - F_0)/(F_{max} - F_0)]$.

Pulse Labeling HDX-MS of H1N1 PR8 Influenza

The pulse labeling reactions described in this chapter were performed by Chengbo Chen under the supervision of Mark Benhaim. Pulse labeling HDX-MS of H1N1 PR8 influenza virus at pH 5.1 was performed identically as described previously [2]. For each reaction, a stock of purified influenza virus kept at 37°C and containing 10.0 µg of HA in HDX HBS pH 7.50 buffer was rapidly diluted 1:1 with HDX HBS Acidification buffer (150 mM NaCl, 10 mM HEPES, 80 mM Citrate, and 0.02% NaN_3) to a final pH of 5.10 at 37°C. Virus was acidified for 5 seconds, 10 seconds, 15 seconds, 30 seconds, 45 seconds, 1 minute, 3 minutes, 5 minutes, and 10 minutes. Following acidification, each reaction was rapidly pulse labeled with deuterium for 5 seconds at room temperature (22°C) by dilution into Pulse Deuteration Buffer (25 mM Phosphate, 150 mM NaCl, 0.02% NaN_3, and 85% D_2O (Cambridge Isotope Laboratories))

to a final pH* 8.0. The pulse labeling reactions were then rapidly quenched by dilution 1:1 with ice-cold quench buffer (8 M Urea, 200 mM TCEP [tris(2-carboxyethyl) phosphine] and 0.2% formic acid (FA)) with 30 μg/mL of porcine pepsin (Worthington Labs) to a final pH of 2.50 and digested on ice for 5 minutes. The labeled HA peptides were separated from intact virions by high speed centrifugation at 25,000 rcf and 0°C for 2 minutes. The supernatant was collected and immediately flash frozen in liquid nitrogen then stored at -80°C until analysis. Undeuterated samples were prepared identically to the deuterated samples with water in place of D_2O. A no acidification or "0 second" control was also prepared where the acidification buffer was included with the Pulse Deuteration Buffer and was otherwise treated identically to acidified reactions. All samples were prepared containing 0.25 μg/mL of each PPPI and PPPF tetrapeptides (AnaSpec) as internal exchange standards [68]. Pulse labeling reactions were performed in triplicate by manual pipetting. All HDX buffers were prepared with LC-MS grade Optima Water (Fischer Scientific). Totally deuterated (TD) samples were prepared by collecting purified peptide eluent following reverse phase LC separation of a pepsin digested undeuterated sample. Following evaporation of the LC elution buffer the peptides were resuspended in HDX HBS pH 7.50 Buffer, deuterated in Pulse Deuteration Buffer for 2 hours at 37°C, and quenched and frozen as described above.

Detergent Solubilization of X-31 HA

For each reaction, a stock of purified X-31 influenza virus kept at 37°C and containing 10.0 μg of HA in HDX HBS pH 7.50 buffer was rapidly diluted 1:1 with HDX HBS Acidification buffer (150 mM NaCl, 10 mM HEPES, 80 mM Citrate, and 0.02% NaN_3) to a final pH of 5.10 at 37°C. Virus was acidified for 0 seconds or 10 minutes. Following acidification, each reaction was rapidly "pulse labeled" for 5 seconds at room temperature (22°C) by dilution into Mock Pulse Deuteration Buffer (25 mM HEPES, 150 mM NaCl, 0.02% NaN_3) to a final pH 8.0. The pulse labeling reactions were then rapidly quenched by dilution

1:1 with ice-cold quench buffer (8 M urea, 200 mM TCEP [tris(2-carboxyethyl) phosphine], 0.2% DDM, and 0.2% formic acid (FA)) to a final pH of 2.50, vortexed and stored on ice for 30 seconds. Following detergent solubilization 10 μL of ice-cold zirconium oxide resin slurry (300 mg/mL) in 0.1% FA was added to the quenched sample, immediately vortexed, incubated on ice for 1 minute and vortexed again. The quenched sample was then transferred to a pre-chilled 0.2 μm spin filter and centrifuged for 1 minute at 0°C to remove the zirconium oxide resin and viral core. The filtrate was immediately transferred to a fresh 0.6 mL tube and flash frozen in liquid nitrogen. All samples were prepared containing 0.25 μg/mL of each PPPI and PPPF tetrapeptides (AnaSpec) as internal exchange standards [68]. All HDX buffers were prepared with LC-MS grade Optima Water (Fischer Scientific).

Reverse Phase Liquid Chromatography and Mass Spectrometry

Analysis by LC-MS was performed as previously described [2]. Samples were thawed for 5 minutes on ice and manually injected into a custom built HDX-MS LC sample manager kept at 0°C (manuscript in preparation, Watson et al.). Whole virus PR8 HA samples were trapped on a Waters ACQUITY UPLC CSH C18 VanGuard 130Å, 1.7 μm, 2.1 mm by 5 mm trap column for 3 minutes with a flow of solvent A [2% acetonitrile, 0.1% FA, 0.025% trifluoroacetic acid (TFA)] at a rate of 150 μL/min. Detergent solubilized X-31 HA samples were digested online with immobilized pepsin for 5 minutes and trapped as previously described [2, 69]. Peptides were resolved over a Waters ACQUITY UPLC CSH C18 130Å, 1.7 μm, 1 x 100 mm column using a 20 minute linear gradient of 3% to 50% solvent B (Solvent B: 100% acetonitrile and 0.1% FA) and analyzed using a Waters Synapt G2-Si Q-TOF with ion mobility enabled. Source and desolvation temperatures were 70°C and 130°C respectively. The StepWave ion guide settings were tuned to prevent non-uniform gas phase proton exchange in the source [70]. A series of trap column wash steps were implemented between each injection to minimize carryover [71].

Figures

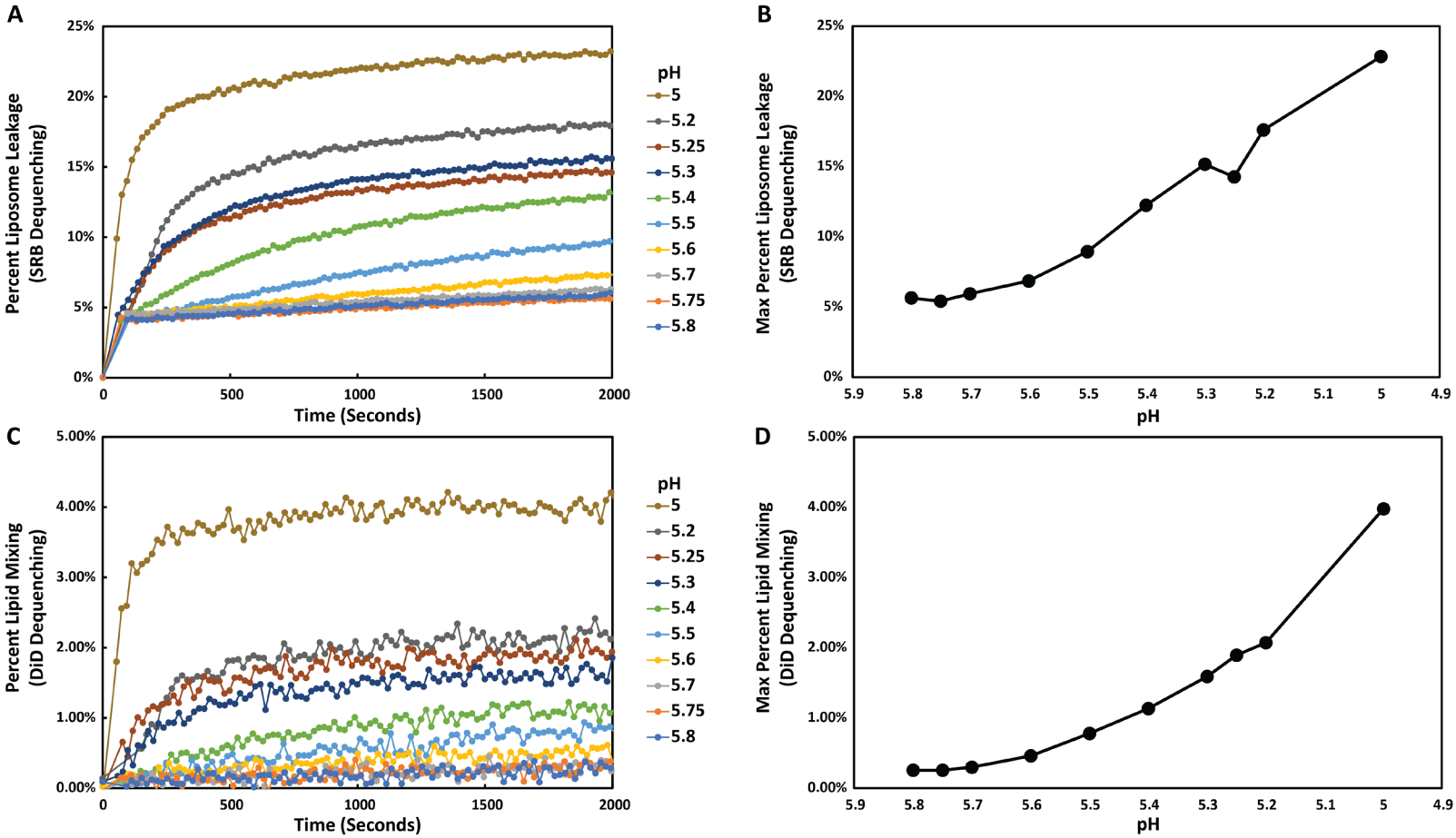

Figure 4.1 H1N1 PR8 Influenza Fluorescence Monitored Membrane Fusion. (A) Normalized liposome leakage as a function of activation pH reports on fusion peptide release and disruption of the liposomal membrane over time. (B) Maximum liposome leakage shows the pH dependence of HA fusion activation. (C) Normalized lipid mixing reports on HA mediated membrane fusion between H1N1 PR8 virions and synthetic liposomes. The kinetics and efficiency of membrane fusion increase as a function of activation pH. (D) Maximum lipid mixing shows the final efficiency of membrane fusion. In contrast to H3N2 X-31 membrane fusion is relatively inefficient and does not show a strong dependence on pH (Data not shown). Fluorescence dequenching was normalized using a maximum dequenched value resulting from detergent solubilization of liposomes and virus.

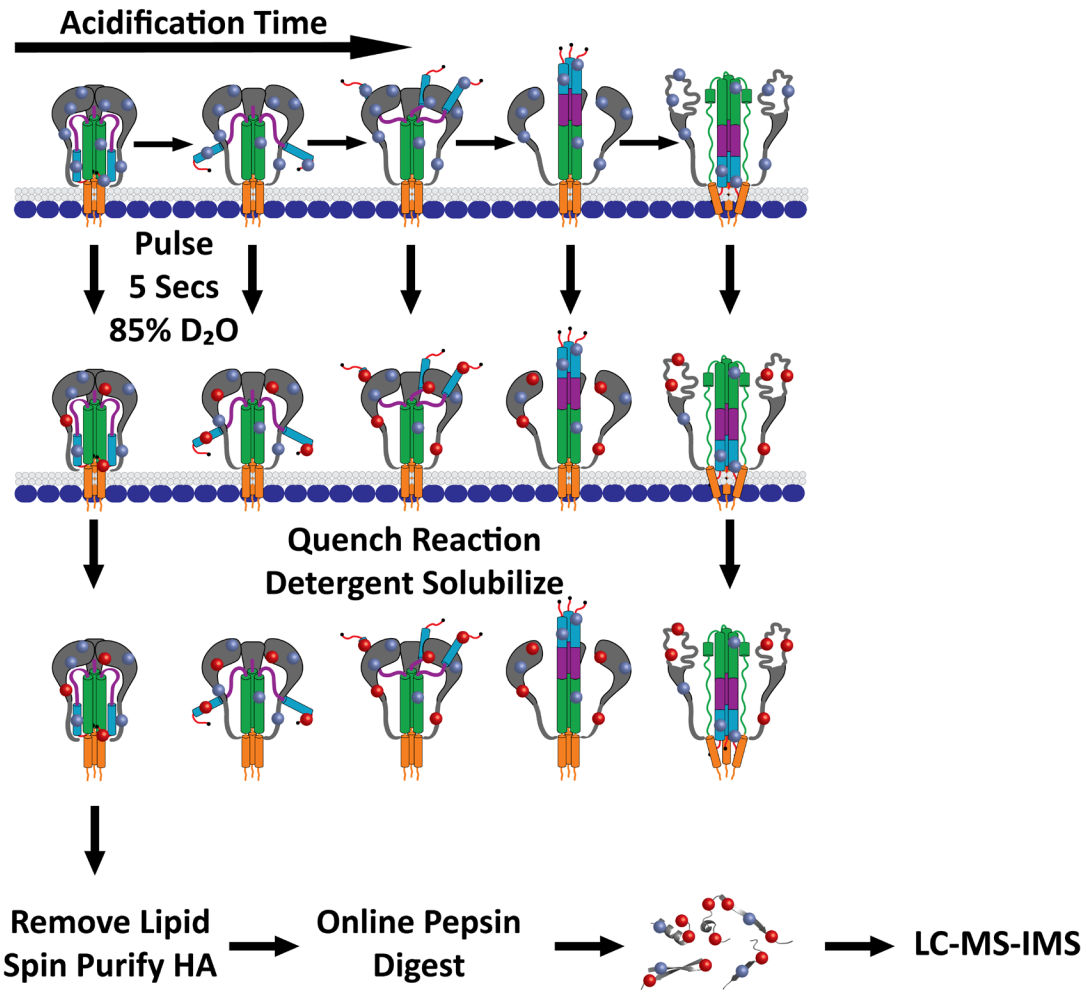

Figure 4.2 Schematic of Improved Pulse Labeling Workflow with Detergent Solubilization. Following pulse labeling of HA on the surface of Influenza virions as previously described the samples are quenched in buffer containing 0.2% DDM on ice. Following a 30 second incubation with the DDM containing quench buffer a slurry of ZrO_2 resin is added in order to deplete the free phospholipids from solution prior to MS analysis. The slurry and viral core is removed from solution following filtration through a 0.2 µm spin filter and the supernatant containing solubilized and labeled HA is rapidly flash frozen in liquid nitrogen and analyzed as previously described using a custom build HDX UPLC system with online pepsin digestion.

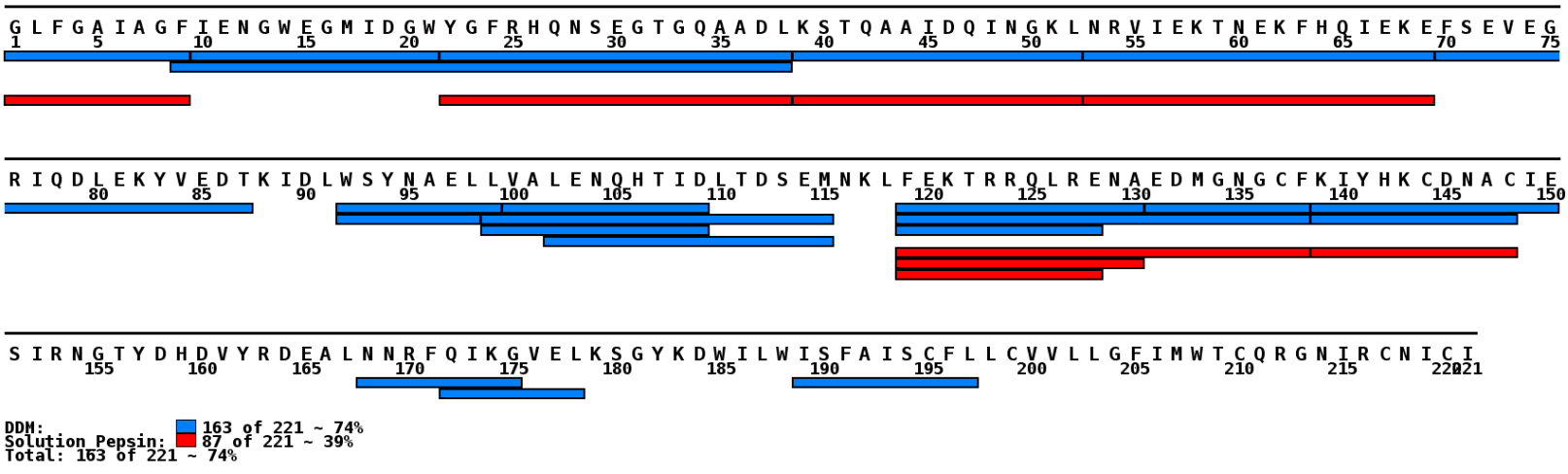

Figure 4.3 Peptide Coverage of X-31 HA2. Coverage map of the HA2 fusion domain from X-31 influenza virus comparing peptide coverage obtained from previous digestion conditions (Red) and the improved detergent solubilization and online pepsin digestion workflow (Blue). Sequence coverage improved dramatically throughout all of HA2 as a result of detergent solubilization and online pepsin digestion. Coverage map generated using MSTools [72].

References

1. Das, D.K., et al., *Direct Visualization of the Conformational Dynamics of Single Influenza Hemagglutinin Trimers.* Cell, 2018. **174**(4): p. 926-937 e12.
2. Benhaim, M., et al., *Structural monitoring of a transient intermediate in the hemagglutinin fusion machinery on influenza virions.* Sci Adv, 2020.
3. Benhaim, M.A. and K.K. Lee, *New Biophysical Approaches Reveal the Dynamics and Mechanics of Type I Viral Fusion Machinery and Their Interplay with Membranes.* Viruses, 2020. **12**(4).
4. Benton, D.J., et al., *Structural transitions in influenza haemagglutinin at membrane fusion pH.* Nature, 2020.
5. Schrauwen, E.J., et al., *Amino Acid Substitutions That Affect Receptor Binding and Stability of the Hemagglutinin of Influenza A/H7N9 Virus.* J Virol, 2016. **90**(7): p. 3794-9.
6. Costello, D.A., G.R. Whittaker, and S. Daniel, *Variations in pH sensitivity, acid stability, and fusogenicity of three influenza virus H3 subtypes.* J Virol, 2015. **89**(1): p. 350-60.
7. Cotter, C.R., H. Jin, and Z. Chen, *A single amino acid in the stalk region of the H1N1pdm influenza virus HA protein affects viral fusion, stability and infectivity.* PLoS Pathog, 2014. **10**(1): p. e1003831.
8. Zaraket, H., O.A. Bridges, and C.J. Russell, *The pH of activation of the hemagglutinin protein regulates H5N1 influenza virus replication and pathogenesis in mice.* J Virol, 2013. **87**(9): p. 4826-34.
9. Galloway, S.E., et al., *Influenza HA subtypes demonstrate divergent phenotypes for cleavage activation and pH of fusion: implications for host range and adaptation.* PLoS Pathog, 2013. **9**(2): p. e1003151.
10. DuBois, R.M., et al., *Acid stability of the hemagglutinin protein regulates H5N1 influenza virus pathogenicity.* PLoS Pathog, 2011. **7**(12): p. e1002398.
11. Maurer-Stroh, S., et al., *A new common mutation in the hemagglutinin of the 2009 (H1N1) influenza A virus.* PLoS Curr, 2010. **2**: p. RRN1162.
12. Yang, H., P. Carney, and J. Stevens, *Structure and Receptor binding properties of a pandemic H1N1 virus hemagglutinin.* PLoS Curr, 2010. **2**: p. RRN1152.
13. Reed, M.L., et al., *The pH of activation of the hemagglutinin protein regulates H5N1 influenza virus pathogenicity and transmissibility in ducks.* J Virol, 2010. **84**(3): p. 1527-35.
14. Garcia, N.K., et al., *Dynamic changes during acid-induced activation of influenza hemagglutinin.* Structure, 2015. **23**(4): p. 665-76.
15. Lakadamyali, M., et al., *Visualizing infection of individual influenza viruses.* Proc Natl Acad Sci U S A, 2003. **100**(16): p. 9280-5.
16. Lin, X., et al., *Atomistic simulations indicate the functional loop-to-coiled-coil transition in influenza hemagglutinin is not downhill.* Proc Natl Acad Sci U S A, 2018. **115**(34): p. E7905-E7913.
17. Murakami, S., et al., *Enhanced growth of influenza vaccine seed viruses in vero cells mediated by broadening the optimal pH range for virus membrane fusion.* J Virol, 2012. **86**(3): p. 1405-10.
18. Koerner, I., et al., *Altered receptor specificity and fusion activity of the haemagglutinin contribute to high virulence of a mouse-adapted influenza A virus.* J Gen Virol, 2012. **93**(Pt 5): p. 970-979.
19. Stauffer, S., et al., *Stepwise priming by acidic pH and a high K+ concentration is required for efficient uncoating of influenza A virus cores after penetration.* J Virol, 2014. **88**(22): p. 13029-46.
20. Beigel, J.H., et al., *Avian influenza A (H5N1) infection in humans.* N Engl J Med, 2005. **353**(13): p. 1374-85.

21. Klenk, H.D. and R. Rott, *The molecular biology of influenza virus pathogenicity.* Adv Virus Res, 1988. **34**: p. 247-81.
22. Yoshimura, A. and S. Ohnishi, *Uncoating of influenza virus in endosomes.* J Virol, 1984. **51**(2): p. 497-504.
23. Imai, M. and Y. Kawaoka, *The role of receptor binding specificity in interspecies transmission of influenza viruses.* Curr Opin Virol, 2012. **2**(2): p. 160-7.
24. Imai, M., et al., *Experimental adaptation of an influenza H5 HA confers respiratory droplet transmission to a reassortant H5 HA/H1N1 virus in ferrets.* Nature, 2012. **486**(7403): p. 420-8.
25. Reed, M.L., et al., *Amino acid residues in the fusion peptide pocket regulate the pH of activation of the H5N1 influenza virus hemagglutinin protein.* J Virol, 2009. **83**(8): p. 3568-80.
26. Garten, R.J., et al., *Antigenic and genetic characteristics of swine-origin 2009 A(H1N1) influenza viruses circulating in humans.* Science, 2009. **325**(5937): p. 197-201.
27. Watanabe, Y., et al., *Characterization of H5N1 influenza virus variants with hemagglutinin mutations isolated from patients.* mBio, 2015. **6**(2).
28. Mair, C.M., et al., *Receptor binding and pH stability - how influenza A virus hemagglutinin affects host-specific virus infection.* Biochim Biophys Acta, 2014. **1838**(4): p. 1153-68.
29. Di Lella, S., A. Herrmann, and C.M. Mair, *Modulation of the pH Stability of Influenza Virus Hemagglutinin: A Host Cell Adaptation Strategy.* Biophys J, 2016. **110**(11): p. 2293-2301.
30. Mair, C.M., et al., *A histidine residue of the influenza virus hemagglutinin controls the pH dependence of the conformational change mediating membrane fusion.* J Virol, 2014. **88**(22): p. 13189-200.
31. Mittal, A., T. Shangguan, and J. Bentz, *Measuring pKa of activation and pKi of inactivation for influenza hemagglutinin from kinetics of membrane fusion of virions and of HA expressing cells.* Biophys J, 2002. **83**(5): p. 2652-66.
32. Lin, Y.P., et al., *Adaptation of egg-grown and transfectant influenza viruses for growth in mammalian cells: selection of hemagglutinin mutants with elevated pH of membrane fusion.* Virology, 1997. **233**(2): p. 402-10.
33. Harrison, J.S., et al., *Role of electrostatic repulsion in controlling pH-dependent conformational changes of viral fusion proteins.* Structure, 2013. **21**(7): p. 1085-96.
34. Xu, R. and I.A. Wilson, *Structural characterization of an early fusion intermediate of influenza virus hemagglutinin.* J Virol, 2011. **85**(10): p. 5172-82.
35. Byrd-Leotis, L., et al., *Influenza hemagglutinin (HA) stem region mutations that stabilize or destabilize the structure of multiple HA subtypes.* J Virol, 2015. **89**(8): p. 4504-16.
36. Thoennes, S., et al., *Analysis of residues near the fusion peptide in the influenza hemagglutinin structure for roles in triggering membrane fusion.* Virology, 2008. **370**(2): p. 403-14.
37. Lin, X., et al., *Order and disorder control the functional rearrangement of influenza hemagglutinin.* Proc Natl Acad Sci U S A, 2014. **111**(33): p. 12049-54.
38. Park, H.E., J.A. Gruenke, and J.M. White, *Leash in the groove mechanism of membrane fusion.* Nat Struct Biol, 2003. **10**(12): p. 1048-53.
39. Williams, J.A., et al., *Dissection of epitope-specific mechanisms of neutralization of influenza virus by intact IgG and Fab fragments.* J Virol, 2017.
40. Gui, L., et al., *Visualization and Sequencing of Membrane Remodeling Leading to Influenza Virus Fusion.* J Virol, 2016. **90**(15): p. 6948-62.
41. Lee, K.K., *Architecture of a nascent viral fusion pore.* EMBO J, 2010. **29**(7): p. 1299-311.
42. Hoekstra, D., et al., *Fluorescence method for measuring the kinetics of fusion between biological membranes.* Biochemistry, 1984. **23**(24): p. 5675-81.

43. Chen, J., J.J. Skehel, and D.C. Wiley, *N- and C-terminal residues combine in the fusion-pH influenza hemagglutinin HA(2) subunit to form an N cap that terminates the triple-stranded coiled coil.* Proc Natl Acad Sci U S A, 1999. **96**(16): p. 8967-72.
44. Bullough, P.A., et al., *Structure of influenza haemagglutinin at the pH of membrane fusion.* Nature, 1994. **371**(6492): p. 37-43.
45. Eddy, N.R. and J.N. Onuchic, *Rotation-Activated and Cooperative Zipping Characterize Class I Viral Fusion Protein Dynamics.* Biophys J, 2018. **114**(8): p. 1878-1888.
46. Boonstra, S., et al., *Hemagglutinin-Mediated Membrane Fusion: A Biophysical Perspective.* Annu Rev Biophys, 2018. **47**: p. 153-173.
47. Benton, D.J., et al., *Influenza hemagglutinin membrane anchor.* Proc Natl Acad Sci U S A, 2018. **115**(40): p. 10112-10117.
48. Ahn, J., et al., *Accessing the reproducibility and specificity of pepsin and other aspartic proteases.* Biochim Biophys Acta, 2013. **1834**(6): p. 1222-9.
49. Ahn, J., et al., *Pepsin immobilized on high-strength hybrid particles for continuous flow online digestion at 10,000 psi.* Anal Chem, 2012. **84**(16): p. 7256-62.
50. Wales, T.E., et al., *High-speed and high-resolution UPLC separation at zero degrees Celsius.* Anal Chem, 2008. **80**(17): p. 6815-20.
51. Zhang, H.M., et al., *Enhanced digestion efficiency, peptide ionization efficiency, and sequence resolution for protein hydrogen/deuterium exchange monitored by Fourier transform ion cyclotron resonance mass spectrometry.* Anal Chem, 2008. **80**(23): p. 9034-41.
52. Wang, L., H. Pan, and D.L. Smith, *Hydrogen exchange-mass spectrometry: optimization of digestion conditions.* Mol Cell Proteomics, 2002. **1**(2): p. 132-8.
53. Guttman, M. and K.K. Lee, *Isotope Labeling of Biomolecules: Structural Analysis of Viruses by HDX-MS.* Methods Enzymol, 2016. **566**: p. 405-26.
54. Redhair, M., A.F. Clouser, and W.M. Atkins, *Hydrogen-Deuterium Exchange Mass Spectrometry of Membrane Proteins in Lipid Nanodiscs.* Chemistry and Physics of Lipids, 2019. **220**(Proceedings of the National Academy of Sciences 114 2017): p. 14-22.
55. Martens, C., et al., *Direct protein-lipid interactions shape the conformational landscape of secondary transporters.* Nature Communications, 2018. **9**(1): p. 4151.
56. Li, M., M. Guttman, and W.M. Atkins, *Conformational dynamics of P-glycoprotein in lipid nanodiscs and detergent micelles reveal complex motions on a wide time scale.* Journal of Biological Chemistry, 2018. **293**(17): p. 6297-6307.
57. Reading, E., *Structural Mass Spectrometry of Membrane Proteins within Their Native Lipid Environments.* Chemistry - A European Journal, 2018. **24**(51): p. 13391-13398.
58. Wijesinghe, K.J., et al., *Detection of lipid-induced structural changes of the Marburg virus matrix protein VP40 using hydrogen/deuterium exchange-mass spectrometry.* Journal of Biological Chemistry, 2017. **292**(15): p. 6108-6122.
59. Adhikary, S., et al., *Conformational dynamics of a neurotransmitter:sodium symporter in a lipid bilayer.* Proc Natl Acad Sci U S A, 2017.
60. Reading, E., et al., *Interrogating Membrane Protein Conformational Dynamics within Native Lipid Compositions.* Angewandte Chemie International Edition, 2017. **56**(49): p. 15654-15657.
61. Duc, N.M., et al., *Effective application of bicelles for conformational analysis of G protein-coupled receptors by hydrogen/deuterium exchange mass spectrometry.* J Am Soc Mass Spectrom, 2015. **26**(5): p. 808-17.
62. Hodge, E.A., M.A. Benhaim, and K.K. Lee, *Bridging protein structure, dynamics, and function using hydrogen/deuterium-exchange mass spectrometry.* Protein Sci, 2019.

63. Vadas, O. and John E. Burke, *Probing the dynamic regulation of peripheral membrane proteins using hydrogen deuterium exchange–MS (HDX–MS).* Biochemical Society Transactions, 2015. **43**(5): p. 773-786.
64. O'Brien, D.P., et al., *Hydrogen/Deuterium Exchange Mass Spectrometry for the Structural Analysis of Detergent-Solubilized Membrane Proteins*, in *Expression, Purification, and Structural Biology of Membrane Proteins*. 2020. p. 339-358.
65. Harrison, R.A. and J.R. Engen, *Conformational insight into multi-protein signaling assemblies by hydrogen-deuterium exchange mass spectrometry.* Curr Opin Struct Biol, 2016. **41**: p. 187-193.
66. Rey, M., et al., *Effective Removal of Nonionic Detergents in Protein Mass Spectrometry, Hydrogen/Deuterium Exchange, and Proteomics.* Analytical Chemistry, 2010. **82**(12): p. 5107-5116.
67. Lim, X.X., et al., *Conformational changes in intact dengue virus reveal serotype-specific expansion.* Nat Commun, 2017. **8**: p. 14339.
68. Zhang, Z., A. Zhang, and G. Xiao, *Improved protein hydrogen/deuterium exchange mass spectrometry platform with fully automated data processing.* Anal Chem, 2012. **84**(11): p. 4942-9.
69. Verkerke, H.P., et al., *Epitope-Independent Purification of Native-Like Envelope Trimers from Diverse HIV-1 Isolates.* J Virol, 2016. **90**(20): p. 9471-82.
70. Guttman, M., et al., *Tuning a High Transmission Ion Guide to Prevent Gas-Phase Proton Exchange During H/D Exchange MS Analysis.* J Am Soc Mass Spectrom, 2016. **27**(4): p. 662-8.
71. Fang, J., et al., *False EX1 signatures caused by sample carryover during HX MS analyses.* Int J Mass Spectrom, 2011. **302**(1-3): p. 19-25.
72. Kavan, D. and P. Man, *MSTools—Web based application for visualization and presentation of HXMS data.* International Journal of Mass Spectrometry, 2011. **302**(1-3): p. 53-58.

Chapter 5: Conclusions, Perspectives, and Future Directions

Infection by all enveloped viruses requires fusion of the viral and host membranes in order to deliver the viral genome and replication machinery across the cellular membrane and into the cytosol. The process of viral protein mediated membrane fusion is facilitated by highly specialized protein fusion machines that decorate the surfaces of enveloped viruses [1-8]. The goals of this dissertation were to interrogate and characterize the structural mechanics and conformational dynamics of class 1 viral fusion proteins *in situ* on the surface of authentic or engineered virions using structural mass spectrometry and solution phase biophysical approaches. Collectively the works presented in this dissertation provide unprecedented insight into the structural mechanism by which the influenza hemagglutinin fusion protein becomes activated and mediates the membrane fusion reaction; and describe a robust and broadly applicable HDX-MS platform with which the structural and conformational dynamics of any viral surface antigen can be profiled and characterized. Furthermore, these works underscore the importance of studying the structure and functions of viral fusion proteins and other viral surface antigens using native, or near native, biological systems as opposed to isolated and engineered soluble ectodomains.

Profiling the Structural and Conformational Dynamics of HIV-1 Env

Historically the structure and functions of viral membrane fusion proteins has been characterized using classical high-resolution structural techniques such as X-ray crystallography or cryo-EM [2, 3, 9-11]. However, as previously discussed these approaches provide a limited snapshot of a proteins structure, thus masking a majority of the ever present structural dynamics and conformational fluctuations that are critical to a protein's function, and are often limited to analysis of engineered and stabilized soluble ectodomain constructs [1, 2, 9, 10, 12-18]. Recent evidence has highlighted how these

high-resolution structural studies and engineered protein constructs do not capture or recapitulate the native structural dynamics and conformational ranges of these highly dynamic viral fusion proteins; such as the HIV-1 Env fusion glycoprotein [1-3, 9, 10, 12-26]. Thus, as described in chapter 2, we utilized continuous labeling HDX-MS in combination with cryo-EM and cryo-ET to characterize the structural dynamics and conformational homogeneity of the full length HIV-1 Env fusion glycoprotein on the surface of authentic and engineered viral systems and provided a direct comparison to the soluble and stabilized ectodomain construct. This work demonstrated that HDX-MS can be used to characterize the structural dynamics and conformational homogeneity of viral surface antigens *in situ*. However, peptide sequence coverage was severely limited and thus we were unable to make meaningful conclusions about the structural and conformational dynamics of the native Env trimer in comparison to the soluble ectodomain construct. Despite these limitations these studies provided an invaluable and quantitative assessment of the conformational homogeneity of Env trimers present in the samples, which was critical for developing these platforms for use as vaccine constructs. As discussed in chapter 2, future efforts are aimed at improving sequence coverage so that we can properly and completely assess the structural and conformational dynamics of native Env. These efforts include adapting the modified and improved detergent solubilization aided HDX-MS workflow described in chapter 4 for use with other viral systems outside of influenza virus. Furthermore, efforts are underway to develop a nanoflow-UHPLC HDX-MS sample handling system which will dramatically expand the capabilities of the approach by reducing sample quantity requirements and improving peptide separation which is critical with complex matrices. With these improvements we are confident that this continuous labeling HDX-MS approach will prove to be a robust structural tool for characterizing the native structural and conformation dynamics of the HIV-1 Env, and other, viral fusion proteins that have long eluded characterization. These future studies will provide invaluable insight into the native conformational dynamics of diverse native HIV-1 Env

isolates and aid in the development of vaccine immunogens capable of eliciting a broad immune response [21, 26-42].

Characterizing the Mechanism of HA Fusion Activation

The influenza virus hemagglutinin (HA) fusion protein has served as the prototypical class 1 viral fusion protein for nearly 40 years [1, 2, 8, 14, 43, 44]. Much our understanding of all class 1 fusion proteins and their functions is based upon our understanding of HA. However, much of this understanding had been informed through low resolution biochemical characterization of HA's structure and function and atomic resolution structures of the pre- and post-fusion states of the HA ectodomain [1, 2, 5, 8, 14, 23, 43-61]. As outlined in the introduction and chapter 3, our mechanistic understanding of how HA mediates viral membrane fusion was rooted in the spring-loaded mechanistic model which described HA as a high energy spring-loaded fusion machine, that upon activation rapidly and irreversibly reorganized to the post-fusion state [53, 57]. Despite there being limited structural support for this mechanistic model it persisted as the prevailing model for nearly 30 years, and only recently has the perspective on HA's structural characteristics and mechanism began to shift. One central feature of the spring-loaded model that has defined the structural and behavioral characterization of HA, and thus all class 1 fusion proteins, was the perception of HA as a static, high-energy, spring-loaded fusion "trap" [2, 11, 12, 53, 57, 60, 62, 63]. This perception defined the way researchers thought about how HA behaved and functioned, both at rest and during activation [2, 14, 47]. However, recent studies have began to change this perception and HA is increasingly being viewed as the highly dynamic fusion machine that it truly is [1, 2, 5, 10, 14, 20, 23, 46, 47, 60, 64]. By using techniques such as cryo-ET, sm-FRET, and HDX-MS researchers have been able to capture these dynamics in stunning detail and visualize the dynamic structural and conformational changes in real-time [1, 14, 46, 47, 65]. However, until recently our understanding of HA's mechanism of fusion activation and HA mediated membrane

fusion was still limited. While a competing mechanistic model, the fusion peptide release model, had emerged more recently the fields perception of HA was still dominated by the spring-loaded model despite there being concrete high resolution structural information that directly challenged the model's features [2, 11, 14, 45, 47, 48, 65, 66]. Such works by Fontana et al., Garcia et al., and most recently Das et al. have shown that not only is HA highly dynamic at rest, but upon activation it adopts a dynamic fusion peptide released intermediate state [1, 14, 47, 65]. However, these works failed to describe the complete mechanism of HA fusion activation and HA mediated membrane fusion. Thus, as presented in chapter 3, we developed a pulse labeling HDX-MS approach that enabled us to characterize the mechanism of HA fusion activation and HA mediated membrane fusion in the most complete detail to date [1]. Our data showed that fusion peptide release and reorganization of the HA1-HA1 interface occurred together and enabled the formation of a dynamic fusion peptide released intermediate ensemble whereby the structurally dynamic HA2 fusion domain sampled conformational space in search of a target membrane to engage with. Using cryo-ET we also demonstrated that this intermediate state is not a discrete isolatable state but a dynamic conformational ensemble state, like that proposed by Das et al. [14]. Importantly, our work provided the first direct comparison between how full length HA on the viral surface and the BHA ectodomain responded to activation and showed that once activated BHA reorganized directly to the post-fusion state and did not adopt any intermediate state. This finding clearly demonstrates the importance of studying the mechanics of viral fusion proteins using the native and complete biological systems as the soluble ectodomains cannot accurately recapitulate their native functions.

However, our data was unable to fully resolve some details of HA's reorganization to the post-fusion state that are essential for understanding the complete mechanism of HA mediated membrane fusion. Furthermore, our study was limited to a single group-2 H3 isolate of influenza virus, X-31 H3N2, and thus it remains unclear if there is a single generalizable mechanism for HA fusion activation and HA

mediated membrane fusion. As described in chapter 4, efforts are currently underway to improve the pulse labeling HDX-MS workflow so that we can monitor all of HA's conformational changes during activation and fusion, including the HA2 C-terminal reorganization that drives the N-and C-terminal recombination event during fusion [1, 14, 45, 67]. Currently, the improved HDX-MS workflow resulted in nearly 100% sequence coverage across all of HA including HA2, thus allowing us to monitor all of HA's conformational changes. As previously discussed, by coupling the improved workflow with new sample handling techniques we can dramatically reduce our sample quantity requirements. These improvements will enable us to interrogate the structural mechanics of HA's from diverse isolates and directly investigate how mechanistically and clinically relevant mutations manifest during activation [1, 2, 14, 45, 47, 68-76]. Thus, we believe the pulse labeling HDX-MS platform presented in chapters 3 and 4 of this dissertation will prove itself as an invaluable and highly adaptable biophysical tool for studying the structural mechanics of all class 1 viral fusion proteins.

Final Perspectives

Much of the work presented in this dissertation was aimed at developing a robust and broadly applicable HDX-MS platform for the study of the structural and conformational dynamics of class 1 viral fusion proteins. Furthermore, my primary goal was to use pulse labeling HDX-MS to resolve a nearly 40-year long debate about how the influenza virus HA fusion protein behaved during activation and membrane fusion. These works contribute to a growing body of work using emerging solution based structural approaches to solve challenging problems in structural biology and cement HDX-MS as a powerful and versatile tool in structural biology. These emerging biophysical and structural approaches, including sm-FRET, cryo-ET and HDX-MS, will continue to provide untold insight into the structure and functions of dynamic biological machines and systems.

References

1. Benhaim, M., et al., *Structural monitoring of a transient intermediate in the hemagglutinin fusion machinery on influenza virions.* Sci Adv, 2020.
2. Benhaim, M.A. and K.K. Lee, *New Biophysical Approaches Reveal the Dynamics and Mechanics of Type I Viral Fusion Machinery and Their Interplay with Membranes.* Viruses, 2020. **12**(4).
3. Rey, F.A. and S.M. Lok, *Common Features of Enveloped Viruses and Implications for Immunogen Design for Next-Generation Vaccines.* Cell, 2018. **172**(6): p. 1319-1334.
4. White, J.M. and G.R. Whittaker, *Fusion of Enveloped Viruses in Endosomes.* Traffic, 2016. **17**(6): p. 593-614.
5. Blijleven, J.S., et al., *Mechanisms of influenza viral membrane fusion.* Semin Cell Dev Biol, 2016. **60**: p. 78-88.
6. Harrison, S.C., *Viral membrane fusion.* Virology, 2015. **479-480**: p. 498-507.
7. Colman, P.M. and M.C. Lawrence, *The structural biology of type I viral membrane fusion.* Nat Rev Mol Cell Biol, 2003. **4**(4): p. 309-19.
8. White, J., J. Kartenbeck, and A. Helenius, *Membrane fusion activity of influenza virus.* Embo j, 1982. **1**(2): p. 217-22.
9. Lu, M., et al., *Associating HIV-1 envelope glycoprotein structures with states on the virus observed by smFRET.* Nature, 2019. **568**(7752): p. 415-419.
10. Garcia, N.K. and K.K. Lee, *Dynamic Viral Glycoprotein Machines: Approaches for Probing Transient States That Drive Membrane Fusion.* Viruses, 2016. **8**(1).
11. White, J.M., et al., *Structures and mechanisms of viral membrane fusion proteins: multiple variations on a common theme.* Crit Rev Biochem Mol Biol, 2008. **43**(3): p. 189-219.
12. Benton, D.J., et al., *Structural transitions in influenza haemagglutinin at membrane fusion pH.* Nature, 2020.
13. Yang, Z., et al., *Asymmetric opening of HIV-1 Env bound to CD4 and a coreceptor-mimicking antibody.* Nat Struct Mol Biol, 2019. **26**(12): p. 1167-1175.
14. Das, D.K., et al., *Direct Visualization of the Conformational Dynamics of Single Influenza Hemagglutinin Trimers.* Cell, 2018. **174**(4): p. 926-937 e12.
15. Stadtmueller, B.M., et al., *DEER Spectroscopy Measurements Reveal Multiple Conformations of HIV-1 SOSIP Envelopes that Show Similarities with Envelopes on Native Virions.* Immunity, 2018. **49**(2): p. 235-246 e4.
16. Liu, Y., et al., *Conformational States of a Soluble, Uncleaved HIV-1 Envelope Trimer.* J Virol, 2017. **91**(10).
17. Guttman, M., et al., *CD4-induced activation in a soluble HIV-1 Env trimer.* Structure, 2014. **22**(7): p. 974-84.
18. Munro, J.B., et al., *Conformational dynamics of single HIV-1 envelope trimers on the surface of native virions.* Science, 2014. **346**(6210): p. 759-63.
19. Das, D.K., et al., *Conformational changes in the Ebola virus membrane fusion machine induced by pH, Ca2+, and receptor binding.* PLoS Biol, 2020. **18**(2): p. e3000626.
20. Boonstra, S., et al., *Hemagglutinin-Mediated Membrane Fusion: A Biophysical Perspective.* Annu Rev Biophys, 2018. **47**: p. 153-173.
21. Wang, H., et al., *Partially Open HIV-1 Envelope Structures Exhibit Conformational Changes Relevant for Coreceptor Binding and Fusion.* Cell Host Microbe, 2018. **24**(4): p. 579-592 e4.
22. Ozorowski, G., et al., *Open and closed structures reveal allostery and pliability in the HIV-1 envelope spike.* Nature, 2017. **547**(7663): p. 360-363.

23. Lin, X., et al., *Lowered pH Leads to Fusion Peptide Release and a Highly Dynamic Intermediate of Influenza Hemagglutinin.* J Phys Chem B, 2016. **120**(36): p. 9654-60.
24. Wang, H., et al., *Cryo-EM structure of a CD4-bound open HIV-1 envelope trimer reveals structural rearrangements of the gp120 V1V2 loop.* Proc Natl Acad Sci U S A, 2016. **113**(46): p. E7151-E7158.
25. Ward, A.B. and I.A. Wilson, *Insights into the trimeric HIV-1 envelope glycoprotein structure.* Trends Biochem Sci, 2015. **40**(2): p. 101-7.
26. Sanders, R.W., et al., *A next-generation cleaved, soluble HIV-1 Env trimer, BG505 SOSIP.664 gp140, expresses multiple epitopes for broadly neutralizing but not non-neutralizing antibodies.* PLoS Pathog, 2013. **9**(9): p. e1003618.
27. Ou, L., et al., *Preclinical Development of a Fusion Peptide Conjugate as an HIV Vaccine Immunogen.* Scientific Reports, 2020. **10**(1).
28. Torrents de la Pena, A., et al., *Similarities and differences between native HIV-1 envelope glycoprotein trimers and stabilized soluble trimer mimetics.* PLoS Pathog, 2019. **15**(7): p. e1007920.
29. Sliepen, K., et al., *Structure and immunogenicity of a stabilized HIV-1 envelope trimer based on a group-M consensus sequence.* Nat Commun, 2019. **10**(1): p. 2355.
30. Murin, C.D., I.A. Wilson, and A.B. Ward, *Antibody responses to viral infections: a structural perspective across three different enveloped viruses.* Nat Microbiol, 2019. **4**(5): p. 734-747.
31. Bresk, C.A., et al., *Induction of Tier 1 HIV Neutralizing Antibodies by Envelope Trimers Incorporated into a Replication Competent Vesicular Stomatitis Virus Vector.* Viruses, 2019. **11**(2).
32. Alsahafi, N., et al., *SOSIP Changes Affect Human Immunodeficiency Virus Type 1 Envelope Glycoprotein Conformation and CD4 Engagement.* J Virol, 2018. **92**(19).
33. Burton, D.R., *Advancing an HIV vaccine; advancing vaccinology.* Nature Reviews Immunology, 2018. **19**(2): p. 77-78.
34. Pancera, M., A. Changela, and P.D. Kwong, *How HIV-1 entry mechanism and broadly neutralizing antibodies guide structure-based vaccine design.* Curr Opin HIV AIDS, 2017. **12**(3): p. 229-240.
35. Torrents de la Pena, A., et al., *Improving the Immunogenicity of Native-like HIV-1 Envelope Trimers by Hyperstabilization.* Cell Rep, 2017. **20**(8): p. 1805-1817.
36. Stano, A., et al., *Dense Array of Spikes on HIV-1 Virion Particles.* J Virol, 2017. **91**(14).
37. Racine, T., G.P. Kobinger, and E.J. Arts, *Development of an HIV vaccine using a vesicular stomatitis virus vector expressing designer HIV-1 envelope glycoproteins to enhance humoral responses.* AIDS Res Ther, 2017. **14**(1): p. 55.
38. Liang, Y., et al., *Probing the Impact of Local Structural Dynamics of Conformational Epitopes on Antibody Recognition.* Biochemistry, 2016. **55**(15): p. 2197-213.
39. Guttman, M., et al., *Antibody potency relates to the ability to recognize the closed, pre-fusion form of HIV Env.* Nat Commun, 2015. **6**: p. 6144.
40. Rabinovich, S., et al., *A novel, live-attenuated vesicular stomatitis virus vector displaying conformationally intact, functional HIV-1 envelope trimers that elicits potent cellular and humoral responses in mice.* PLoS One, 2014. **9**(9): p. e106597.
41. Davenport, T.M., et al., *Isolate-specific differences in the conformational dynamics and antigenicity of HIV-1 gp120.* J Virol, 2013. **87**(19): p. 10855-73.
42. Leaman, D.P. and M.B. Zwick, *Increased functional stability and homogeneity of viral envelope spikes through directed evolution.* PLoS Pathog, 2013. **9**(2): p. e1003184.
43. Skehel, J.J., et al., *Changes in the conformation of influenza virus hemagglutinin at the pH optimum of virus-mediated membrane fusion.* Proc Natl Acad Sci U S A, 1982. **79**(4): p. 968-72.

44. Wilson, I.A., J.J. Skehel, and D.C. Wiley, *Structure of the haemagglutinin membrane glycoprotein of influenza virus at 3 A resolution.* Nature, 1981. **289**(5796): p. 366-73.
45. Benton, D.J., et al., *Influenza hemagglutinin membrane anchor.* Proc Natl Acad Sci U S A, 2018. **115**(40): p. 10112-10117.
46. Fontana, J. and A.C. Steven, *Influenza virus-mediated membrane fusion: Structural insights from electron microscopy.* Arch Biochem Biophys, 2015. **581**: p. 86-97.
47. Garcia, N.K., et al., *Dynamic changes during acid-induced activation of influenza hemagglutinin.* Structure, 2015. **23**(4): p. 665-76.
48. Xu, R. and I.A. Wilson, *Structural characterization of an early fusion intermediate of influenza virus hemagglutinin.* J Virol, 2011. **85**(10): p. 5172-82.
49. Leikina, E., et al., *Reversible stages of the low-pH-triggered conformational change in influenza virus hemagglutinin.* EMBO J, 2002. **21**(21): p. 5701-10.
50. Chen, J., J.J. Skehel, and D.C. Wiley, *N- and C-terminal residues combine in the fusion-pH influenza hemagglutinin HA(2) subunit to form an N cap that terminates the triple-stranded coiled coil.* Proc Natl Acad Sci U S A, 1999. **96**(16): p. 8967-72.
51. Kozlov, M.M. and L.V. Chernomordik, *A mechanism of protein-mediated fusion: coupling between refolding of the influenza hemagglutinin and lipid rearrangements.* Biophys J, 1998. **75**(3): p. 1384-96.
52. Korte, T., et al., *Transient changes of the conformation of hemagglutinin of influenza virus at low pH detected by time-resolved circular dichroism spectroscopy.* J Biol Chem, 1997. **272**(15): p. 9764-70.
53. Carr, C.M., C. Chaudhry, and P.S. Kim, *Influenza hemagglutinin is spring-loaded by a metastable native conformation.* Proc Natl Acad Sci U S A, 1997. **94**(26): p. 14306-13.
54. Steinhauer, D.A., et al., *Studies using double mutants of the conformational transitions in influenza hemagglutinin required for its membrane fusion activity.* Proc Natl Acad Sci U S A, 1996. **93**(23): p. 12873-8.
55. Chen, J., et al., *A soluble domain of the membrane-anchoring chain of influenza virus hemagglutinin (HA2) folds in Escherichia coli into the low-pH-induced conformation.* Proc Natl Acad Sci U S A, 1995. **92**(26): p. 12205-9.
56. Bullough, P.A., et al., *Structure of influenza haemagglutinin at the pH of membrane fusion.* Nature, 1994. **371**(6492): p. 37-43.
57. Carr, C.M. and P.S. Kim, *A spring-loaded mechanism for the conformational change of influenza hemagglutinin.* Cell, 1993. **73**(4): p. 823-32.
58. Godley, L., et al., *Introduction of intersubunit disulfide bonds in the membrane-distal region of the influenza hemagglutinin abolishes membrane fusion activity.* Cell, 1992. **68**(4): p. 635-45.
59. Kemble, G.W., et al., *Intermonomer disulfide bonds impair the fusion activity of influenza virus hemagglutinin.* J Virol, 1992. **66**(8): p. 4940-50.
60. White, J.M. and I.A. Wilson, *Anti-peptide antibodies detect steps in a protein conformational change: low-pH activation of the influenza virus hemagglutinin.* J Cell Biol, 1987. **105**(6 Pt 2): p. 2887-96.
61. Klenk, H.D., et al., *Activation of influenza A viruses by trypsin treatment.* Virology, 1975. **68**(2): p. 426-39.
62. Hamuro, Y. and S.J. Coales, *Optimization of Feasibility Stage for Hydrogen/Deuterium Exchange Mass Spectrometry.* Journal of The American Society for Mass Spectrometry, 2018. **29**(3): p. 623-629.
63. Walls, A.C., et al., *Tectonic conformational changes of a coronavirus spike glycoprotein promote membrane fusion.* Proc Natl Acad Sci U S A, 2017. **114**(42): p. 11157-11162.

64. Lin, X., et al., *Order and disorder control the functional rearrangement of influenza hemagglutinin.* Proc Natl Acad Sci U S A, 2014. **111**(33): p. 12049-54.
65. Fontana, J., et al., *Structural changes in Influenza virus at low pH characterized by cryo-electron tomography.* J Virol, 2012. **86**(6): p. 2919-29.
66. Kielian, M., *Mechanisms of Virus Membrane Fusion Proteins.* Annu Rev Virol, 2014. **1**(1): p. 171-89.
67. Park, H.E., J.A. Gruenke, and J.M. White, *Leash in the groove mechanism of membrane fusion.* Nat Struct Biol, 2003. **10**(12): p. 1048-53.
68. Schrauwen, E.J., et al., *Amino Acid Substitutions That Affect Receptor Binding and Stability of the Hemagglutinin of Influenza A/H7N9 Virus.* J Virol, 2016. **90**(7): p. 3794-9.
69. Byrd-Leotis, L., et al., *Influenza hemagglutinin (HA) stem region mutations that stabilize or destabilize the structure of multiple HA subtypes.* J Virol, 2015. **89**(8): p. 4504-16.
70. Cotter, C.R., H. Jin, and Z. Chen, *A single amino acid in the stalk region of the H1N1pdm influenza virus HA protein affects viral fusion, stability and infectivity.* PLoS Pathog, 2014. **10**(1): p. e1003831.
71. Mair, C.M., et al., *Receptor binding and pH stability - how influenza A virus hemagglutinin affects host-specific virus infection.* Biochim Biophys Acta, 2014. **1838**(4): p. 1153-68.
72. Galloway, S.E., et al., *Influenza HA subtypes demonstrate divergent phenotypes for cleavage activation and pH of fusion: implications for host range and adaptation.* PLoS Pathog, 2013. **9**(2): p. e1003151.
73. Maurer-Stroh, S., et al., *A new common mutation in the hemagglutinin of the 2009 (H1N1) influenza A virus.* PLoS Curr, 2010. **2**: p. RRN1162.
74. Reed, M.L., et al., *The pH of activation of the hemagglutinin protein regulates H5N1 influenza virus pathogenicity and transmissibility in ducks.* J Virol, 2010. **84**(3): p. 1527-35.
75. Reed, M.L., et al., *Amino acid residues in the fusion peptide pocket regulate the pH of activation of the H5N1 influenza virus hemagglutinin protein.* J Virol, 2009. **83**(8): p. 3568-80.
76. Thoennes, S., et al., *Analysis of residues near the fusion peptide in the influenza hemagglutinin structure for roles in triggering membrane fusion.* Virology, 2008. **370**(2): p. 403-14.